2014

# Characterisation of a dual detector probe for medical physics applications

Christopher James Pinn
*University of Wollongong*

UNIVERSITY OF WOLLONGONG

Faculty of Engineering and Information Sciences - School of Physics

# Characterisation of a Dual Detector Probe for Medical Physics Applications

CHRISTOPHER JAMES PINN

This thesis is presented as part of the requirement for the

Award of the Degree of

Masters of Science – (Research) – Theoretical Physics

Supervisors - Associate Professor Anatoly Rosenfeld and Doctor Marco Petasecca

University of Wollongong

December 2014

# ACKNOWLEDGEMENTS

A number of people deserve acknowledgement in the production of this thesis. First and foremost should be the members from the University of Wollongong - Centre for Medical Radiation Physics (UOW-CMRP). I would not have started this exciting project without their intervention. Individuals deserving independent citation are Doctors: Marco Petasecca, Anatoly Rosenfeld and Michael Lerch. They are not stated in any particular order and are thanked for their advice regarding theoretical and physical approaches during the Liana Dual Detector Design System ($^3$DS) investigation. In addition, I specifically thank Anatoly Rosenfeld for his patience and time in helping me overcome my technical writing difficulties which ultimately led to the development of this document.

In a similar way CMRP Technicians Peter Ihnat and Martin Morillas provided technical assistance with the apparatus. Marco Petasecca should be acknowledged more extensively. Therefore I would like to individually thank him for his aid in the construction of this paper and for his guidance throughout the entire research work of this project. In particular I thank him for his patience across these 2+ years.

Members of the Australian Nuclear Science and Technology Organisation (ANSTO) should also be acknowledged. In no particular order I thank Doctors: Mark Reinhardt, Dale Prokopovich, and Ramin Raifei. Additional aid from the CMRP was given by Technician Adam Sarbutt, whose involvement in the physical development of the testing chamber and components was highly valued. Dr. Dale Prokopovich provided similar aid as Adam Sarbutt and in addition provided a wealth of theoretical and experimental understanding on detector functionality during the research.

There are many others' who deserve acknowledgement, but space is limited, my parents Michael and Gay Pinn. My sister Melissa Pinn and her new husband Timothy Lukins for both supporting and loving me. My two closest friends, and Kings, Michael Breen and Elliot Yee for providing me with a means to "blow out the much suppressed steam". Nathan Thorpe and Vanja Gracinan should also be thanked for keeping me functional during the closing stages of this Masters work.

Last but certainly not the least in my opinion, I would like to thank God. The one who I believe made me and the universe and sent his one and only son Jesus to die for me upon the cross. For giving me the capacity to do what is presented in this work. In the hope that this device helps others whether suffering from Cancer, or through one of the many other amazing applications this device is capable of. I pray that it brings Glory to him who was, and is, to come.

# ABSTRACT

Non-invasive surgery is an increasing requirement in modern day surgical theatres. A patient's recovery experience, and even their long term quality of life, can be affected by the amount of extensive invasion required in surgery. This issue is particularly prevalent in Cancer based surgical wards, where the removal of all cancer afflicted cells from a human body is critical to success. The difficulties associated with achieving this task are numerous: Identification of the correct cells for removal, removal of afflicted tissue that ensures complete cancer cell absence in the patient, non-excessive removal of tissue to improve the patient's quality of life and recovery time after surgery.

In an attempt to address these problems, Lymphoscintigraphy was developed to locate afflicted cells prior to surgical removal. Lymphoscintigraphy provides the surgeon with a map illustrating the location of afflicted cells throughout a patients' body. This allows the surgeon to plan the most minimally invasive procedure whilst still acquiring the maximum afflicted tissue possible. The timeframe between a Lymphoscintigraphic scan and surgery however means that cancer cells can develop and spread further throughout the patient's body. In short, a more immediate time frame between detection and removal of cancer cells is required to ensure surgical success.

An intraoperative Lymphoscintigraphy device needs to be developed that caters for the needs of the Radio-guided surgical theatre, a fast radionuclide detection response time, highly accurate physical localisation of the emission source point, adjustable and Active Collimation to allow for wide to narrow detection windows in

performing this localisation, the capacity to resolve the isotopes commonly preferred for implementation in the medical theatre.

CMRP has developed in the last decade an innovative solution to cope with the requirements of an intraoperative probe: the Liana Dual Detection Probe (DDP). The focus of this study is the characterisation of detectors with their related electronics for the purpose of further development to the DDP. Though Liana is intended as a medically based instrument, it is not limited to medically based functions. Liana's wide to narrow digital Active Collimation will be explored using characterisation from a pure physics perspective. The results of the exploration are then addressed back to the requirements of the medical theatre.

Characterisation of the Liana probe provided significant physical insight into the fundamentals of detector operation. Characterisation of the probes energy and localisation resolution explored effects such as Compton induced Background Scattering events and Penumbra. IV (Current vs Voltage) and CV (Capacitance vs Voltage) characteristics of the photodiode investigated the dependence of the wavelength absorption region upon the impurities present within the diode. The impact of an electronics design change from a previous study by Bradley Franks was assessed to identify improvements in managing the physical phenomena occurring within the detector.

These unique facets illustrated how the design of a dual detector must account for the physical phenomena associated with the interactions of energy emissions with matter.

# TABLE OF CONTENTS

# TABLE OF FIGURES

# INTRODUCTION

The Liana Probe is based on the Dual Detector Design System (DDDS or $^{3}$DS) and is a handheld radiation detector the size of a very large pen. The probes applications are diverse ranging from security to medical as its size makes it suitable for operating in tight enclosed spaces. This design aspect is absent among many current detectors and is due to a unique technological solution. The same solution also makes the probe suitable for both gamma (γ) and beta (+) ($\beta^{+}$) detection.

The Liana probe design provides a number of useful features:-

1. Immediate response to the detection of radioactive materials
2. Digital adjustment of the sensitivity.
3. Digital adjustment of the detection window (Spatial Resolution)
4. Detection of gamma emissions (up to 800 KeV) and detection of beta (+) particles by direct interaction in silicon.
5. “Electronic shielding” of the probe from background radiation by implementation of dual probe functionality. (Background Suppression)
6. Improved resolution of lower energy events

7. Selective emission detection by dual channel operation by event subtraction.

The Liana Probe is a dual detector unit designed for the precise localisation of user specified radioactive events. The dual detector achieves this task by comparing the detected events occurring inside each of the two detectors. An understanding of radiation physics allows for specific emissions to be identified based on the interaction of these events with each probe media. Electronic processing of this data using flat field compensation then allows the user to precisely focus the probe on the region of interest. The probes capacity to reliably recognise events from a specific area allows for the accurate localisation of emission sources. The localisation procedure is dependent on situational application and is adjustable between event subtraction and event addition.

The interaction between radiation and matter provides the basis for the Liana Probes Dual Detector Design System (referred to as DDDS or $^{3}$DS for short). This design allows for specific events within a region of interest to be targeted and identified by rejecting the remaining events entering the detector from outside of this domain.

The primary function of the dual detection unit is to act as an Active Collimator by specifically cancelling events passing through the IC to the OC. This function allows the user to physically localise the position of an emission source by confining the detection area to within a specified physical window. This function eliminates the impact of a Compton induced Background Penumbra found within the scintillator, and allows for more precise localisation of the emission source.

Comparison of the Liana Probes design functionality is made with respect to other modern devices. Comparing these devices gives a greater understanding of the

detectors properties and fundamentals. The Liana Probes advantages naturally emerge from this comparison and allows for greater insight into its operation.

# PROJECT GOALS

The aims of the project were to assess the Liana Probes capacity to:-

1. Resolve emission spectra from various substances:-
    a. Co-57 (122.1 KeV)
    b. Cs-137 (661.657 KeV)
    c. Na-22 (511 KeV and 1275 KeV)
    d. Am-241 (59 KeV)
2. Maintain stable sensitivity and performance consistency over extended periods of time.
3. Spatially resolve the physical position of radioactive substances (localisation).
4. Function using the different design modes for the DDP.
5. Function as a Gamma Probe.

The results provide information regarding future designs for radiation detectors across numerous fields. They also provide an outline for designing detectors focussing on applications. For the purpose of medical based Lymphoscintigraphy, the substances selected for energy characterisation align with those utilised in the medical theatre. This allows for the direct assessment of the probes performance for its intended application.

As an aid for envisioning the detector, a design illustration of the Liana Probe as a handheld unit has been provided in the Appendix.

# WHAT IS LYMPHOSCINTIGRAPHY?

Lymphoscintigraphy (LS) is the identification and removal of cancer cells by the injection of a radionuclide near the site of affliction for lymph node accumulation [1]. Lymph nodes produce the antibodies called lymphocytes found in the bloodstream. Lymph nodes are also responsible for the supply and removal of materials used by organs and tissue throughout the body.

Afflicted material travels through the lymphatic system in the earliest stages of cancer cell development resulting in the metastasis of lymph nodes. Radionuclide bonding with the lymph nodes allows for the accurate 3D mapping of afflicted tissue. The stage progression of cancer cell development can be forecasted from this information by identifying the metastasis rate of the nodes throughout the lymphatic system. This is achieved by the localisation of the Sentinel Lymph Node (SLN), which is classified as the site of first contact of the cancer cells with the lymphatic system. [2]

Breast cancer and melanoma are two very frequent cancers where surgery plays a major role [3]. Currently, dissecting the regional or axillary lymph nodes is considered the standard staging procedure in breast cancer also including some melanoma patients. Evidence is becoming increasingly available that suggests dissection of the sentinel node may provide the same or even better staging information. [2] Targeting the sentinel node should therefore be the research focus in the development of Lymphoscintigraphic intraoperative probe development.

Morbidity can be reduced significantly by the use of SLN dissection in clinical node-negative patients. In the case of melanoma, it is proven that the histological characteristics of the SLN reflect the histological characteristics of the distal part of

the lymphatic basin. Currently, the management of the SLN for melanoma and breast cancer is done by Lymphoscintigraphy and includes the detection of parathyroid adenoma as a standard procedure. Technetium-99m ($^{99m}$Tc) ($T_{1/2}$ = 6.02 hours, $E_\gamma$ = 141 KeV) labeled nanocolloid particles are pre-operatively injected at four points around the primary tumor with a total activity of ~60 MBq. The flow of $^{99m}$Tc isotope is directed towards a specific node, typically the first or sentinel node (SN), which will demonstrate the highest node activity in the axilla. The depth of the internal mammary lymph nodes varies between 1 cm and 7 cm, with an average of 3.0 ± 1.1 cm. For surgical purposes an intraoperative probe must therefore be capable of precisely localising the position of the nodes at these depths. Refining the acceptance region of a detector allows for this capability.

Localisation of the SLN allows the surgeon to perform a biopsy upon the afflicted node. The biopsy of this node illustrates the severity and duration of the cancers presence in the patient's body. Information from this biopsy is also used to identify the source of the cancer and the likely organs it may spread to outside of the lymphatic system. The role of the radio-guided probe has been to locate with high accuracy the SLN allowing the surgeon to perform this biopsy.

Recent developments to radio-guided instrumentation are responses to fundamental needs in the surgical theatre. These needs are: small size for maneuvrability in the patient; greater sensitivity for easier localisation of afflicted tissue; collimation for limiting the detection window angle and the capacity to operate with multiple isotopes without changing the probe.

The number of developments addressing these needs are large and diverse:-

1. High sensitivity for detecting Sentinel Node's with low radiopharmaceutical uptake (Point Source detection).
2. Active and Passive Collimation for wide to fine localisation of afflicted material.
3. High quality energy resolution for accepting multiple isotope types. (100-800 KeV)
4. Real time presentation of the detected data.
5. Accurate, reliable and consistent detection over extended periods of time.
6. Small size and portability of probe.
7. Internal (digital) event processing (energy windowing).

Modern medical theatres have preferred the application of low energy gamma emitters such as Tc-99m with emission energy of 141 KeV. Relatively low energy gamma emissions of Tc-99m allow effective detection using high Z scintillating detectors like CsI(Tl) , NaI(Tl) , GSO, LYSO and others. High detection efficiency of low energy gamma emissions allows for the non-invasive localisation of cancer cells. This high attenuation feature of low energy gamma emissions allows for the non-invasive localisation of cancer cells. Radioguided devices are often called "Gamma Probes" because of this gamma absorption function. Gamma Probes however are not strictly limited to detecting only gamma events.

Implementation of modern day Gamma probes has grown to facilitate detection of beta emitters. Beta emitters have become increasingly popular due to their short emission path. This allows for finer localisation of the afflicted material in the modern day theatre. [4].

Another consideration of probe development is Positron Emission Tomography (PET) utilised with substances such as FDG (Fluorodeoxyglucose). 511 KeV photons are released from the collision of an electron by a positron at an angle of $180^0$. Measuring the time difference between the 511 KeV photons (γ) colliding with the detector means the depth of the affliction can be determined using Time of Flight (TOF) PET imaging systems. Localisation of the afflicted tissue is then determined directly from this analysis. Intraoperative PET however has not been able to perform accurate identification for lesions smaller than 9mm without the aid of an additional beta probe. [4] This is due to the higher energies utilised in PET resulting in Compton scattering interactions between human tissue and the emission prior to reaching the detector. This is also because of an inherent physical spatial resolution limit with PET in managing these events.

The interactions of gamma and beta emissions within an intraoperative probe constitutes a difficulty which must be overcome to ensure accurate localisation of afflicted tissue. As radioisotope application can vary between surgeons, it is important that the Intraoperative probe be capable of accepting:-

1. Different emitter types mainly $\beta^+$ (F-18, Ga-68,…) and γ (Tc-99m, In-111,…) emitters
2. A wide range of emitter energies (approximately 200-800 KeV), which corresponds to the radioisotopes commonly found and used by surgeons in the medical theatre.

Developments over the last 20 years have been focussed at addressing these problems encountered by radiation detectors. Two recent and iconic developments

within the field in the last 10 years provide a graphic insight for resolving these issues and shall be explored in the coming sections.

The basis for a detectors operation and design is found in the interaction between the emitted energy types and matter. A full understanding of these interactions must first be established before these developments can be properly explored and appreciated.

## RELEVANT PHYSICS CONSIDERATIONS

Emitted energy from a radioisotope will interact with matter in a number of ways dependent on the energy type and amount contained within the emission. The fundamental operation of a dual detector requires understanding two of these processes.

1. The Photoelectric Effect
2. Compton scattering

### *THE PHOTOELECTRIC EFFECT*

When a photon of sufficient energy strikes the diode, it creates an electron pair. This mechanism is also known as the inner photoelectric effect. If the absorption occurs in the junction's depletion region, or one diffusion length away from it, these carriers are swept from the junction by the built-in electric field of the depletion region.

The Photoelectric Effect is a key property of detectors as the interaction between the scintillate material and the radiated emission produces optical photons. The optical photons produced then travel to the photodiode located at the base of the scintillator material. The optical photons then collide with the doped semiconductor material which releases an electron-hole pair as per the inner photoelectric effect.

Releasing electrons for each optical photon combined with a voltage bias across the semiconductor results in the development of photocurrent. The amount of photocharge (current) produced is proportional to the number of the optical photons absorbed in a photodetector.

The charge produced by the photoelectric effect results in an electronic signal being developed which can be analysed to identify the energy of the radiated emission.

## *COMPTON SCATTERING*

Compton scattering is the deflection of a photon from an electron orbiting a nucleus. The result of this interaction is that:-

1. The incident photon scatters away from the electron with less energy than it started.
2. The electron is deflected out of its orbit.

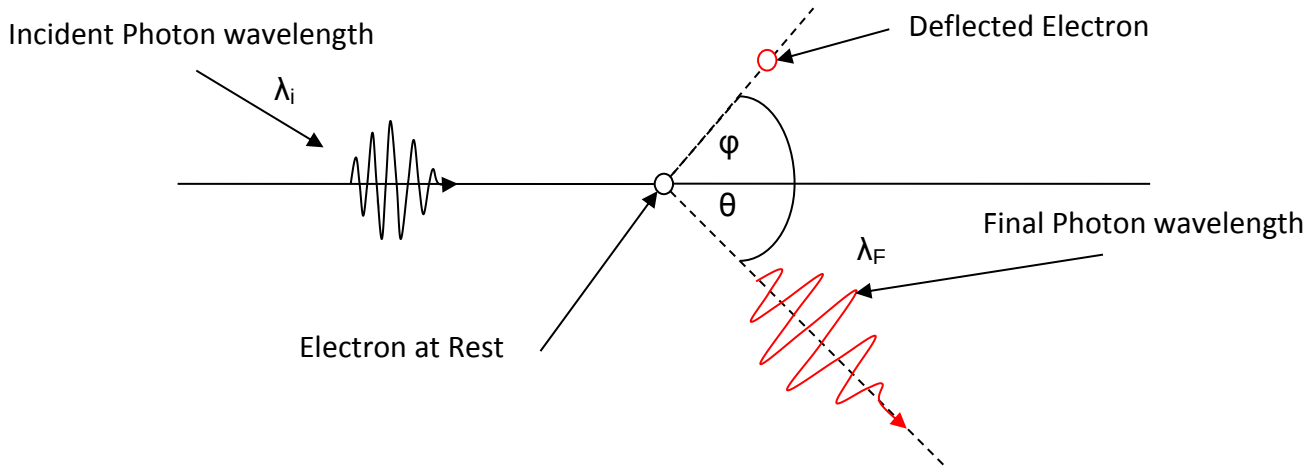


**FIG. 1:- DIAGRAM OF COMPTON SCATTERING, FORMULA FOLLOWS.**

Compton scattering causes problems in Lymphoscintigraphy due to "Detector intrinsic sensitivity (being) highly dependent on the effective atomic number of the detector material." [5] The Liana Probes detection material, a crystal of Caesium

Iodine (CsI(TI)) is effective in spectroscopy for photons in the energy range of 100-200 KeV. CsI(Tl) is ideal for detecting sources such as Tc-99m and Co-57 with emission energies of 140 and 122 KeV respectively. [5].

Compton scattering produces a number of problems for detectors attempting to localise the physical position of a specific emission energy source:-

1. Higher energy emissions can scatter out of the detector leaving a partial energy deposited in the detector
2. Scattering can cause the direction of an emission to change.
    a. This means that the detector can be ‘deceived’ into recording events that would actually be outside of this detection window.
    b. This subsequently reduces the fine localisation capacity of the probe as events outside of the intended window may be detected.

All possibilities result in the detector inaccurately identifying the emission and producing false feedback data. The user is then unable to accurately identify the position of the emission source due to the false data obscuring the real data. The detectors system resources are also wasted in the electronic processing of the false events with the real data. Management of Compton events due to interactions with tissue is especially critical for the accurate localisation of low energy emitters when approaching the emission source. This is because the Compton events from tissue deflect into the probe from outside the intended detection window. [6] This makes precise localisation very difficult for singular probe units as they have no way of controlling the size of their physical acceptance window. This results in the detector being unable to precisely locate of the emitter, increasing the amount of invasion necessary to procure the emission source from the patient.

$$\lambda_f - \lambda_i = \frac{h}{m_e c}\left[1 - \cos\theta\right]$$

**EQUATION 1:- CANONICAL COMPTON SCATTERING FORMULA AS DERIVED FROM CONSERVATION OF ENERGY. $\lambda$ DESIGNATES THE WAVELENGTH, $\lambda_f$ IS THE FINAL WAVELENGTH AND $\lambda_i$ THE INITIAL WAVELENGTH. $h$ IS PLANCKS CONSTANT, $m_e$ THE ELECTRON MASS, $c$ IS THE SPEED OF LIGHT AND FINALLY $\theta$ IS THE SCATTERED ANGLE.**

One technique for managing background induced Compton events due to the interaction of beta and gamma emissions with body tissue is to remove these events from the data collection. Two ways of achieving this task are by Passive and/or Active Collimation with the detector.

Passive Collimation involves implementing a high density material to block photons entering the detector from a side direction and provide photon detection from one direction only. Active Collimation is the implementation of a second detector which is used to identify events entering the detector from all directions except one. Events identified by the second detector are vetoed from the overall data collection leaving only the real events to be analysed. Both techniques are also useful in suppressing background events which interfere with the accuracy of the detectors recording for a specific region.

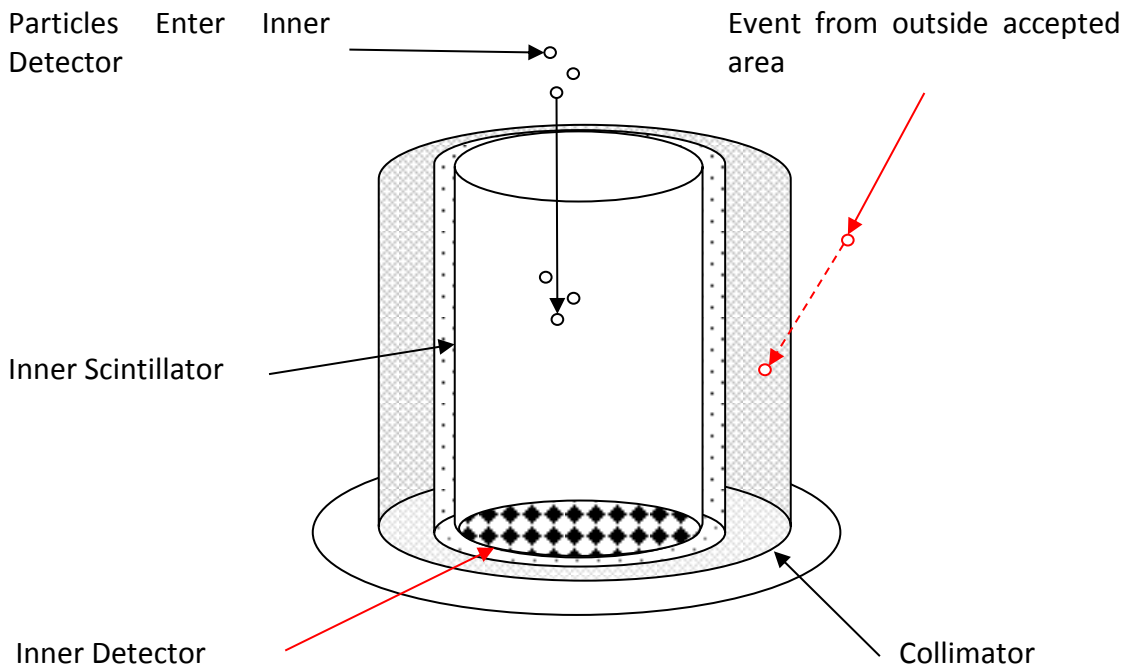


**FIG. 2:- EXAMPLE OF PASSIVE COLLIMATION. EVENT OUTSIDE THE ACCEPTED PHYSICAL WINDOW IS STOPPED BY THE COLLIMATION MATERIAL PREVENTING ENTRY TO THE INNER DETECTOR. ONLY EVENTS ENTERING THE TOP OF THE DETECTOR ARE PERMITTED ENTRY TO THE INNER DETECTOR.**

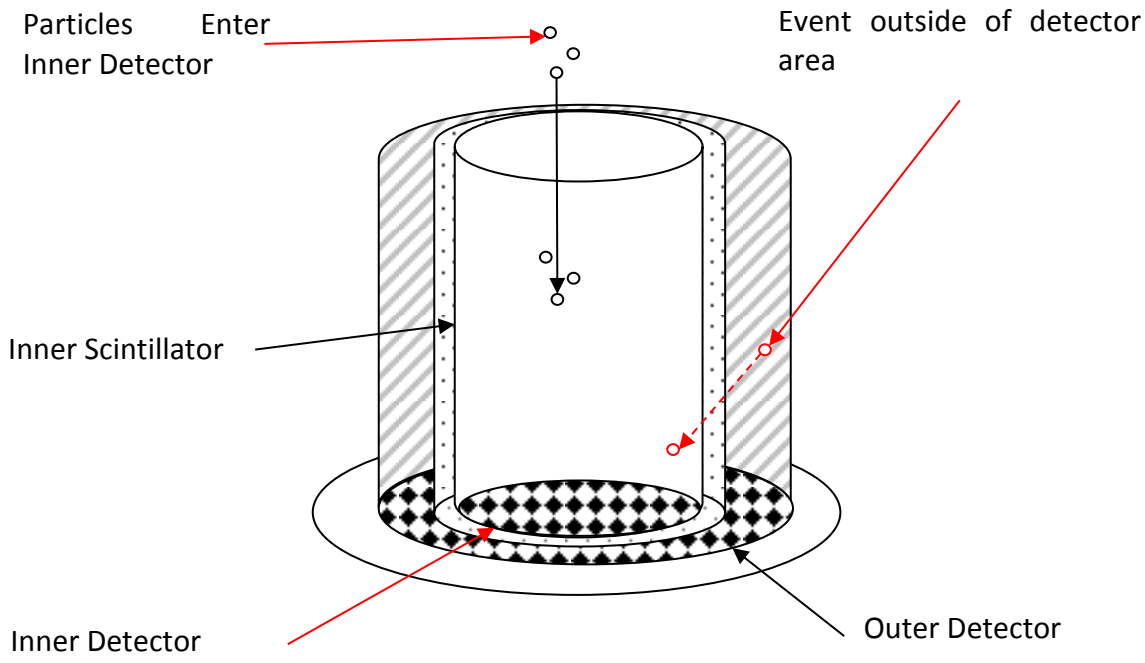


**FIG. 3:- EXAMPLE OF ACTIVE COLLIMATION WHERE THE EVENT OUTSIDE THE WINDOW IS ABLE TO ENTER THE INNER DETECTOR. AS THE OUTER DETECTOR HAS IDENTIFIED THIS EVENT IT IS SUBTRACTED FROM THE COUNT. THIS SUBTRACTION LEAVES ONLY THE EVENTS ENTERING THE INNER DETECTOR FROM THE TOP IN**

The techniques displayed in Fig. 2 and Fig. 3 are designed to prevent events entering the detector from anywhere except directly from the top of the inner detector. Suppression of these emissions significantly reduces the amount of background events recorded in the lower energy domain. Furthermore these techniques ensure that the source of the emissions is confined to a specific physical window by rejecting events attempting to enter the detector from any other angle. It

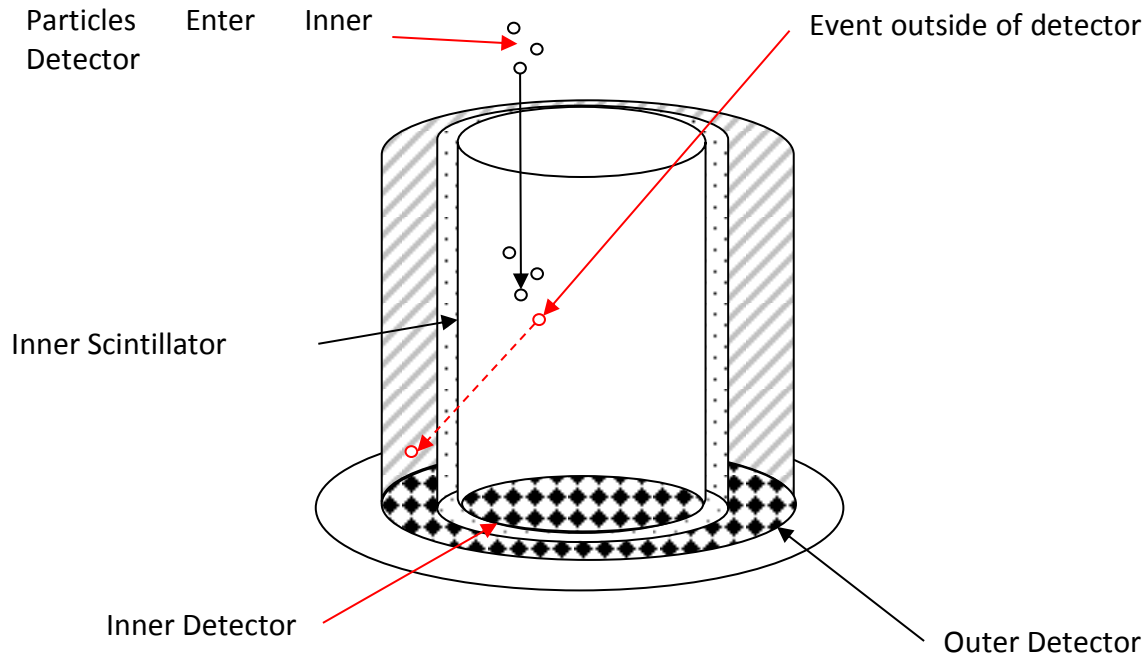


**FIG. 4:- EMISSION ENTERING INNER DETECTOR ON AN ANGLE CONTINUES THROUGH THE SCINTILLATE INTO THE OUTER DETECTOR. SUBTRACTING THESE EVENTS ENSURES THAT ONLY EMISSIONS DIRECTLY IN FRONT**

does not restrict the case observed in the figure below however.

These techniques independently cannot manage Compton events occurring either within or outside of the detector. Passive and Active Collimation working simultaneously can however manage this problem. Two additional forms of screening are required for this *in-partisan* approach to work. The first is the inclusion of a coincidence function between the two channels. This function rejects events that

occur within the negligibly small time frame required for an emission to travel between the two scintillates. This approach is suitable for suppressing the Background Induced Compton Events and will result in a cylindrical detection area. The second type of screening is the inclusion of an energy windowing scheme which only counts events that have the specific energy level of the expected emitter. This second type of screening is only suitable for internal Compton event suppression where the scattering is recorded in the first detector and is matched with an event in the second detector by its energy level.

For Internal Compton Suppression these forms of screening would require the scintillator to be of a large size to ensure complete deposition within the scintillate material. As intraoperative application requires the detector to be of a small size for entering incisions within a patient, Internal Compton Suppression is technologically impossible for medical application at present. The second type of screening for externally induced Compton Background events is discussed in the literature review. [8] [9] [10]

Historically the management of events entering the detector from outside of the accepted physical window has been achieved by Passive Collimation. In modern day radio guided surgery wards the collimation substance of choice is Tungsten Carbide. This selection is due to Tungsten's high density, material strength and non-toxicity compared to Lead (Pb). Higher density allows for a smaller volume of collimation material to be used permitting greater maneuvrability within a patients' body.

Active collimation as explained above is not limited to vetoing events coming from the radial side of the detector. Events entering the inner detector from the top at an angle may pass through the inner detector and exit out the radial side similar to

internally Compton scattered events. Active Collimation using a second detector can be used to veto these background events and ensure that the only events recorded are emissions coming from directly in front of the detector. Passive Collimation can be used in conjunction with Active Collimation to further increase the accuracy of these event vetoes by ensuring events entering the outer detector only come from the inner detector.

A secondary detector can also use Active Collimation to create a 3D image of an emission source. This design aspect is found in Gamma Camera's (GC's) and mimics the function of two eyes on a human face. The energy collected by each detector is compared to find the distance between the emission source and each detector. This means the emission sources depth can be determined which allows the 3D image to be created.

This detector configuration is useful for determining if any radioisotope and subsequent afflicted Node is remaining. It can be detrimental in surgery however for the reason that if the Node cannot be accurately localised unnecessary surgical invasion results, adversely impacting the patient's treatment experience. [7]

Surgeons require highly accurate localisation to ensure the correct identification and removal of afflicted material. Active collimation in conjunction with Passive Collimation could improve localisation precision, patient survival and recovery rate post-surgery. The applications of a system utilising this dual collimation would not be restricted to medical application, and would only be limited by the size to which the components could be reliably manufactured.

A system with the ability to remove Background events from a detection window would have a higher capacity to fine localise the physical position of an emission

source. It may also improve its ability to resolve the energy spectra of an emission source. If this system could be made handheld the applications would be numerous.

## *LITERATURE REVIEW: HANDHELD PROBE SOLUTION DEVELOPED FOR LYMPHOSCINTIGRAPHY*

Devices have been developed in an attempt to resolve the problems encountered in Lymphoscintigraphy. A large percentage of these devices are based on the implementation of different radionuclide energy types. These radionuclides' utilise properties such as shorter mean free travel paths for emitted photons or positrons. The resulting deposition is close to the emission point and allows for simpler localisation of the SLN. The commonly used radionuclide for this purpose is Iodine 125 (I-125) and Tc-99m. Other substances used are purely beta emitting radionuclides for a similar purpose, but also to avoid the problem of background counts which exist as gamma events.

Energy selection and rejection windows are another means for improving localisation of the emission point. Energy selection and rejection windows create fixed energy criteria where emissions are only recorded if their energy is between two pre-set points. A simplified example of this is determining the number of emissions coming from a Cs-137 peak. Setting an energy window accepting events between 660 – 662.5 KeV ensures to high accuracy that events within this domain come from the Cs-137 source. This can be applied surgically to perform localisation by adjusting the acceptance width of this energy window. The result is that as the energy window is narrowed, the background events caused by tissue attenuation are rejected. [8] The number of events collected by this approach are usually fewer and typically result in slower peak acquisitions. [9] This requires a longer acquisition time due to reduced sensitivity but is useful for fine localising an emission source. [10]

Pattern based recognition, or "coincidence detection" is another method for performing the localisation of an emission source. Indium-111 is a radionuclide which

produces multiple energy photons. The validity of an Indium emission can be achieved by comparing the sources recorded energy spectrum with the expected decay pattern of Indium-111 [4].

Coincidence detection is used in PET to record the events of positron annihilation with an electron. The nature of the positron colliding with the electron results in the emission of two gamma photons with a separation angle of $180^0$. The detector is shaped like a large ring for the purpose of intercepting these gamma emissions. Localisation is achieved by determining the time difference of these gamma emissions once they have both been collected by the detector. This provides a 3D image of the afflicted tissue allowing for the depth of the affliction to be accounted for prior to surgery.

A handheld PET probe was developed in 2010 which conjunctively used a second detector to refine localisation by tracking beta emissions. [4] As beta emissions carry their energy over short distances this system was able to localise tumours of size slightly under 1cm. Characterisation of the probe demonstrated the success rate of the combined probe operation for localising malignant tissue of 1cm or less to be greater than 80%. The beta probe specifically was able to achieve this task with accuracy greater than 93% and approaching 100% for specific isotopes. This is one example which illustrates the operational capacity available to a dual functioning probe and its benefits to localisation in surgery.

The PET probe developed by Brader is an example of a Dual Detector Probe (DDP's) which is another form of coincidence detection. Designs for DDP's involve the presence of two or more detectors. Their operation is similar to the pattern recognition based method with respect to determining the depth of the emission

point. Three examples of dual detection systems are presented and explored in the following sections.

The third design concludes the review and is a large scale Internal Compton Suppression device that implements coincidence detection and subtraction methods for targeting specific events. This device by Parus's research group closely emulates the background suppression function of the Liana $^{3}$DS with some minor modification.

*DUAL SURFACE BARRIER DETECTION PROBE (DSP) - [11]*

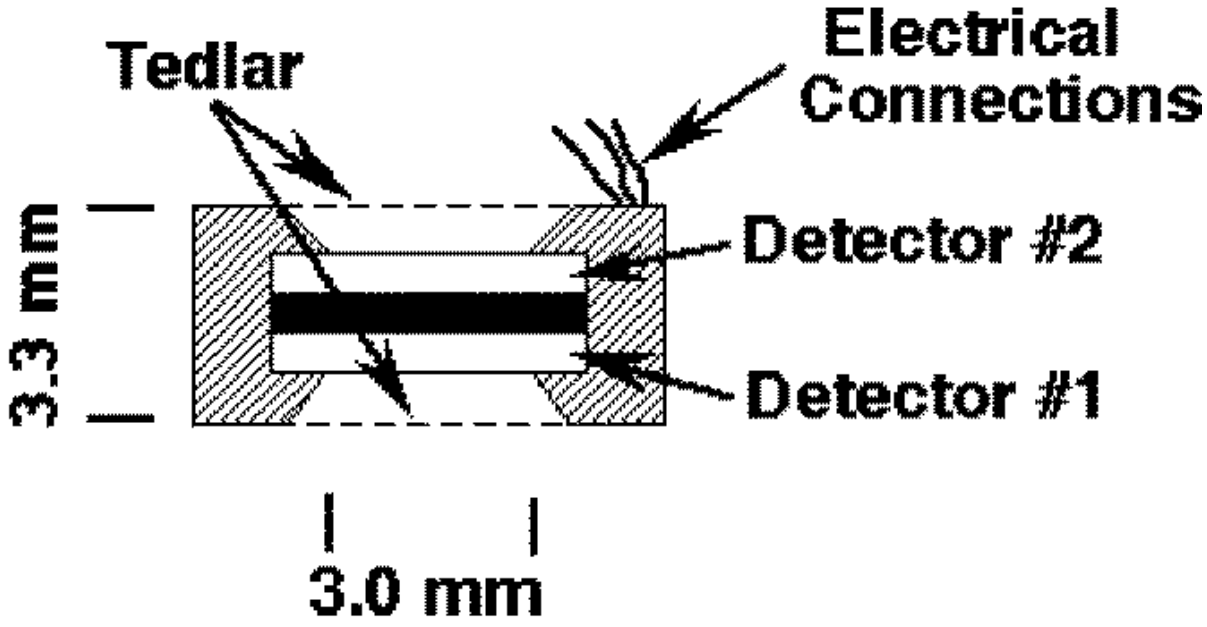


**FIG. 5:- DUAL SURFACE BARRIER DETECTION PROBE. A BETA EMISSION IS ABLE TO ENTER ONLY ONE OF THE DETECTORS. IF BOTH DETECTORS RECORD AN EVENT THE EVENT IS DISCOUNTED FROM THE FIRST DETECTOR AS IT IS ASSUMED TO BE A FALSE READING FROM A GAMMA EMISSION. [11]**

The DSP designed in 2004 utilises two probe layers. The first detector is sensitive to gamma emissions and beta emissions, the second detector is sensitive only to gamma emissions. The configuration ensures that if the second detector records an emission, then the first detector, assuming it has recorded an emission, has incorrectly interpreted this event as a beta emission, and vetoes this event from the count. [11]

This design function is achieved by shielding Detector #2 from all emission types from every side except from the front. The common grounding plate located between Detector's #1 and #2 prevents beta emissions from entering Detector #2 from #1. The grounding plate does not impede the passage of gamma emissions and thus ensures that events recorded in Detector #2 are purely gamma emissions.

The operational effectiveness of this device is described as excellent. It cannot account for Compton induced Background scattering however and can only use Passive Collimation to refine its localisation capacity.

The DSP's dual function has several operating modes:-

1. Individual threshold adjustment for each detector allowing for energy windowing.
2. Coincidence detection for isolating either beta or gamma events.
3. Pattern recognition for multiple decay nuclides.

To ensure the accuracy and simplicity for its intended function, Detector's #1 and #2 are comprised of the same ion implanted silicon. The Ion implanted silicon detectors functioned sufficiently well at room temperature to be applicable for intraoperative utilisation.

A problem is encountered by the DSP in the form of low energy gamma emissions depositing entirely in the first detector. Fine localisation of beta emissions can be clouded by low energy gamma deposits in Detector #1 due to Compton scattering in the surrounding tissue. Gamma energy windowing is used in this study as an attempt to rectify this problem.

## *MULTIPLE DETECTOR PROBE (MDP) - [12]*

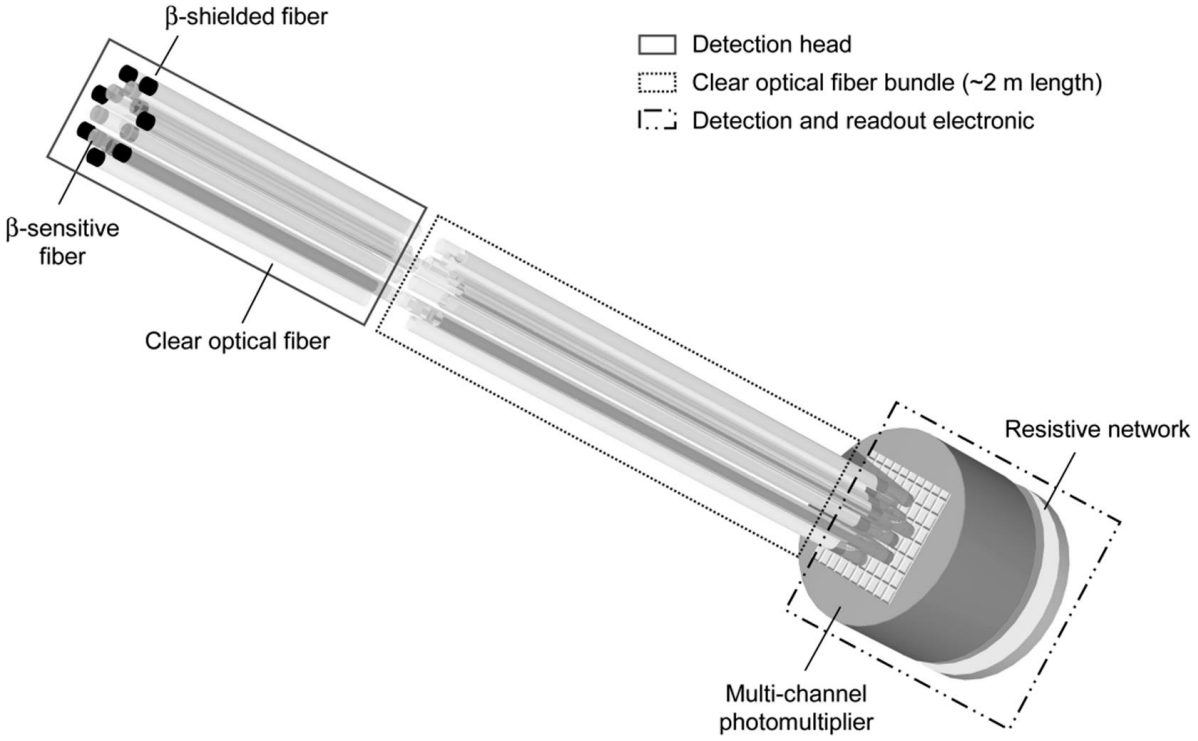


**FIG. 6:- MULTIPLE DETECTOR PROBE. THIS PROBE IS DESIGNED FOR THE DETECTION OF PURE BETA EMISSIONS BY DISCOUNTING CONTAMINANT READINGS ($B^+$ INDUCED GAMMA EVENTS) FROM THE DETECTION COUNT. THE EVENT VETO RELIABILITY IS ACHIEVED BY CLOSE POSITIONING OF THE SHIELDED FIBRES TO THE SENSITIVE FIBRES. [12]**

The MDP developed in 2007 operates similar to the DSP by seeking to distinguish between beta and gamma emissions for the purpose of localisation. Optical fibres were used to transfer event interactions out of the hand held unit to a processing unit external to the surgical implement. External event data processing lowered the weight and increased the portability of the handheld device. An excision implement was intended to be coupled directly to the probe to ensure precise clinical removal of cancer tissue.

Bonzom's study found that improving localisation required bundling the numerous detectors closely together. Half of the detectors were covered with a thin stainless

steel layer for the purpose of beta shielding. The remaining half of the detectors were uncoated and intended for the detection of beta counts. The purpose was to veto gamma events which would be mistaken for beta emissions due to the scintillators capacity to interact with both energy types.

The gamma rejection efficiency was found to improve as the distance between the shielded and unshielded fibres decreased.

A problem was identified for photons travelling from the scintillator into the fibre optic. These photons are impeded by the refractive index induced by the difference in index between the scintillator and the fibre optic. This problem is exacerbated by the adhesive used to bond the scintillator with the fibre optic and additionally by the presence of bubbles. Research shows that fibre optic transfer efficiency due to refractive factors is typically quite poor in most applications. (See [13] and [14]) This factor is manageable with suitable electronics.

The MDP does not manage background events for precise localisation of emission sources but it is also described as an effective working model warranting further study. [12]

## *SUMMARY*

No intra-operative device seems to have ever been developed that performs both Active and Passive collimation for the purpose of highly precise localisation of emission events from a small emission source.

Many designs currently exist which could be used to isolate such events. They require minor modification to their operation in order to do so. This modification would improve their functional capacity without impeding any original function. An example of an Internal Compton event suppressor is provided by J. Parus [15], and illustrates a novel technique for actively identifying and isolating events entering the detector through a specific physical window.

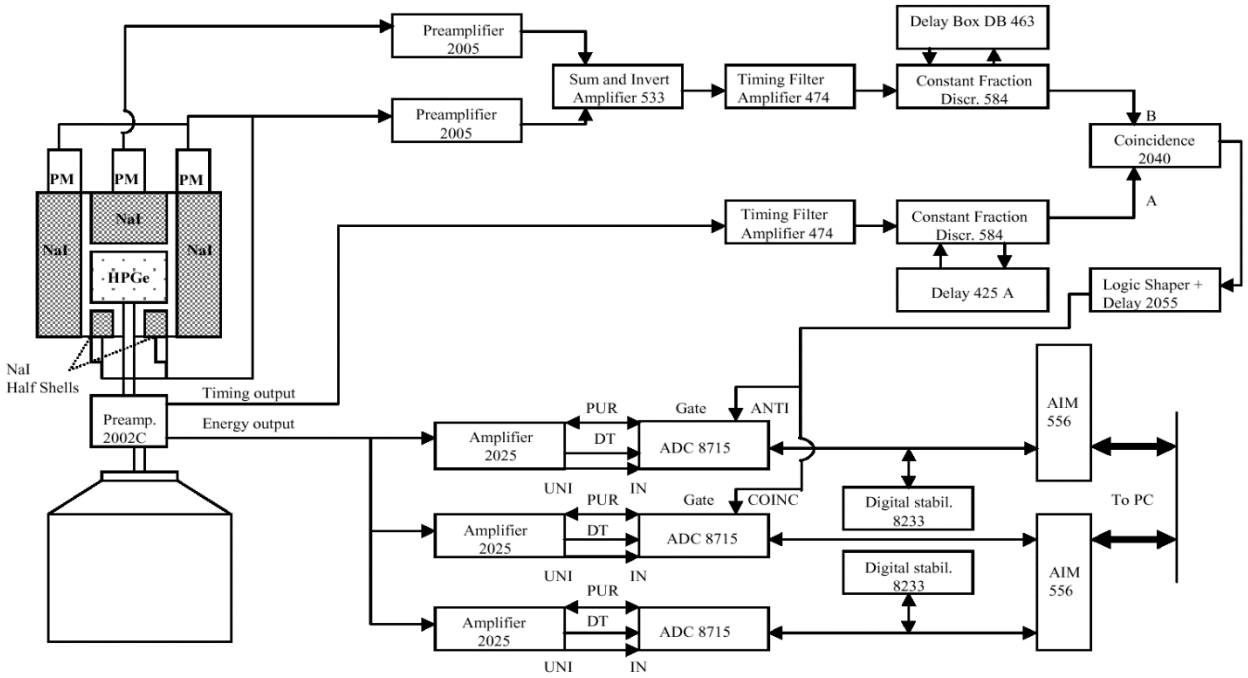


**FIG. 7:- FROM J. PARUS ET. AL. [15] IN THIS SETUP THE TIMING OUTPUT OF THE HPGE IS CORRELATED WITH THE TIMING OUTPUT OF THE NAI DETECTORS. IF THERE'S A CO-INCIDENT TIME FRAME THE MESSAGE IS PASSED TO THE LOGIC SHAPER WHERE THE ANTI-INCIDENCE ALONG WITH THE CO-INCIDENT ARE RECORDED SEPARATELY.**

## *INTERNAL COMPTON SUPPRESSION USING OUTER DETECTOR EXPLANATION*

Compton scattering inside the detector is a problem as the signal processing depends on the amount of energy deposited inside the inner scintillate and subsequently into the NaI. When a collision between a photon and an orbiting electron occurs the photons energy decreases and its direction is changed. If Compton scattering occurs inside the detector then not all the energy will be deposited.

The direct consequence of Compton Scattered events are inaccurate and false readings in the detector. These false readings create unnecessary noise in the electronics which lead to reduced energy resolution during signal processing. The end result of a detection phase involving Compton Scattered events are decreased energy and spatial resolution.

The second detector in Parus's study manages Compton scattering events by implementation of the coincidence detection technique. Events occurring in the High Purity Germanium (HPGe) inner detector are compared with the events occurring in the NaI outer detector. The comparison is based on two factors:

1. The magnitude of energy released.
2. The time recorded between the events deposited in each detector, as the velocity of high energy emissions is approximately the speed of light.

If an event is recorded in each detector within the time frame for an emission to move between the two channels. This event is likely to have been Compton Scattered, and is rejected from the results.

Signals from Parus's study [15] are recorded with both a coincidence and anti-incidence electronics scheme. If the signal time from the NaI does not match up with HPGe it is recorded as anti-incident. If the signal time between the two detectors does correlate to be within the time frame then it is recorded as co-incident. Since with the Compton event, an emission is recorded in both the HPGe and the NaI within the scattering time frame. Coincident events in this circuit are recorded as Compton events. The coincident events are automatically vetoed from the system by subtracting the appropriate event from the count. The veto in Parus's design occurs directly after signal processing but shortly before the signal is officially recorded by the computer.

The response time of the electronics however is slower than the speed of the emissions passing between the HPGe and the NaI. The electronics therefore interprets the timeframe between emissions passing from the HPGe to the NaI as effectively "Zero" and interprets them as occurring simultaneously.

All legitimate events by the detectors design must enter the HPGe before the NaI for the coincident function to correctly identify the Compton events. Events that enter the NaI before entering the HPGe are treated as background events which trigger the anti-incident line. The anti-incident lines function is to record background events for later comparison with the spectra produced after Compton suppression. The comparison reduces the impact of background counts in the lower energy domain by a factor of 8. The anti-incident line also provides a means of actively diagnosing the electronics during event recording.

The results of the study indicate a high suppression factor implying that the method of Compton suppression used is highly effective.

Active Compton Suppression as illustrated in Parus's study for an intraoperative probe is technologically impossible at time of writing. A Compton Suppressed intraoperative probe would be able to localise events simply by adjusting the rejection conditions. The scattering time would be a fixed factor predetermined by the volume of the dual detector. Energy windowing could be achieved by adjusting the energy acceptance threshold individually for each channel. Emissions scattered by tissue before entering the probe would then be rejected due to having lost energy from earlier interactions. Specific radionuclide emission types could be identified and isolated by the same method. Energy windowing therefore improves localisation.

Compton Suppression therefore removes these tissue Compton scattered events from the low energy range. This makes substances such as Tc-99m and other low energy gammas used by surgeons resolvable. Beta emissions are also resolvable using this configuration. Eliminating the bulkiness of Parus's probe would result in an intraoperative probe capable of resolving and localising any radionuclide. The extent of which would need to be quantified.

## *IMPLICATIONS OF THIS INFORMATION UPON DETECTOR DESIGN*

Intraoperative detectors would benefit from combined Passive and Active localisation in order to finely localise the position of an emission source. Compton Suppression demonstrated by Parus is a method of coincidence detection which can provide Active localisation. The coincidence method used in Compton Suppression has also been demonstrated as able to distinguish between emission types. Compton Suppression also diversifies the available detection spectrum in the lower energy domain.

Compton Suppression in a small size detector suitable for intraoperative purposes is technologically impossible at the present time due to requiring a larger volume scintillator. The Suppression technique for isolating specific events however could be used for actively adjusting the physical acceptance window of emissions. Adjustment of this physical window could veto events not entering from directly in front of the detector. This could be used for negating the impact of Compton induced Background interactions with matter. This function would provide the capacity for highly precise localisation, and could be developed in small sizes suitable for surgical application.

Compton scattering occurring within the tissue leads to deflections in the path of the emission travelling to the detector. Such events can be vetoed leaving only the emissions directly in front of the detector to be analysed. An intraoperative probe of this design would suppress events similar to Parus's study, the events selected for veto however are those occurring outside of the detector and not within it. A probe of this design would be called an *Active Background Suppressor* as it suppresses background events which interfere with the precise localisation of sources in the 100-200 KeV domain.

An intraoperative probe with Active Background Suppression has now been developed and is called the Liana $^{3}$DS Gamma Probe. It is patented by the Centre for Medical Radiation Physics (CMRP) [16] [17]. The Liana $^{3}$DS is introduced below.

# EXPLANATION OF INTENDED UNIT – DUAL DETECTOR PROBE

## PHYSICAL AND ELECTRONIC DESIGN

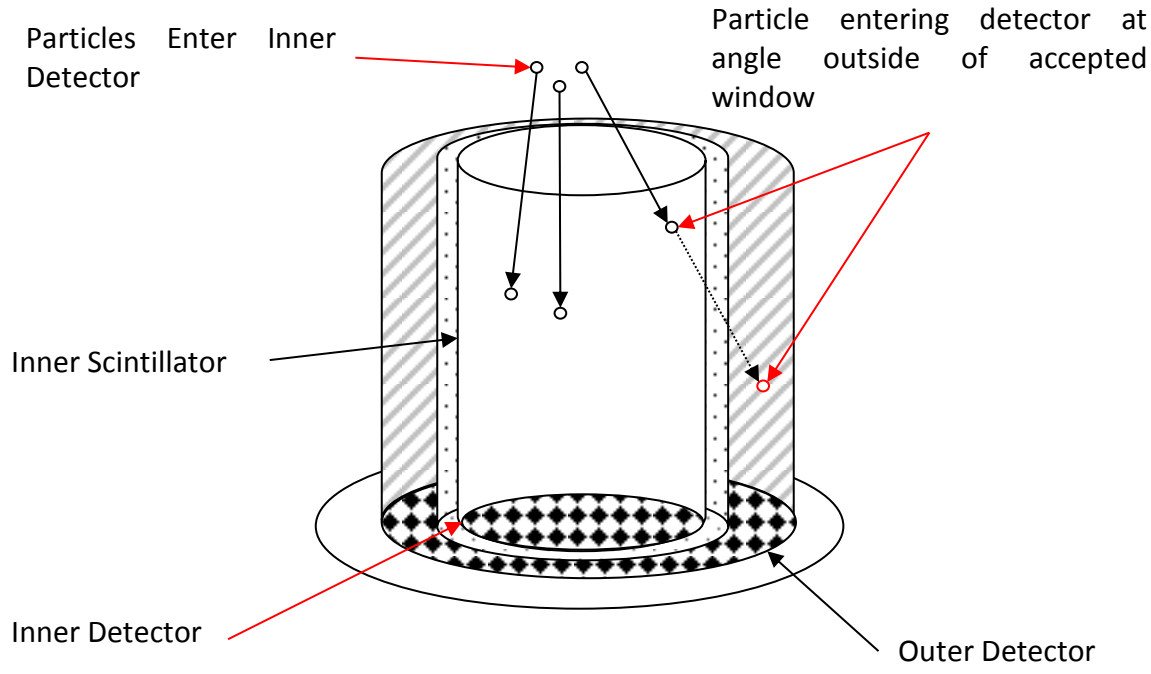


**FIG. 8:- THE LIANA PROBE DESIGN. MATERIAL DESCRIPTION AND DESIGN PURPOSE FOLLOWS.**

### *PHYSICAL*

The Liana Probe comprises of two independently operating channels, an Inner Channel (IC) and Outer Channel (OC). The IC by design is the first to encounter and collect emissions coming from an emitter. If an emission enters the probe at an angle, the event passes from the IC and is collected by the OC as shown in Fig. 8. To ensure the event came from the IC, the OC must be sufficiently passively collimated. The probes passive acceptance window is set by an aperture in Tungsten Carbide which is presented in Fig. 9 as the glass scintillate protection. The Tungsten collimator blocks 99% of events with energy <200 KeV.

The OC is optically separated from the IC by Teflon Tape, which prevents optical cross talk occurring between the channels that would lead to false readings. The intended functions of the OC are:-

1. Active Collimation of the inner detector.
2. Guaranteed detection of events passing through the IC to the OC.

These two design aspects combine to create the Background Suppression function. Assuming all events collected in the OC come from the IC, events that are Compton Scattered prior to entering the probe can be accurately rejected. The localisation window of a probe can therefore be digitally adjusted to ensure only events entering the probe from directly in front are collected and analysed.

The Background Suppression function is implemented by signal processing located within the circuit board which will be discussed shortly.

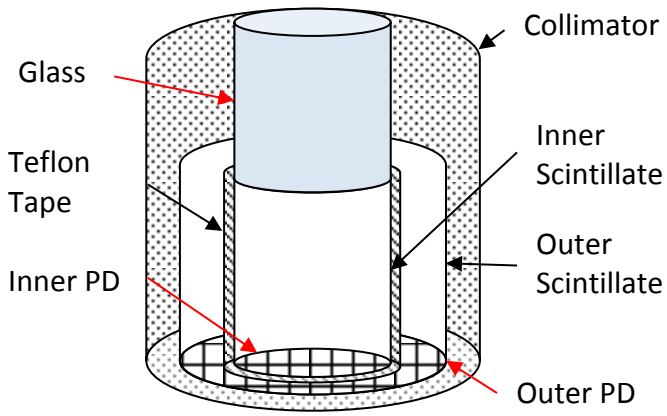


**FIG. 9:- THE TUNGSTEN COLLIMATOR USED TO PREVENT EMISSIONS FROM ENTERING THE OC IS LABELLED. THE COLLIMATOR ONLY ALLOWS PASSAGE INTO THE PROBE BY THE GLASS APERTURE. THE GLASS IS USED TO PROTECT THE SCINTILLATE WITHOUT IMPEDING THE PASSAGE OF**

The last physical aspect of the detector is the photodiodes. The photodiodes in Liana B are located in close proximity to each other. This proximity may produce cross talk. Cross talk is the charge induced between two conductors due to their close proximity.

When emissions from radioactive sources interact with the

scintillator, optical photons are generated which travel to the photodiode. These photons collide with the semiconductor surface and transfer all their energy into orbiting electrons by the inner photoelectric effect.

The orbiting electrons are then excited into the conduction band creating current which is read by the electronics as an energy deposition. Amplitude and wavelength of the signal pulse produced correlates to the deposited energy.

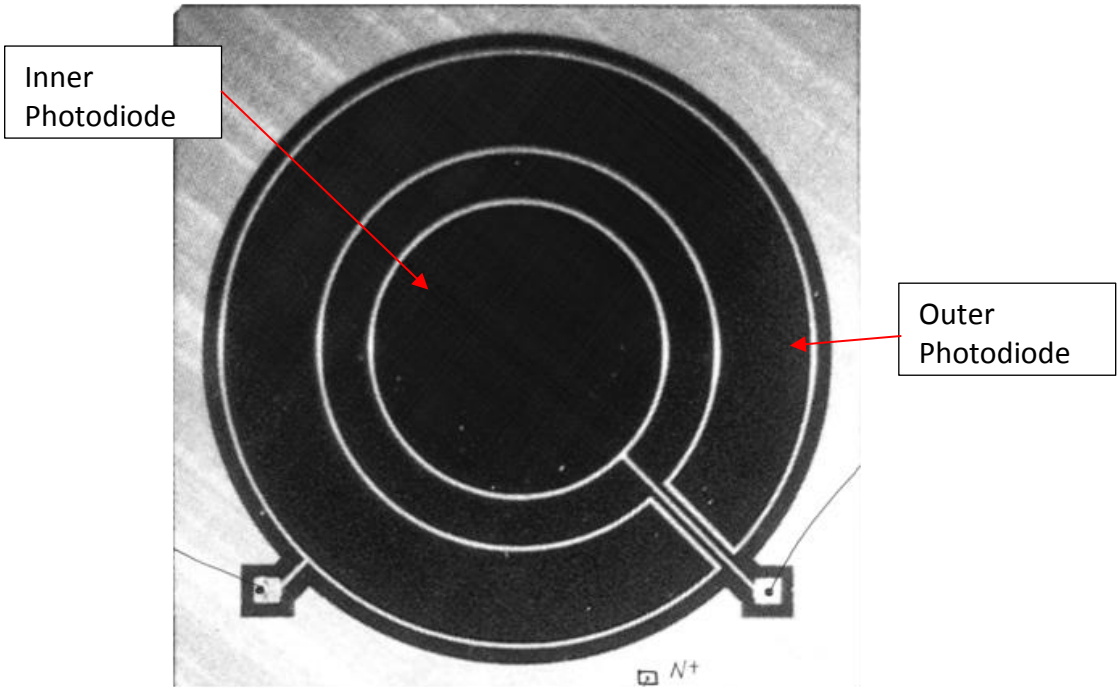


**FIG. 10:- REAL IMAGE OF THE LIANA PHOTODIODES WITHOUT THE SCINTILLATE.**

# TOP VIEW

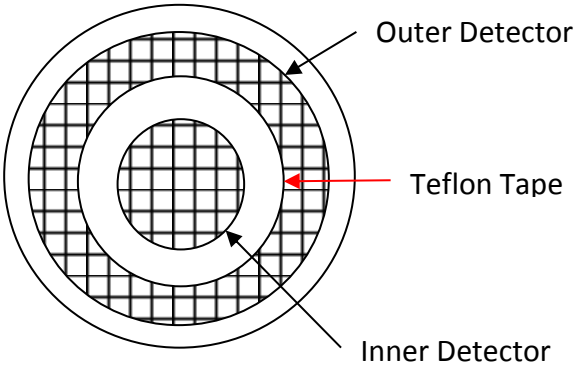


**FIG. 11:- AN IDEALISED DEPICTION OF THE DUAL DETECTOR. THE DETECTION MATERIAL AND SHAPE DIFFERS FROM THE REAL BUT PROVIDES A SIMPLIFIED PICTURE OF THE REAL SITUATION. DIAGRAM ITERATION OF FIG. 10.**

# SIDE VIEW

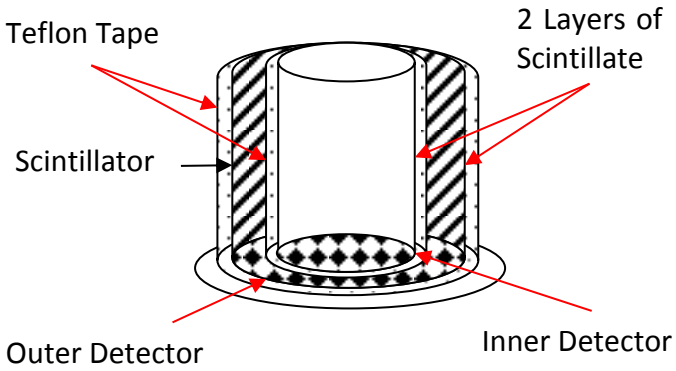


**FIG. 12:- THIS DIAGRAM CONSISTS OF THE UPPER SCINTILLATE THAT REACTS TO THE EMISSION EVENT WHICH PRODUCES AN OPTICAL PHOTON. AT THE BASE THERE IS A PHOTODIODE WHICH ACTS AS A DETECTOR AND IS USED TO COLLECT THIS SIGNAL.**

## *SIGNAL PROCESSING*

To perform Background Suppression and the other functions available to Liana, the electronics must process signals from each scintillator individually. This requires both signal processing channels to be electronically isolated from each other. Each channel therefore operates as a standalone detector, where the outer channel functions as a filter for events entering the inner channel from outside the accepted physical domain.

Each channel of scintillating material converts the source emission event into a flash of light (Optical photons). This light is collected by the photodiode located at the base of the probe, where photoelectrons are released as explained by the Photoelectric Effect. This creates a pulse of current whose height and width are dependent on the intensity and duration of the scintillation event occurring inside the Scintillator. The nature of the signal pulse varies based upon the material used for the scintillator.

The time taken for the peak intensity of a scintillator to reduce to 1/e of its maximum value is called the decay time. The amplitude and width of a signal pulse is dependent upon the number of photons and the rate at which these photons are emitted after radiation particles have interacted with the scintillator. LYSO crystals upon interaction release 20 photons per KeV with a decay time of 40ns. CsI(Tl) releases 65 photons per KeV with a decay time of mostly 900ns. CsI(Tl) therefore produces a higher amplitude pulse as it releases more photons than LYSO Crystals. Furthermore, the duration of the pulse is longer due to the slower decay time of CsI(Tl) vs. LYSO Crystals.

The pulse created by the photodiode is amplified and shaped by the electronics so that it can be processed by a Multi-Channel Analyser (MCA). The MCA's function is

to record and store events for specified voltage windows which correspond to energy

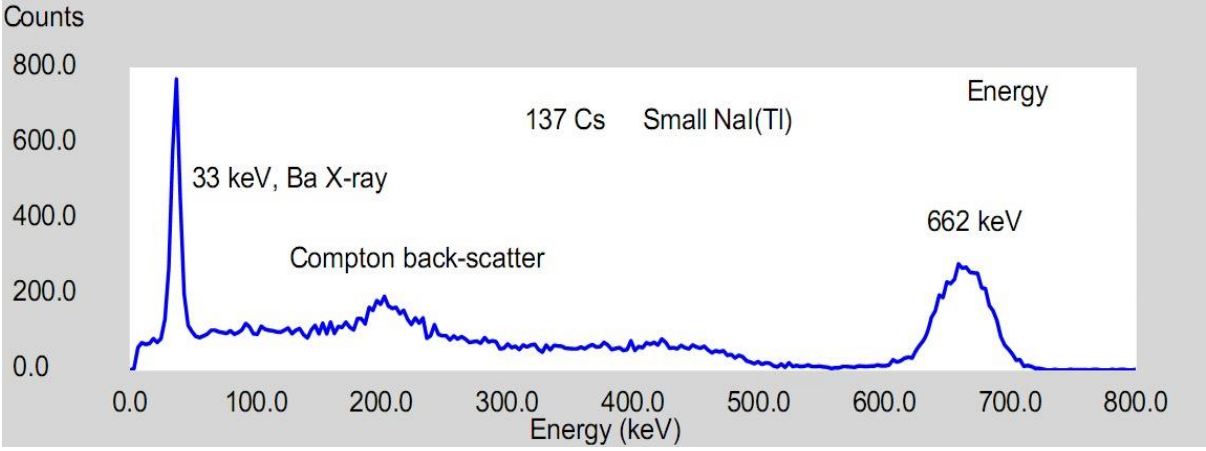


**FIG. 13:- AN EXAMPLE OF A FORMED SPECTRA USING CS-137 DECAYING TO BA-137M. IDEALLY THE PEAKS SHOULD BE DIRAC LIKE AND HAVE NO WIDTH AS THIS REPRESENTS A WIDE ENERGY UNCERTAINTY LIMIT. THIS WIDTH COULD POTENTIALLY OBSCURE EMISSION PEAKS FROM OTHER SUBSTANCES.**

bins. The spectra produced should present itself as it does below.

In an ideal acquisition the peaks should be shaped like a delta function and have no width. This would ensure emissions are accurately identified based on their sources unique emission spectrum signature. The width observed is due to radiations stochastic interaction with matter, which can result in a different number of photons being emitted for the same gamma photon energy. This width is also due to other factors such as: electronic ‘noise’; the photodiode’s intrinsic charge collection properties; and the inconsistent loss of optical photons at the interface between the scintillator and photodiode.

A detectors lower energy operating range can be affected by:

1. Background events produced by Compton scattering.
2. Electromagnetic noise produced by electronic devices.
3. Naturally occurring background radiation.

The first factor listed makes the most significant contribution to the lower energy operating domain and is what Liana was designed to resolve. The two remaining factors contribute significantly less events compared to the first listed point. However, these two remaining factors can interfere with the Liana's operation. Removing or reducing these factors will improve the Liana's resolution in the lower energy domain.

Naturally occurring radiation is managed by the Liana's passive collimation and energy acceptance threshold which must be calibrated before use.

Electromagnetic 'noise' events are more frequent than naturally occurring radiation and will contribute significant error to the lower energy domain. 'Noise' can be severely reduced or removed by placing electromagnetic shielding around the detector.

An intraoperative probe therefore requires EM shielding to resolve lower energy emitters like Co-57 and Tc-99m which are used in surgery.

Suppression of internal Compton scattering within the detector is at present technologically impossible. Resolving low energy emitters like those used in surgery therefore presents a challenge to detector designers. The fraction of events impacting the lower energy domain (<200KeV) can be reduced by implementing an Active and Passive Collimation unit. The Tungsten Carbide Passive Collimator stops events with energy <200KeV, the Active Collimator rejects events entering the IC from an angle outside of the accepted range. Simultaneous implementation of these collimators reduces the impact of background events in the probe by either blocking or discounting their impact.

The Active Collimation uses electronics to reject events by a coincidence circuit configuration which manages the emissions occurring in each channel. Events should only be able to enter the OC if they have first passed through the IC. Therefore events detected in the OC have entered the IC from an angle outside the specified physical window, and must be removed from the count. The time taken for the angled event to travel between the two media is called the rejection time frame. If the IC and OC both detect a signal within the rejection time frame, then the event is identified as outside of the accepted window and rejected.

Intraoperative implementation requires the removal of lower energy events for improving the localisation resolution of medical isotope sources <200KeV. A possible assessment criteria for rejectable events within this domain is the correlation of an energy acceptance window.

Implementation of an energy acceptance window isolates the targeted events by rejecting emissions with energy outside of the accepted range. Emission interactions with matter like Compton scattering result in changing the energy level of an emission. The chances of interaction increase with the amount of tissue between the emission source and the collecting detector. Creating a strict acceptance criteria rejects events that have likely passed through a larger amount of tissue due to the increased probability of interaction. Events whose energy closely aligns with the targeted level are less likely to have interacted with matter and are more likely to have been collected closer to the source.

The electronics rejects emissions by storing the first event recorded by the IC until a second event co-incident with the time difference of the OC arrives. If the event

arrives within the time frame the event is rejected, if it does not then the signal is allowed passage to the MCA for recording. (See

Fig. 7)

The first pulse can be stored by a delay line, this intentionally delays the signal for the rejection time frame required. If scattering has occurred then the signal from the OC would reach the discriminator before the IC. This signal would then be rejected from the spectra count. Ensuring the correct signal is rejected once the signal has entered the electronics requires the rejection time frame to be calculated accurately. This creates the strictest possible Subtraction Criteria and ensures that the correct events are rejected to high accuracy. The electronics response time however is slower than the emissions passing between each of the scintillators. The rejection time frame then is effectively zero and considered to be simultaneous with respect to the operating speed of the electronics. The physical picture of emissions passing between each channel within a time frame however will continue to be discussed in place of “simultaneous events” for the duration of this report.

The scintillate composition affects the probes energy conversion efficiency towards certain emission types and energy levels. Knowledge of the conversion efficiency for each of the probes interactions with an event allows for the background events to be identified. Identification is performed by comparing the peak energies found in each detector and matching them together for subtraction from the results. This allows for accurate localisation of the source by correctly identifying and eliminating the Penumbra generated by background events outside of the acceptance window.

For a Compton scattering event occurring within the probe the signal delay must be adjusted to accommodate for the processing time of the logic gate. This aspect of

the Liana Board processing design was thoroughly investigated by Franks [18]. It was not investigated in this study due to constraints on the research time period. An illustration of the electronics design is provided in **Error! Reference source not found.**.

In the study by Franks, Anti-incidence is also discussed but it is not investigated. Anti-incidence with Liana can be used to exclude events coming from the OC into the IC. This provides an additional method of Active Collimation for events that pass directly through the Passive Collimation. The Lianas $^{3}$DS design includes numerous functions that make the probe versatile and useful for a number of applications. Switching between configurations will be at the push of a button.

The modes are tabulated with a brief description in TABLE I. This table also explains how these modes are advantageous to the probe design. Various constraints prevented thorough assessment to all these modes

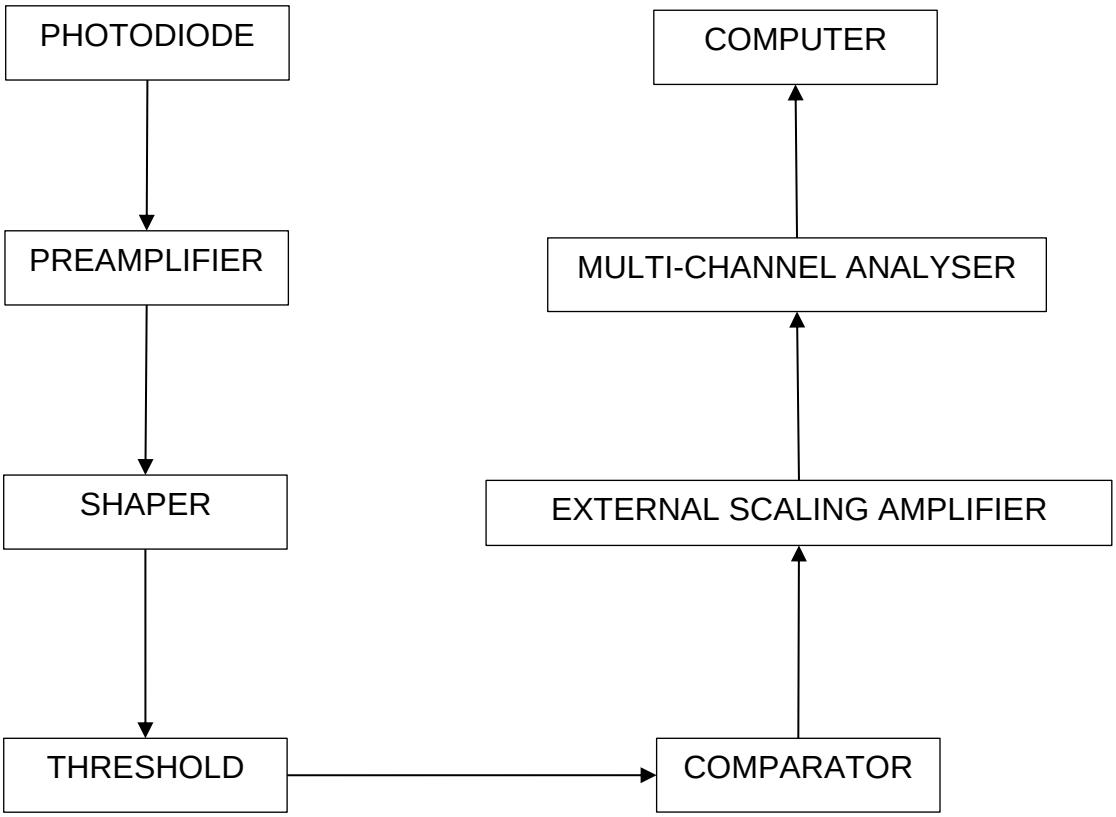


**FIG. 14:- THIS BLOCK DIAGRAM ILLUSTRATES THE STEPS USED BY THE LIANA CIRCUIT BOARD WHEN PROCESSING A SIGNAL. AFTER THE PHOTODIODE RECEIVES INPUT, IT CREATES A SIGNAL WHICH PASSES THROUGH EACH STEP OF THE BLOCK DIAGRAM ABOVE UNTIL FINALLY IT IS OUTPUTTED BY THE MULTI-CHANNEL ANALYSER.**

# EXPERIMENTAL METHOD AND FURTHER EXPLANATION OF DESIGN ASPECTS

The signal amplitude from the Liana board is insufficient to be processed by the Multi-Channel Analyser (MCA). Since this data was required for assessing the probes functionality, the signal would be passed through a ten times non-inverting signal amplifier. This signal amplifier was also designed to manage dual inputs for each channel, however, this function was never used.

The amplifier was tested using a function generator that simulated signals coming from the Liana circuit board. The amplifier's load line was found to function perfectly within the limit of the signals that could be generated by the Liana board. According to external assessment by Adam Sarbutt, an experienced technician from ANSTO, the amplifier's construction was robust, durable and effective. The amplifier would operate reliably, precisely, and with consistency under any conditions in which the Liana probe would be expected to operate.

After the output signal from the Liana Board was externally amplified it was directed into the MCA for data recording and channel "binning".

Signals coming from the Liana board and amplifier were externally assessed by an oscilloscope while they were in operation. This was to ensure:

1. The input signal was a 'pulse' and that the Liana circuit hadn't failed.
2. The output signal was the amplified version of the input signal 'pulse'.

This meant if either of these components failed then the test could be stopped immediately until the problem was rectified. This not only prevented further damage to the circuit, but also provided a means for diagnosing the problem.

All components of the test equipment were EM shielded. EM interference is therefore considered as negligible for all results. The collimator inside the detector container was also grounded for all tests and thus provided additional shielding.

The Liana's electronic circuit was found to be insufficiently grounded. It was observed that improving the boards grounding connections improved the recorded energy resolution result. The low energy spectrum resolution was significantly improved by removing the electronic noise with additional grounding. Whilst further reduction of electronic noise is clearly achievable, this was not resolved during the course of the project.

The modes available to the Liana Probe are described in TABLE I below. The terms A and B are used to represent the activated Channel, "A" designates the Inner Channel and "B" designates the Outer Channel. The scintillator in both channels was comprised of CsI(Tl) as its reduced hygroscopic properties allowed for easier handling of the probes during the project. Another advantage with comprising both channels of the same scintillate was that the optical properties would be identical along with the photon yield. This meant the same circuit layout could be used for each channel when identifying the Background Events for rejection.

The modes presented in TABLE I will only function correctly if the Tungsten Carbide Collimator Cap is present and covering the scintillate material within the handheld unit as illustrated in Fig. 9.

| Modality | Function Purpose | Function Method |
|---|---|---|
| A | Base Level Detection | Using just the IC records all events entering the probe via the aperture as the Passive Collimation shields the probe. This is the standard operating function for a single detector probe. |
| A+B | Widest collection range | Combining both channels increases the detection efficiency and enables the probe to roughly localise a radioactive sources position within the larger area of a patient vs. a specific part of their body. |
| A-B | Low energy beta event resolution | Subtraction of events in A from B.<br>This function provides the sharpest localisation resolution. It is used for identifying the specific location of a radioactive source within the body.<br>The function suppresses background Compton scattered events by subtracting events recorded by the OC from the IC.<br>This leaves only the counts in the inner channel which are related to positron detection. |

**TABLE I: - THE MODES ALONG WITH THEIR FUNCTION ARE LISTED AND EXPLAINED.**

Performance depends on the Scintillator's absorption depth. Activating both channels creates the largest absorption volume with the highest chance of absorption. Activating one channel creates the smallest absorption volume. The dual channel operation is electronically based and performed by logic modules. The

physical structure of the scintillator is carefully designed to ensure Background Events are collected by the OC if they enter the IC.

Energy passing through a Scintillator is more accurately converted to optical photons if the emission energy is only slightly greater than the Scintillators forbidden energy gap. [19] [20] Reducing the volume of the Scintillator reduces the interaction probability of events outside the designed energy range of the Scintillator.

The design of the OC volume corresponds to the maximum absorption volume for emissions within the intended lower energy domain. When both channels A and B are activated the detection volume is at its largest. This larger scintillate volume corresponds to collecting the penumbra like background events passing at an angle across the IC. The maximum absorption volume therefore ensures that tissue scattered events in the lower energy domain are collected. This provides accurate data to the logic module in the circuit for processing in either the event addition

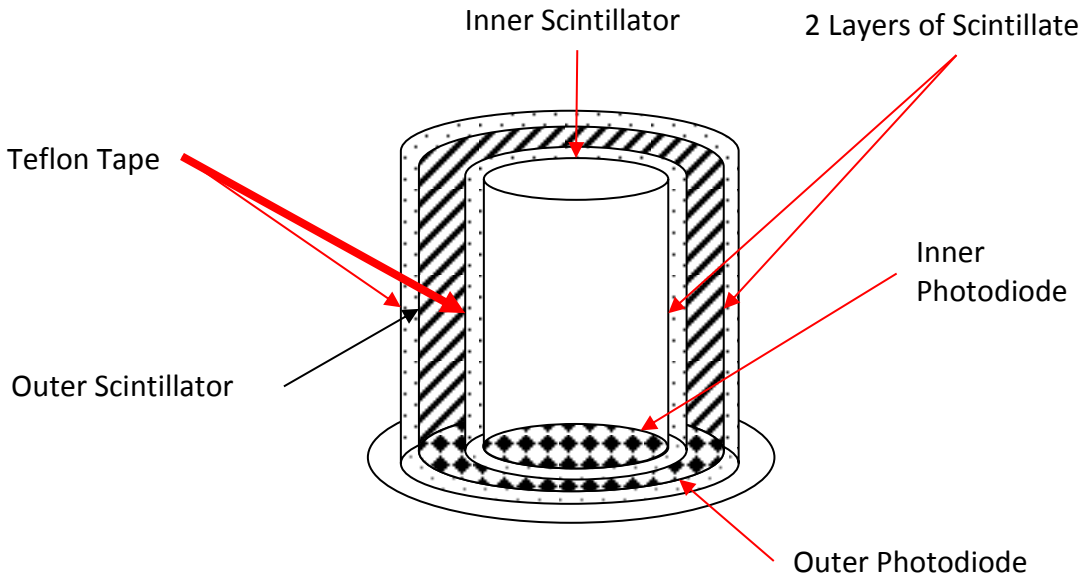


**FIG. 15:- BOTH SCINTILLATORS ARE OPTICALLY ISOLATED BY TEFLON TAPE. THIS PREVENTS CROSS TALK FROM IMPACTING THE PROBES RESULTS. THE PASSAGE OF THE ELECTRONIC LEADS IS OMITTED FROM THIS DIAGRAM.**

(A+B) or event subtraction (A-B) mode. In a significantly larger detector this function could be used for internal Compton suppression but as the scintillator is small it is unable to provide this capacity.

The physical design of each channel must be carefully considered then to balance between two critical detector factors. For the IC, the choice is between spatial resolution and sensitivity. For the OC the choice is between accurate collimation and practical probe size.

The “A+B” mode is the Liana probes widest angle detection setting. The probe enters its widest collection state accumulating events across a much larger physical localisation window. In surgical application this would allow the surgeon to determine if any radioisotope and subsequently afflicted node is remaining within the patient. The direct consequence of this configuration is that the localisation resolution is diminished and requires the probe to be changed to the A-B mode to perform.

The “A-B” setting is the fine resolver for both the energy spectra and localising the emission material in the low energy domain. This function is what the probe was primarily designed and built to perform. Events passing through the IC into the adjacent OC are subtracted. Medical application allows the surgeon to fine localise the position of radioisotopes in a patient’s body to within approx. ≈ 1mm. The surgeon can therefore pinpoint the location of an afflicted cell and excise it from the patient’s body.

Results were collected for investigating the physical fundamentals of detector design. The results illustrate each channels operating capacity independently. Assessing the function of each channel independently provides insight to the probes capabilities when the dual function is active. The physical phenomena managed by

each probe is analysed and a correlation between the experimental and theoretical results is identified. This information allows for diagnosing Liana's capacity to function as a dual channel intraoperative Gamma Probe. A more thorough test would involve implementing the combined modes. Various factors impeded the implementation of the dual modes and were not resolved during the research period.

# CHARACTERISATION OF THE LIANA BOARDS AND PROBES

## INTRODUCTION

The research focussed on the probes and boards characterisation. This provided quality assurance for the results and the capacity to diagnose the boards and scintillator detectors in the event of mishandling.

An important part of the characterisation process was the identification of the best operating board with the best operating scintillator probe. The best operating board was identified by the implementation of "bare detectors" (BD's) i.e. photodiodes alone without a scintillator. The bare detectors had an IV and CV Characteristic performed on them in the reverse bias domain. The tests would assess the response of the photodiode to the voltages it would experience when in operation on the Liana circuit board. The ideal result for the IV test is a reading that shows minimal change to the current (I) with respect to the increase in voltage (V). A low I/V gradient means that the impact of noise from the detector is reduced and that photon yield is treated equally by the photodiode despite minor changes in voltage during device operation.

The bare diodes were redundant for intraoperative application, but were effective for testing the board electronics. Implementing bare diodes ensured safe diagnosis of the untested boards without sacrificing expensive scintillators. Characterisation could

also be conducted on the boards using Am-241's gamma emission source (59 KeV) allowing for early assessment of the board functionality.

The tests were performed inside a sealed, dark and EM shielded container. The darkness allowed for the impact of "dark current" to be measured. Dark current is the random generation of electrons and holes in the depletion region of a photodiode when no optical photons are passing through it. Dark current is a source of noise and its impact must be reduced, assessment of dark current provides insight into achieving this reduction. The darkness of the container also simulates the operating conditions of the scintillator inside an intraoperative probe.

In total 11 samples with two channels each were recorded for the bare diodes (BD's). The data below illustrates only the two best operating probes of this BD batch. A third probe is included to illustrate the results given by a poor detector and contrasts the results given by the better probes. The change in current for the two best functioning operating diodes is minimal with respect to the change in voltage.

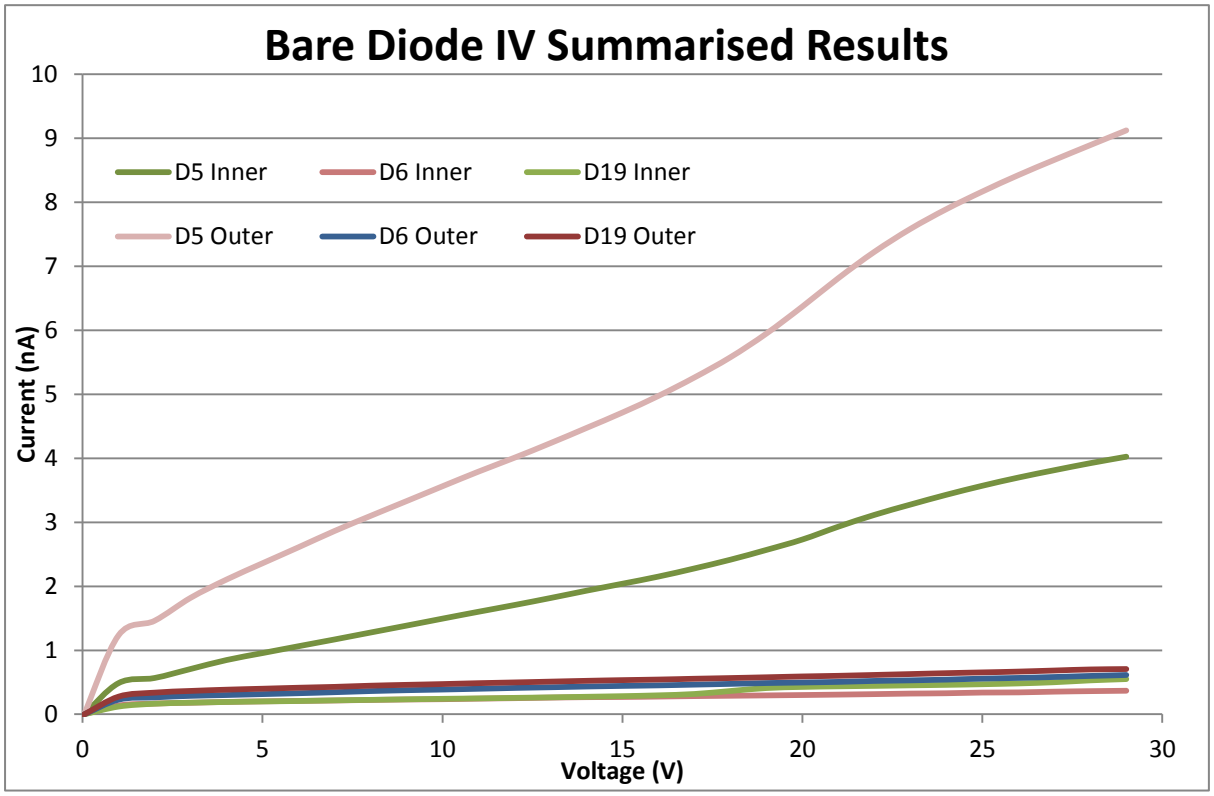


**FIG. 16:- D5 ILLUSTRATES THE WORST PERFORMING PHOTODIODE AS IT HAS THE HIGHEST IV GRADIENT IN COMPARISON TO THE OTHER PROBES OF THE FIRST PROBE BATCH.**

## *BARE DIODES RESULTS*

D6's Inner diode produced a gradient of 0.008268 nA/V which was the flattest result for the probes in the operating voltage domain. D19's OC produced a gradient of 0.01539 nA/V which was also flat in the operating voltage domain. D5 was considered the poorest functioning photodiode and its results provide clarity by contrast to the superior performance of D6 and D19.

D6 and D19 were the highest performing bare diode detectors. D5 was chosen however because it was unclear if the boards could damage the detectors during the characterisation. D6 and D19 became unnecessary as D5 provided sufficient quality results when characterising the boards.

# BOARD CHARACTERISATION

Bare Diode 5 (BD5) was used to record the spectra for Am-241, it was recorded

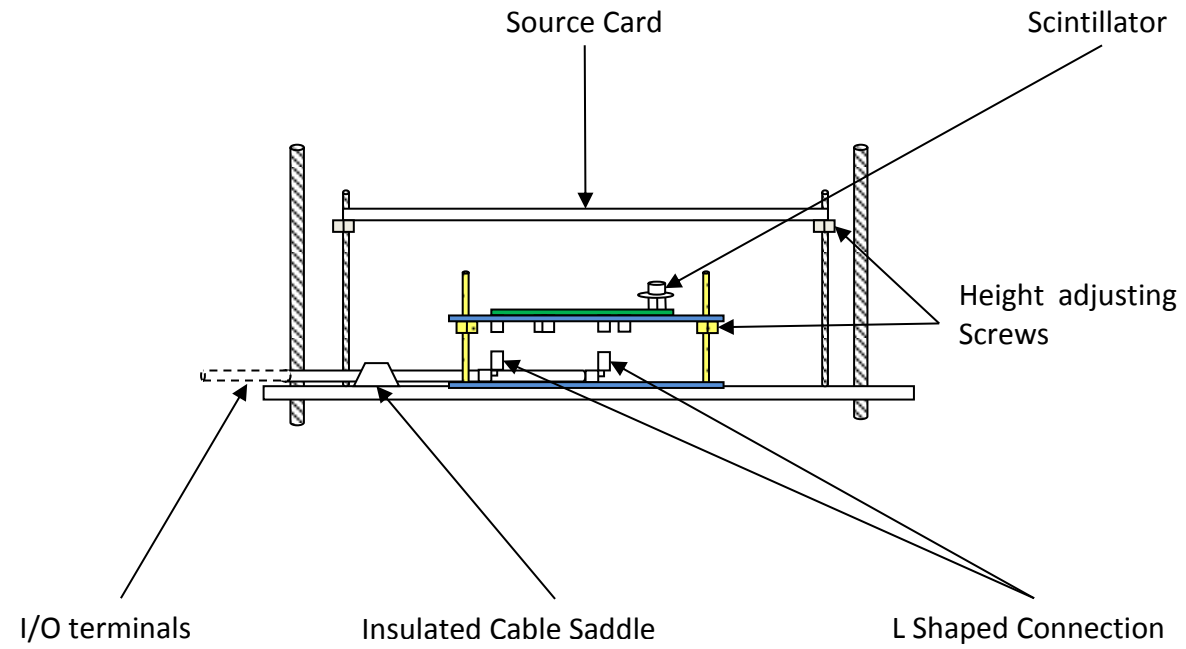


**FIG. 17:- THE ELECTRONICS AND PROBE ARE ENCLOSED WITHIN A SHIELDED VACUUM CHAMBER. THE ELECTRONICS IS ISOLATED FROM THE GROUNDING OF THE CHAMBER BY THE IMPLEMENTATION OF INSULATING MATERIALS DESIGNATED BLUE AND YELLOW.**

within an enclosed vacuum chamber using the experimental setup presented below.

The leads, board and the probe in Fig. 17 were electronically isolated from each other and the chamber. The distance between the probe and emission source was managed by adjusting the screw heights. The vacuum chamber was not used in later tests.

The chamber was capable of producing a vacuum. This wasn't used however as air bubbles in the adhesive between the scintillator and photodiode could jeopardise the probes structural integrity. Furthermore, the Liana probe was designed to function in STP conditions. Testing the probes functionality in a vacuum was therefore

redundant except for diagnosing improvements for the crystal. Fig. 17 depicts a Scintillator when a Bare Diode was used for the first round of tests. The bare diode was replaced with a scintillator for later tests involving the energy resolution.

All boards excluding Board 0 were manufactured prior to testing. Board 0's inclusion in these tests was intended to show a common relationship between each boards functionality. Board 0 was anticipated to be the highest functioning board as it was developed during an independent study by a fellow CMRP student - Ahmad Ulbngali. When compared to the manufactured boards, Board 0 did not produce the highest quality spectra. Energy Characterisation was not used for scaling these results.

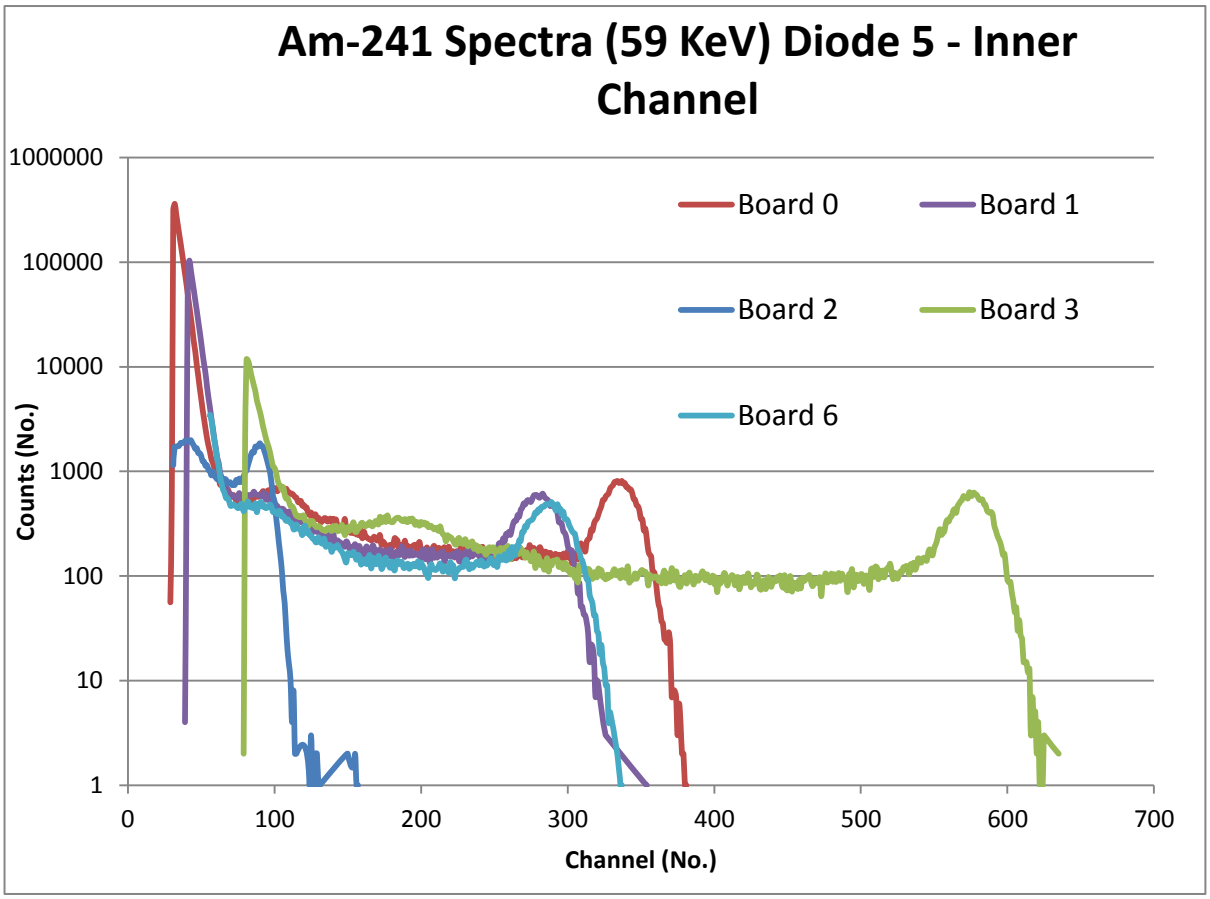


**FIG. 18:- THIS TEST USED AMERICIUM-241 AS THE TEST SOURCE. BOARD 3 AS SHOWN IN THE FIGURE IS THE BEST PERFORMING CIRCUIT. THIS FIGURE DEPICTS THE IC RESULTS ONLY.**

## *BOARD CHARACTERISATION RESULTS*

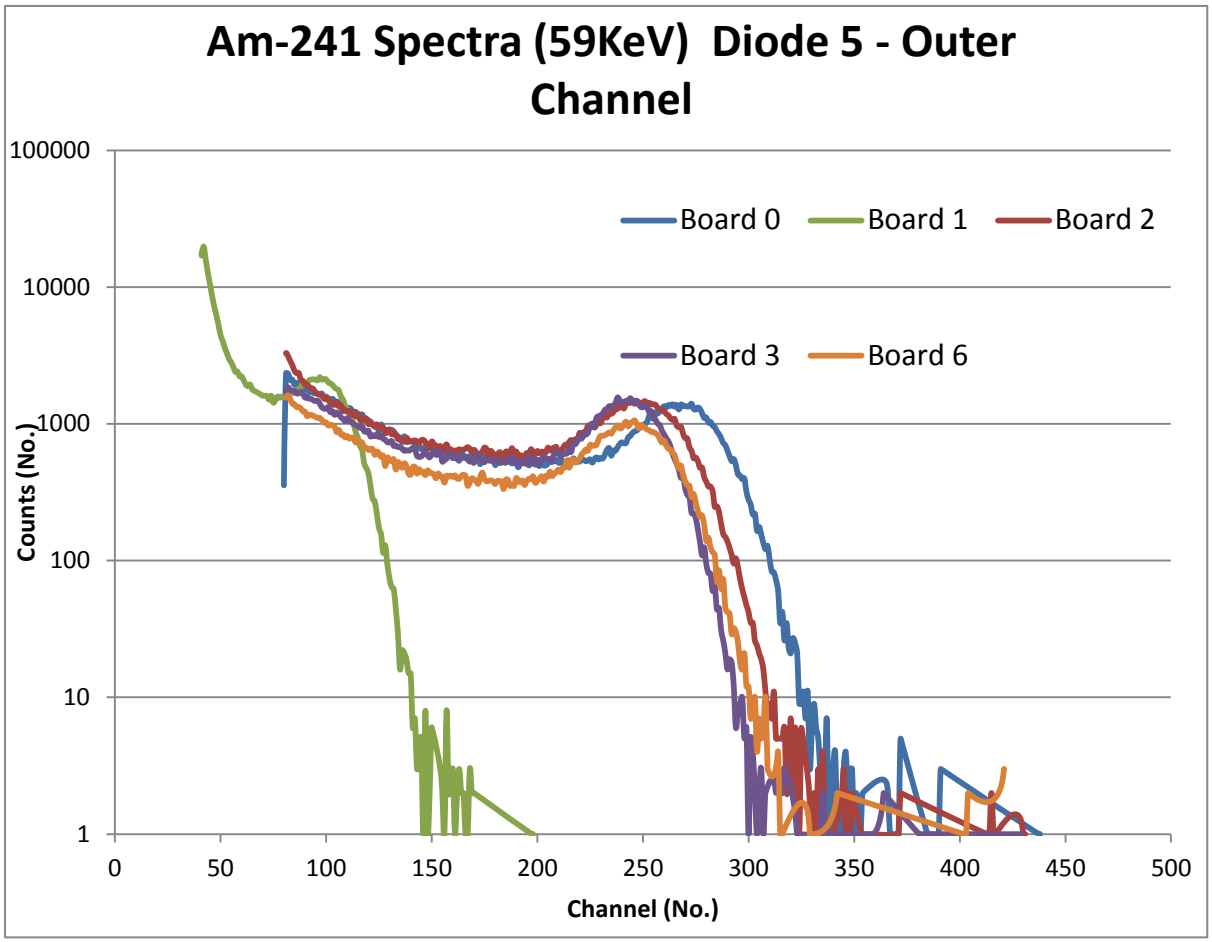


**FIG. 19:- BOARD 3'S OC PERFORMED RELATIVELY POORLY IN COMPARISON TO ITS OWN IC, BUT PERFORMED EQUALLY WELL COMPARED TO THE OTHER BOARDS OC'S. THE SOURCE USED IN THIS TEST WAS AMERICIUM-241.**

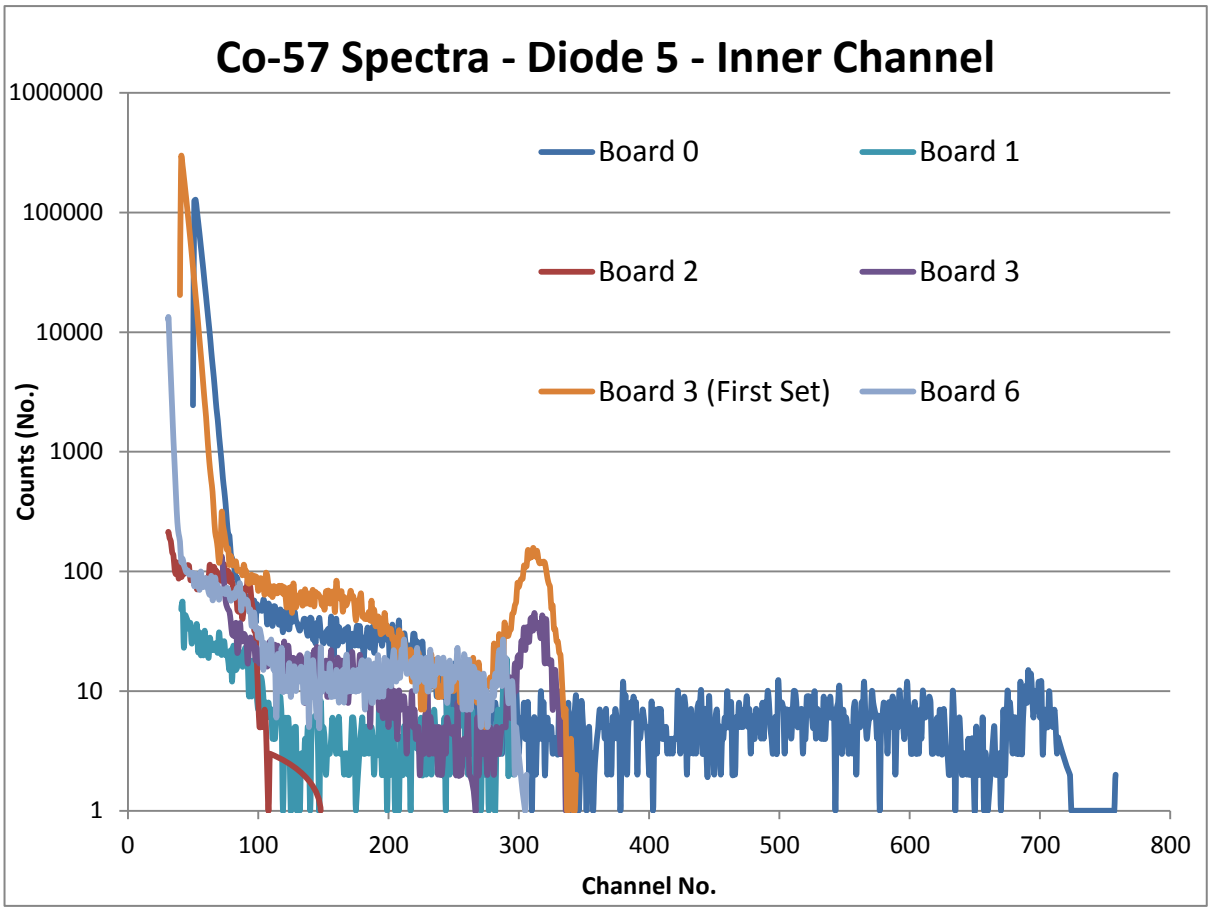


**FIG. 20:- FOR THIS TEST COBALT-57 WAS USED. AT TIME OF TESTING INCONSISTENCIES BEGAN APPEARING IN BOARDS 0 AND 3. BOARD 3'S SENSITIVITY HAD DECLINED BETWEEN THE TIMEFRAME OF THE TWO TESTS (APPROXIMATELY 30 MINUTES). THE CAUSE OF THE SENSITIVITY DECLINE WAS NOT FOUND DURING THE TIMEFRAME OF THE STUDY.**

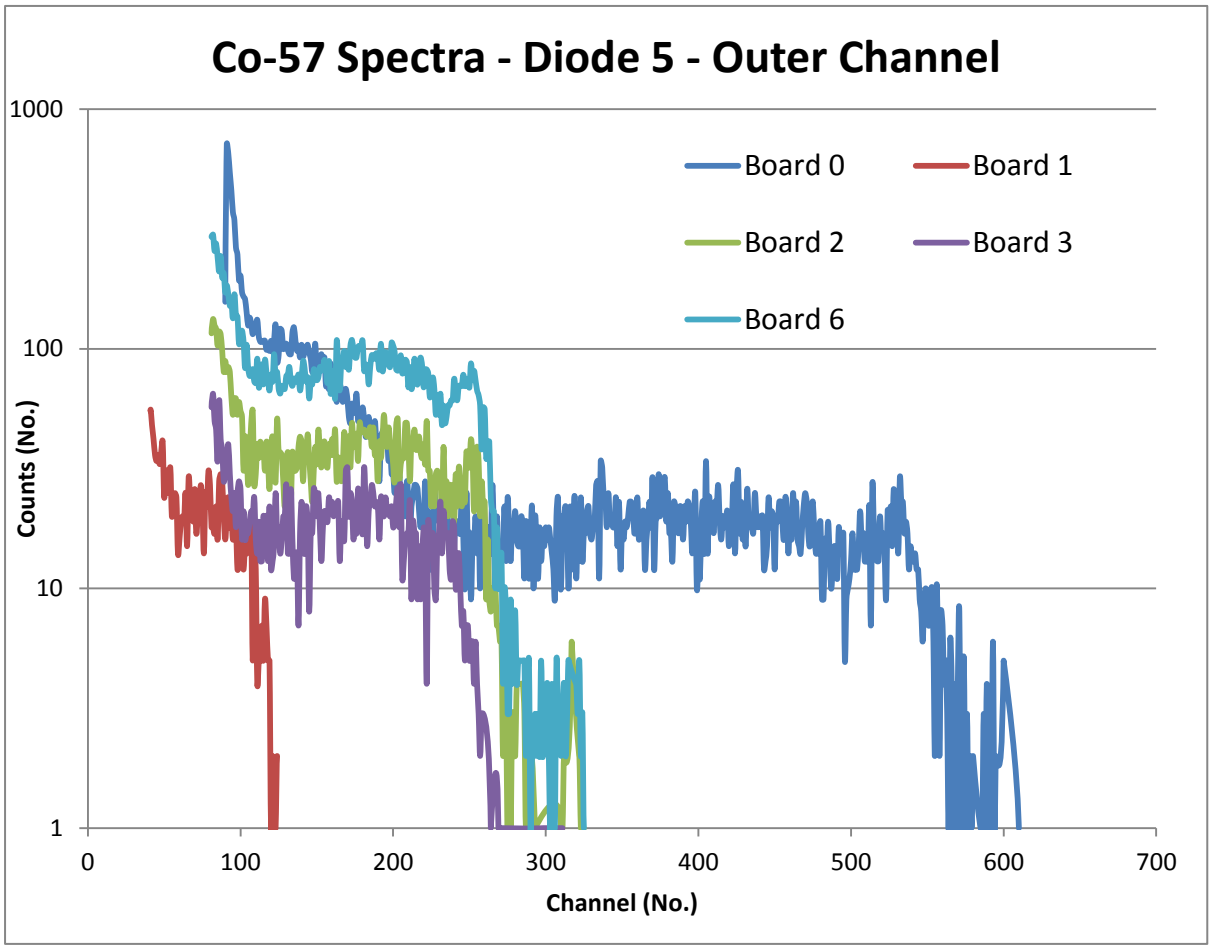


**FIG. 21:- SOURCE USED FOR THIS TEST WAS COBALT-57, BOARD 0'S INCONSISTENCIES ARE FOUND ACROSS BOTH CHANNELS.**

## *DISCUSSION OF BOARD CHARACTERISATION TEST*

Many tests of the board characterisation were conducted, the results chosen provide insight to the board functionality and were consistent with previous tests conducted by Ulbangali and Franks.

Board 3's IC was the most superior functioning of the batch. Board 3's higher signal gain corresponded to improved sensitivity which provided greater energy distinction for resolution. This was because Board 3's bin data was distributed across a wider energy range relative to the other boards.

Co-57's data illustrates Board 3's performance decay with respect to the research period (Fig. 20). The performance decay was investigated extensively and the problem was by deduction isolated to the 0603 capacitors on the Liana board. This is because every other component was individually checked by reading the printed resistance/capacitance rating on the back of each component. After reading the value, these components were then individually tested by removing them from the board and checking their resistance/capacitance rating was the same as their printed value.

The size, number of components and lack of distinguishing markings made testing the 0603 capacitors with this process onerous. Testing was also found to jeopardise the PCB's function as it was designed to have components soldered onto it no more than once. A choice had to be made between finding the factor responsible for increasing the gain and losing the best functioning Liana board.

A more consistently operating board was selected for the remainder of the project as Board 3 required continuous repair and could be investigated later by another study. Board 6 was selected based on the results acquired from the characterisation and its

manufacture quality. Numerous investigations were unable to identify the cause of B3's superior performance, though the cause for the performance decay is anticipated to link with the signal gain.

## DETECTOR WITH SCINTILLATOR CHARACTERISTICS

The process used to assess the bare diodes functionality was replicated for the tests with the scintillator attached. The diodes were placed in a dark EM shielded container.

The IV Characteristics purpose was to assess the photodiodes response to changing voltages across the operating domain. It was discussed that the IV Characteristic reveals dark current, which is due to defects within the photodiode generating holes and free electrons. Measuring the dark current allows for noise contribution from the Scintillator into the signal processing to be assessed. The unmentioned factor of the IV characteristic was the identification of the breakdown voltage. Though already performed by Franks, the breakdown voltage may have changed during the time frame between the two studies. An IV characteristic allows for diagnosis later in the research period if fine assessment of the probes functionality is required. This information is critical when managing electronics consisting of over 100 components that fit into an area effectively the same size as a pen.

CV Characteristics not presented earlier allow for a different investigation to be performed on the probes. The CV allows the detectors doping density to be assessed.

The data garnered from this test was useful as an additional diagnostic test for the probe. It was anticipated that the capacitance experienced by the outer diode would be greater than the inner diode. This was because the surface area of the outer diode is larger than the inner diode. Implementing known physics and previous test comparisons provides useful diagnostic tools for assessing the condition of the

photodiodes. Increasing current in the diode may not significantly affect the CV characteristic, but it would register in I-V characteristics.

The depletion voltage for a semiconductor can be determined from the CV, allowing the probes impurity concentration to be diagnosed. Approximating the IC and OC as parallel plates means the capacitance is expressed as,

$$C = \frac{\varepsilon_0 \varepsilon_r A}{d}$$

Where “d” is the separation between the two plates, “A” is the overlapping area of the two plates, $\varepsilon_0$ is the *electric constant* and $\varepsilon_r$ is the relative dielectric permittivity.

The Depletion Voltage is given by,

$$V = \frac{qN \times d^2}{2\varepsilon_0 \varepsilon_r}$$

Where “N” is the doping density and “d” is the depletion regions thickness. The separation between the two capacitor plates is equal to the depletion region width. The equations can be solved to give.

$$\frac{1}{C^2} = 2\left( \frac{V}{N \times q\varepsilon_0 \varepsilon_r A^2} \right)$$

Which applies when $V < V_{depletion}$, for $V \geq V_{depletion}$,

$$\frac{1}{C^2} = Const.$$

The depletion Voltage can therefore be determined by plotting, $C^{-2}$ vs. V. It is the point on the diagram where the capacitance is reached saturation.

While finding the Photodiodes Breakdown and Depletion Voltage is certainly useful, it isn't vital to the probes function that they be found in this test. This is because the purpose of these tests is to determine whether the photodiode will function correctly within the intended supply voltage domain (between 0 to 30V). Hence, if neither Breakdown nor Depletion is observed in these tests, then the photodiode can be expected to function correctly for all later tests.

The First probe batch's IV and CV characteristics in this study were obtained using equipment from ANSTO's Detector Radiation Group (DRG). The DRG equipment comprised of a top of the line Keithley 2224 electrometer, Boonton capacitance modulator and a dedicated vacuum chamber which was regularly maintained and configured for characterising detector photodiodes.

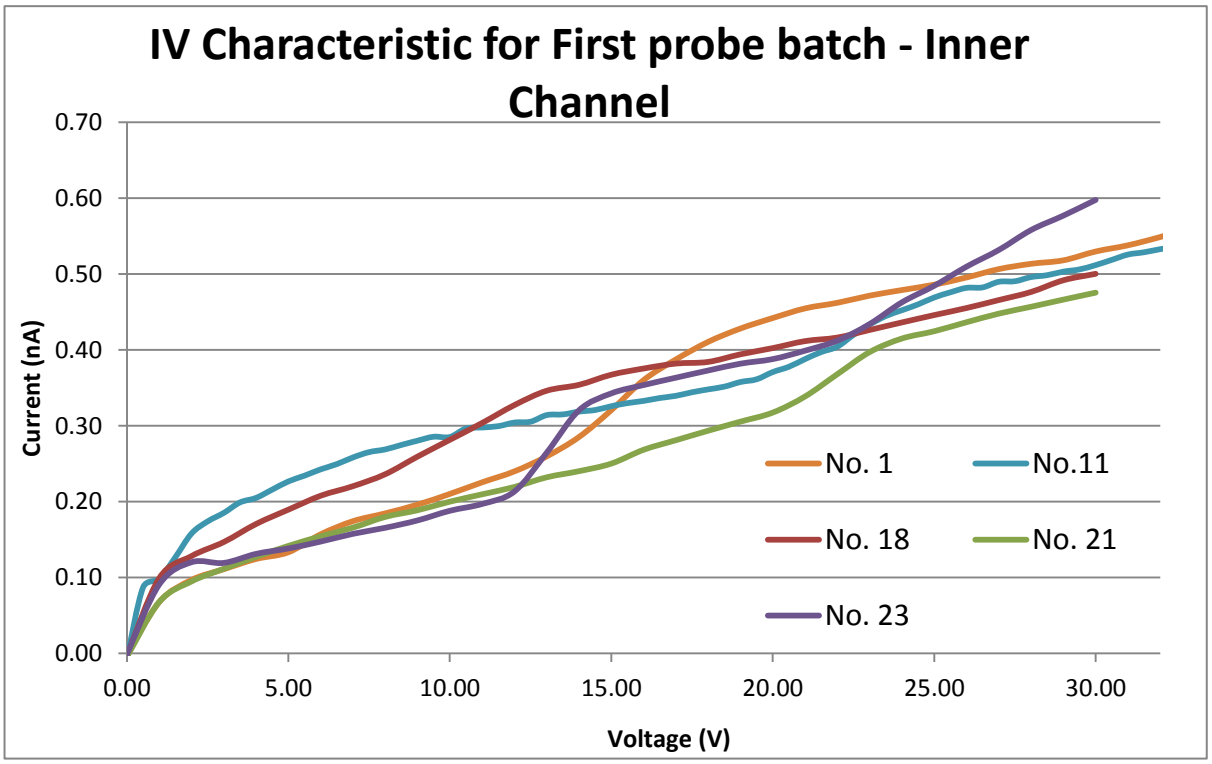


**FIG. 22:- THE IV CHARACTERISTICS HAVE BEEN LIMITED TO THE BEST OPERATING SCINTILLATORS. AT 15V THE AVERAGE WAS APPROXIMATELY 0.3 NA. THE GRADIENT FOR PROBE 21 = 0.00134**

## *1ST SET OF SCINTILLATE IV AND CV CHARACTERISTICS*

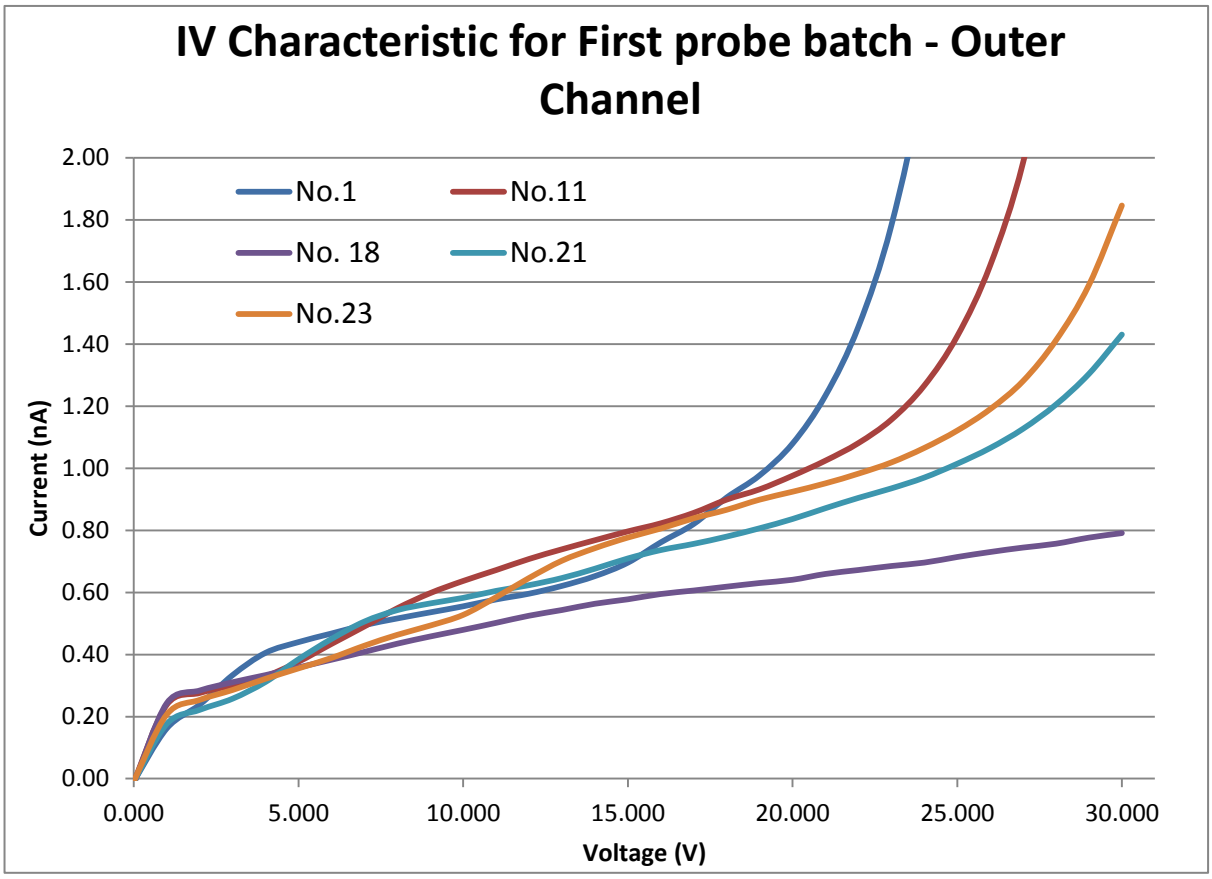


**FIG. 23:- THE OC USING THE SCINTILLATORS IN** ERROR! REFERENCE SOURCE NOT FOUND.**. THOUGH INITIALLY FLAT THE VOLTAGE BREAKDOWN OCCURS MUCH SOONER FOR ALL SCINTILLAORS EXCEPT PROBE 18. AT 15V THE AVERAGE CURRENT WAS 0.707 NANOAMPERES. PROBE 11 AND 23 WERE FOUND TO HAVE A GRADIENT**

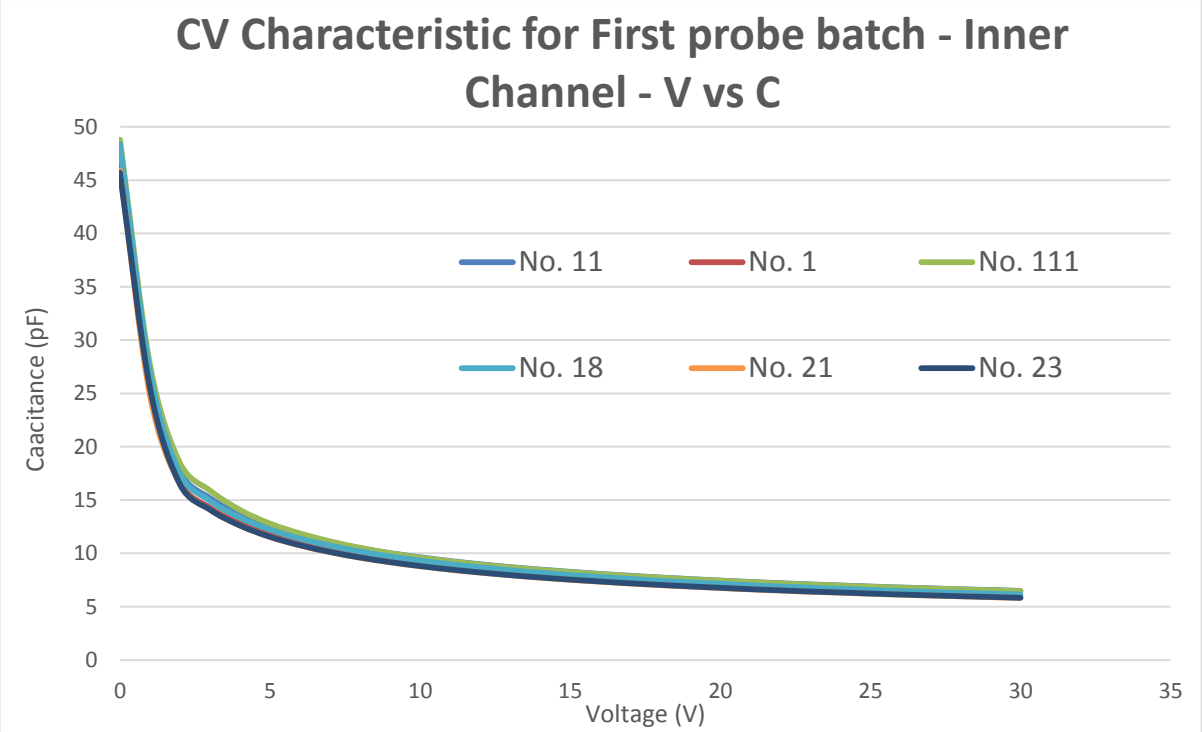


**FIG. 24:- CV FOR ALL DETECTOR IC'S IS ALMOST IDENTICAL AND ONLY NOTICEABLY DEVIATES IN THE 1 → 5 VOLTS DOMAIN.**

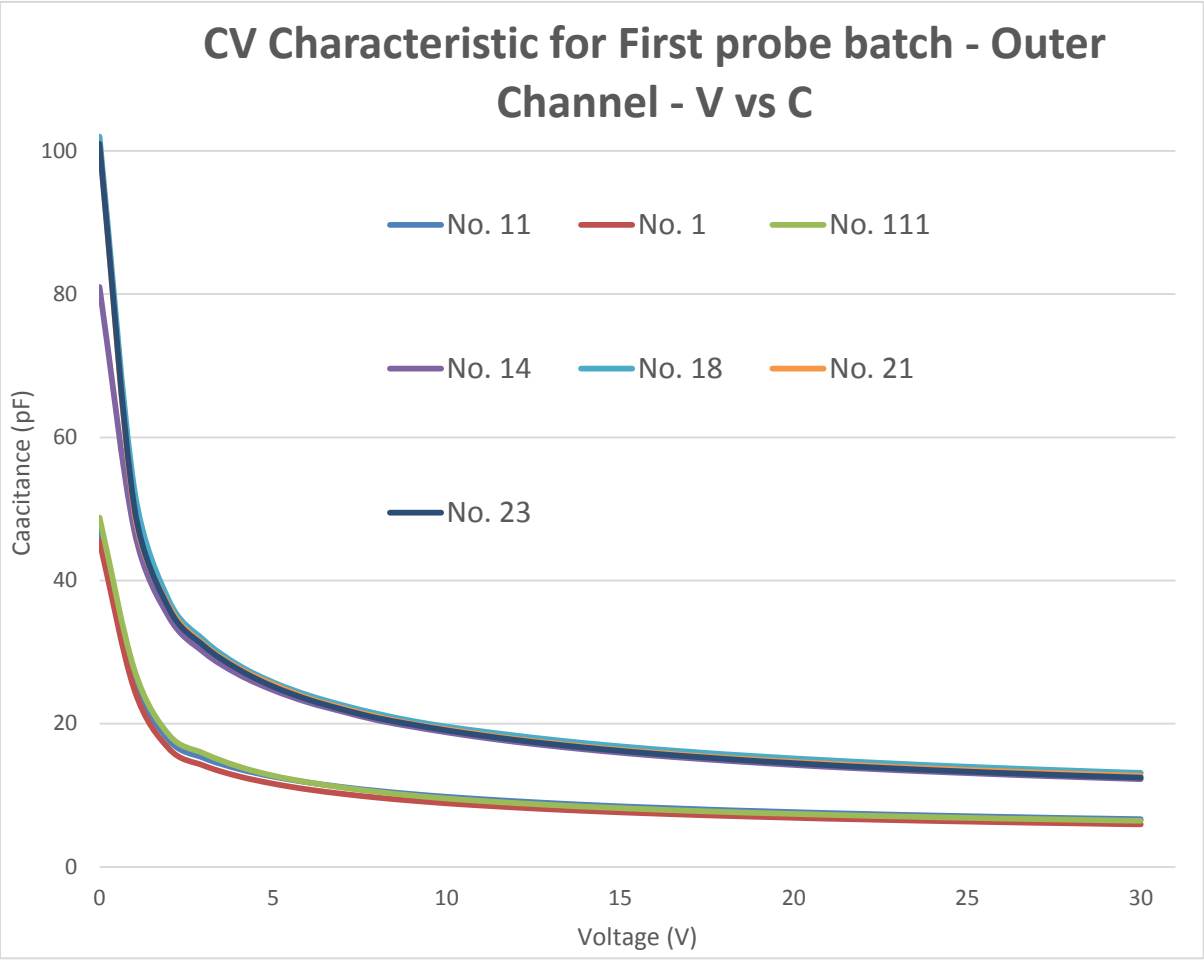


**FIG. 25:- DETECTORS 1 AND 11 HAVE HIGHER CONSISTENCY WITH THEIR IC EQUIVALENTS. THIS RESULT WAS UNEXPECTED AS THEIR OUTER CHANNELS ARE LARGER AND SHOULD PRODUCE RESULTS SIMILAR TO PROBES 18, 21 AND 23.**

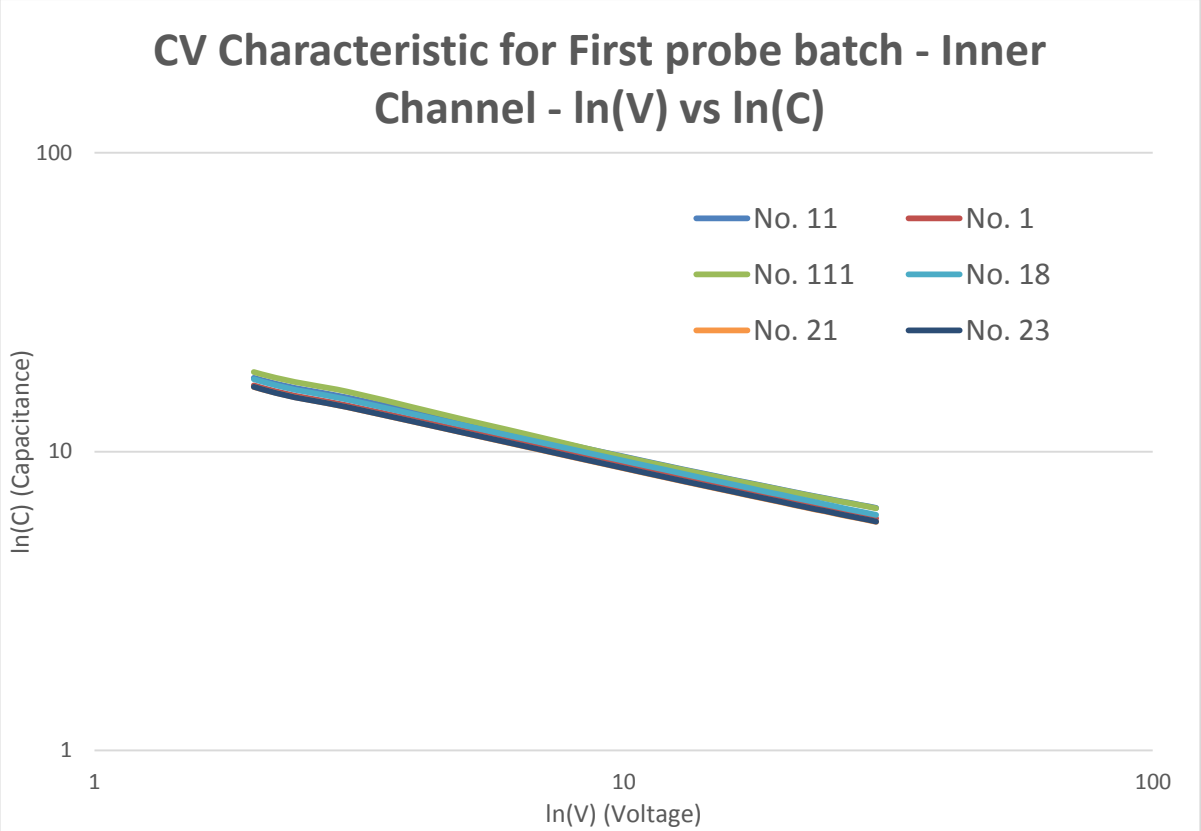


**FIG. 26:- LOGARATHMIC SCALE OF FIG. 24. UPON VOLTAGE SATURATION OF THE PHOTODIODE THE RATE OF CHANGE FOR THE CAPACITANCE WOULD BECOME CONSTANT AND FLATLINE. WITHIN THE DOMAIN OF 0 TO 30 V NO FLATLINE IS OBSERVED IN THE CAPACITANCE DATA. THEREFORE THE PHOTODIODE CAPACITANCE WILL NOT SATURATE WITHIN THE OPERATING VOLTAGE DOMAIN SUPPLIED BY THE $^{3}$DS ELECTRONICS.**

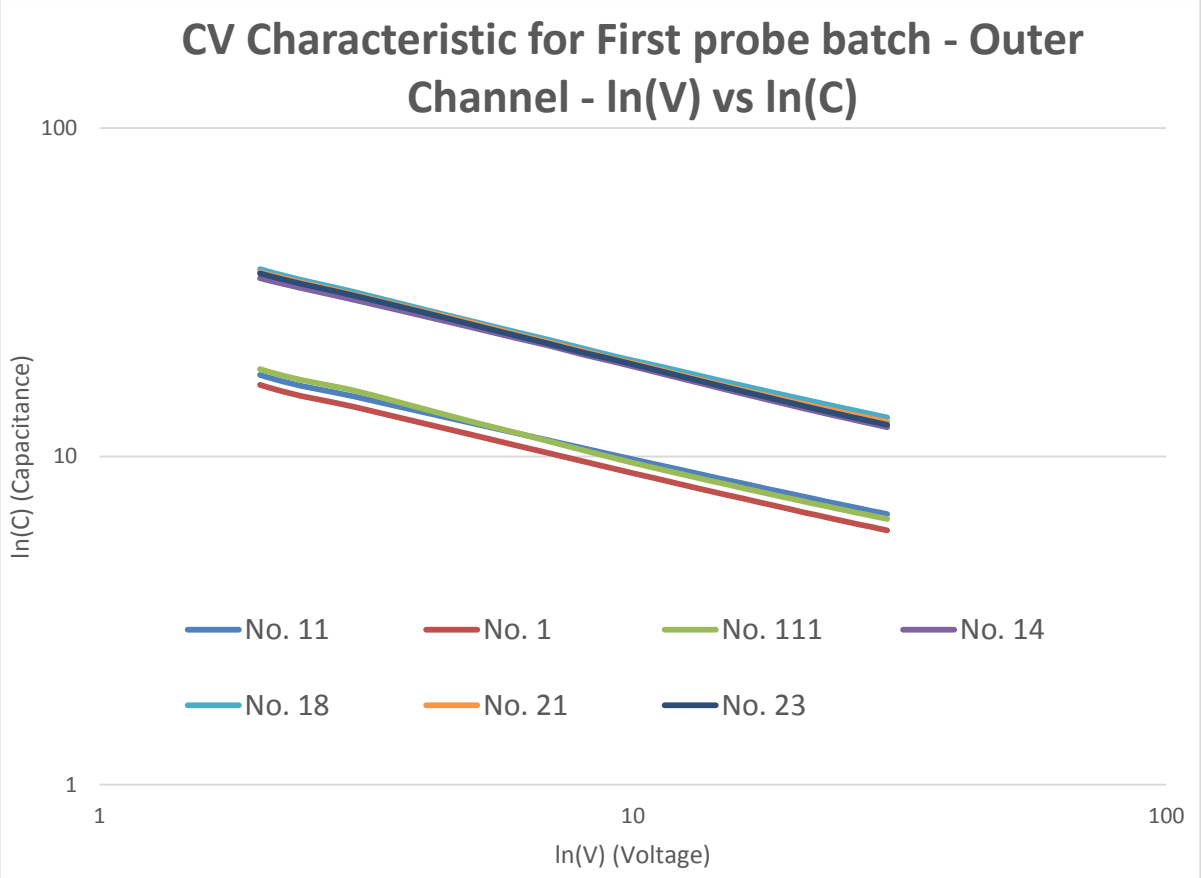


**FIG. 27:- SIMILAR TO FIG. 26 THE PHOTODIODE CAPACITANCE FOR THE OC'S NEVER SATURATES. THE DICHOTOMY OF RESULTS OBSERVED IN** ERROR! REFERENCE SOURCE NOT FOUND. **IS MAINTAINED IN THE LOGARATHMIC SCALE VERSION OF THIS FIGURE.**

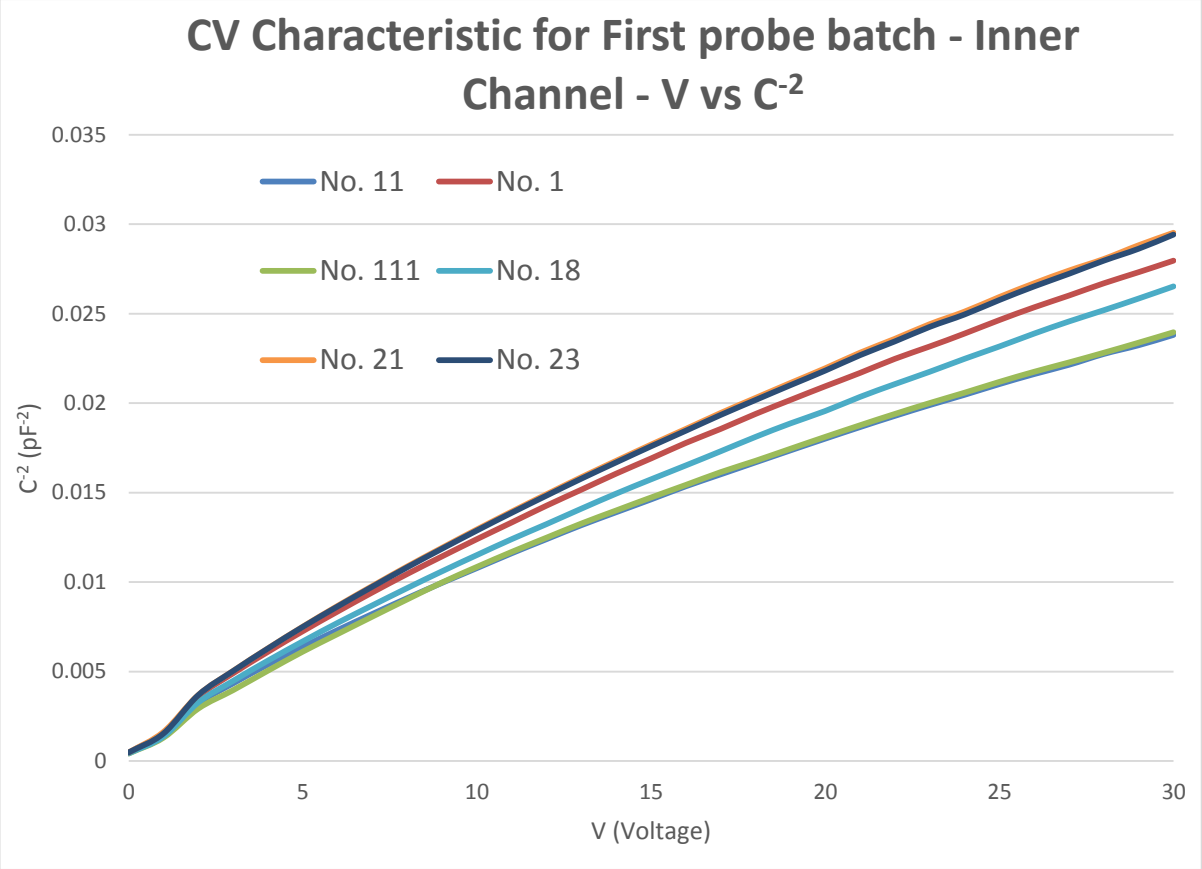


**FIG. 28:- SQUARING THE CAPACITANCE IS INTENDED FOR IDENTIFYING THE SATURATION VOLTAGE. AS WITH THE LOGARATHMIC SCALE A FLAT LINE IS ANTICIPATED FOR THE CAPACITANCE. NO FLAT LINE IS OBSERVED AS WITH FIG. 27 AND SO THE SATURATION VOLTAGE IS NEVER REACHED.**

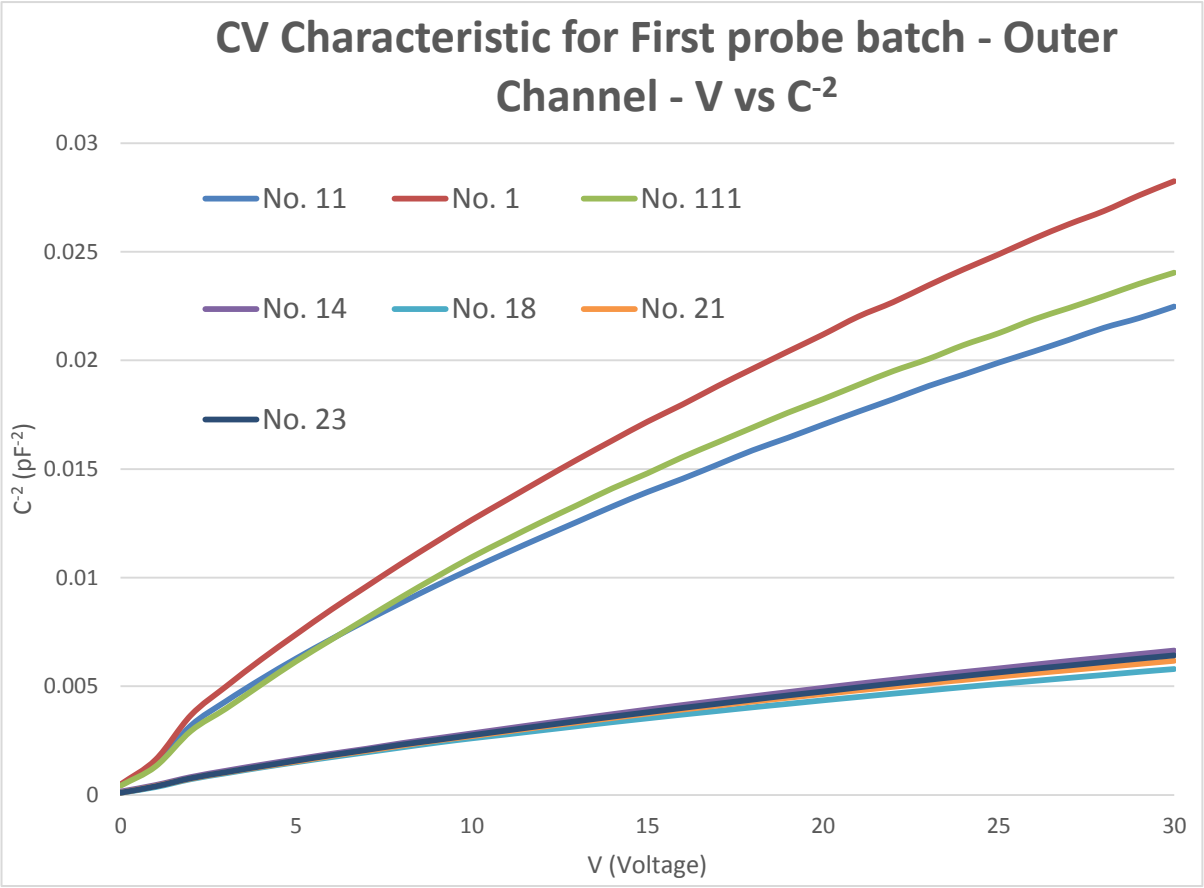


**FIG. 29:- THE RESULT DICHOTOMY IS MORE DISTINCT USING THE $C^{-2}$ EXPRESSION FOR THE CAPACITANCE.**

## *DISCUSSION OF IV AND CV CHARACTERISTICS*

The IV and CV Characteristics obtained by Franks and this study demonstrate a high level of consistency. This implies minimal change to the scintillator integrity during the time frame between the two studies.

The CV Characteristic had the highest similarity between the two studies. The result implied that neither the surface area nor doping density of the probes changed during the time frame between the two studies. A difference is present in the IV calculations. Repeating the IV Characteristic showed that if the container was not completely light sealed, the current to voltage gradient could increase. This is one factor that may explain why the IV Characteristics in Franks study have slightly greater IV gradients than the one recorded during this project.

A pursued factor in photodiode production is reduced leakage current. A reduced leakage current (low IV gradient) implies minimal noise impact from dark current. It also provides a stable voltage operating region for result acquisition prior to signal processing by the electronics.

| *INNER CHANNEL IV CHARACTERISTICS COMPARISON* | | |
|---|---|---|
| Batch No. | Current at 15V (nA) | Gradient (nA/V) |
| First probe batch | 0.25 | 0.016 |
| Franks First probe batch | 1 | 0.081 |

**TABLE II: - RESULTS ARE THE AVERAGE OF EACH SET TO ALLOW FOR BETTER COMPARISON. UNCERTAINTIES ARE OMITTED FROM THIS TABLE.**

| *OUTER CHANNEL IV CHARACTERISTICS COMPARISON* | | |
|---|---|---|
| Batch No. | Current at 15V (nA) | Gradient (nA/V) |
| First probe batch | 0.7 | 0.105 |
| Franks First probe batch | 0.6 | 0.056 |

**TABLE III: - GRADIENT AND CURRENT AT 15V ALIGN MORE CLOSELY ON AVERAGE. UNCERTAINTIES ARE OMITTED.**

Franks study hypothesised that the Liana photodiodes decay with time, the results of this study may contradict this hypothesis. The reduced leakage current result is positive regardless, but it must be further explored.

The recorded IV characteristic for the OC was larger than the IC. This result was anticipated because both channels were made from the same semiconductor. This would mean they have the same impedance index per unit distance. The longer path would have a higher resistance than the shorter path of the same material due to the amount of impedance experienced on the currents traverse. This is why the OC was expected to have a smaller IV gradient in comparison to the IC.

After discussion with supervisors it was explained that some physical phenomena may be in effect, it is possible for the photodiodes conductivity properties to either improve or degrade with time. The conditions for this are dependent on the photodiodes immediate environment and include temperature effects. Special studies are dedicated to exploring the unusual effects of surface physics on silicon photodiodes. In summary, these surface based physical effects can change the conductivity properties of the photodiodes with respect to time. It is therefore possible that these surface effects have affected the IC and OC. It is also possible that each channel has been affected by these changes differently. It is more likely

however that the factor responsible is differences in the acquisition apparatus and temperature.

The impedance concept also applies for the capacitance. In the study performed by Franks, an approximation was made using the parallel plate capacitance formula. Given earlier by,

$$C = \frac{\varepsilon_0 \varepsilon_r A}{d}$$

Where d was the separation between the two plates, A was the overlapping area of the two plates, $\varepsilon_0$ was the *electric constant* and $\varepsilon_r$ was the relative static permittivity. A direct relationship between the areas of the diodes showed that a larger area diode would experience a higher capacitance than a smaller area diode.

The results of the CV characteristic from both studies does correlate with what is explained by the capacitance formula. The capacitance per unit voltage when comparing the OC to the IC is double. This result for the capacitance implies that the Surface Area of the OC with respect to the IC is double. A measurement of the IC area with respect to the OC can approximate to a factor of two but is closer to a factor of three ($R_I$ = 1.5mm with $A_I = 2.25\pi$ mm$^2$ and $R_O$ = 3mm with $A_O = (9 - 2.25)\pi$ mm$^2$ = $6.75\pi$ mm$^2$).

As the CV never plateaued and it cannot be reliably extrapolated it is impossible to calculate the full depletion voltage of the photodiode. This problem was encountered and explained in Franks study as due to the photodiode physical setup being far more complicated than the simple parallel plate capacitance.

There are in reality three sources of capacitance within the dual photodiode configuration itself.

1. The capacitance between the outer P+ layer and the N+ type of the backing. ($C_{OB}$)
2. The capacitance between the inner P+ layer and the N+ type of the backing. ($C_{IB}$)
3. The capacitance of the inner P+ layer and the outer P+ layer. ($C_{IO}$)

All these sources combine to create the following formula as acquired by Franks from mutual supervisor Dr. Marco Petasecca and Professor Anatoly Rosenfeld.

$$C_{total} = \frac{C_{IO} \cdot C_{OB}}{C_{IO} + C_{OB}} + C_{IB}$$

It is simply not possible to determine all of these capacitances using the equipment available to this study. It was recommended by Franks that the manufacturer perform this process. This is because the manufacturer has the capacity to determine each of these capacitances individually during the photodiode production process.

As the data was only required for diagnosing the probes in the event of physical damage, and to ensure the photodiodes functioned correctly within the supplied voltage domain. The depletion voltage was not pursued and the impurity concentration was not calculated. This was also the case for the Second probe batch.

## *SCINTILLATE CHARACTERISATION – SPECTRA ACQUISITION*

A means to assess both the scintillators and boards' functionality was now established. The Scintillators could now be attached to a board and have their spectra's compared. Board 3 was used during these tests as it was still the highest functioning board and had not yet undergone performance decay. The data provided by cross comparison would identify which Scintillator best operated with the electronics on a Board.

The spectra was acquired with four emitters, Am-241, Cs-137, Na-22 and Co-57. The radioisotope selection was based on identifying the probes response to the differing energy types of gamma and beta emitters used in surgery. Once the spectra had been acquired, the resolutions would be compared to the results acquired from the previous studies conducted by Franks and Ulbngali.

The testing chamber used by Ulbngali was reused after considerable repair was performed, a basic diagram of the experimental setup is provided below.

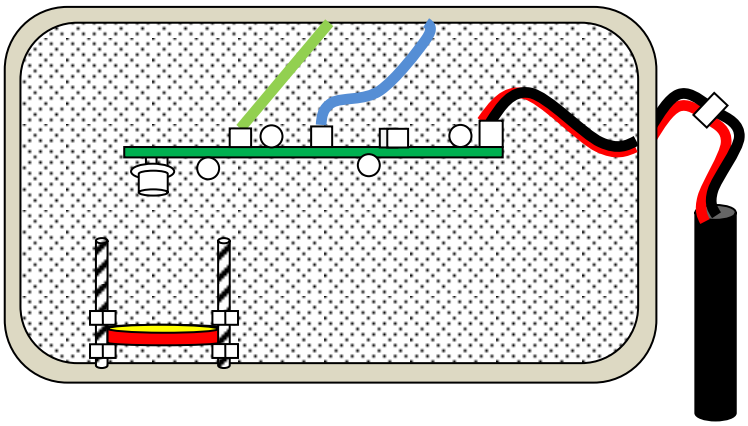

**FIG. 30:- THE BLACK CYLINDER REPRESENTS THE BATTERY. THE BLUE WIRE REPRESENTS THE CHANNEL FEED TO THE MCA. THE GREEN WIRE REPRESENTS THE BOARD GROUNDING. THE RED AND YELLOW DISC REPRESENT THE EMISSION SOURCE.**

The electronics is completely isolated from the conductive chamber by plastic screws and an insulating sheet. This sheet covers the entire containers base and is designated by the haze in Fig. 30.

The probe creates a signal to

be processed by the board after receiving an emission from the source. This signal is monitored by an oscilloscope after leaving the board.

The signal amplitude is too small to be interpreted by the Multi-Channel Analyser (MCA) and requires ten times amplification by a non-inverting amplifier. The signal is again assessed through the oscilloscope to ensure that the amplifier is operating correctly before it is allowed to pass through into the MCA.

In Fig. 30, screws are used to adjust emission sources position with respect to the scintillator. A 4.21 V battery is used to power the Liana circuit board electronics. The battery was placed outside to the container to improve control of the board and negate operational risks to the apparatus.

Only the low energy peaks for the substances were of interest to this study, thus the signal gain did not require adjusting to observe the higher energy peaks for figures 33 to 38.

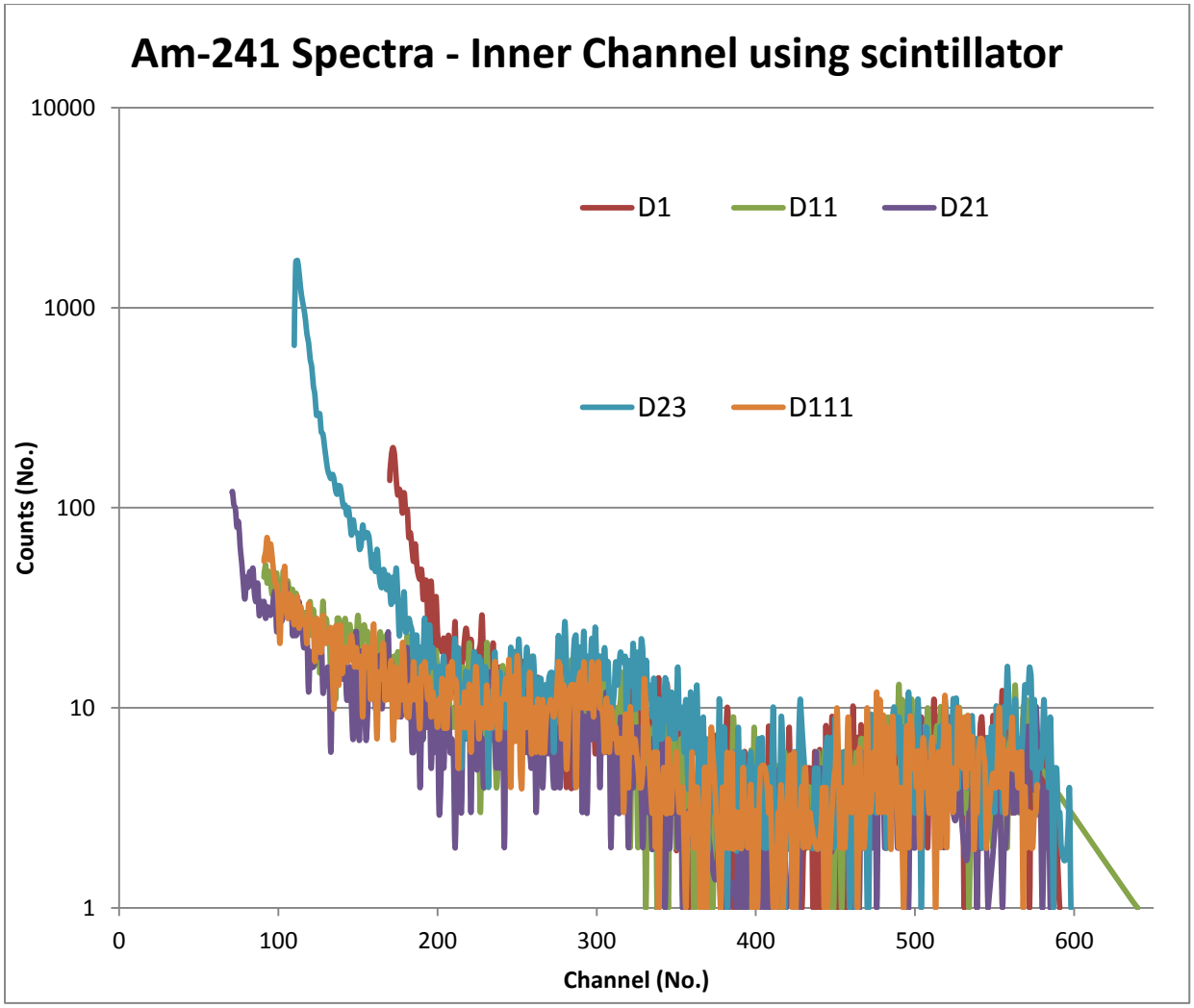


**FIG. 31:- THE SOURCE USED FOR THIS TEST WAS AM-241. AM-241'S COLLECTION IS BLURRED IN COMPARISON TO THE BARE DIODE TEST RESULTS.**

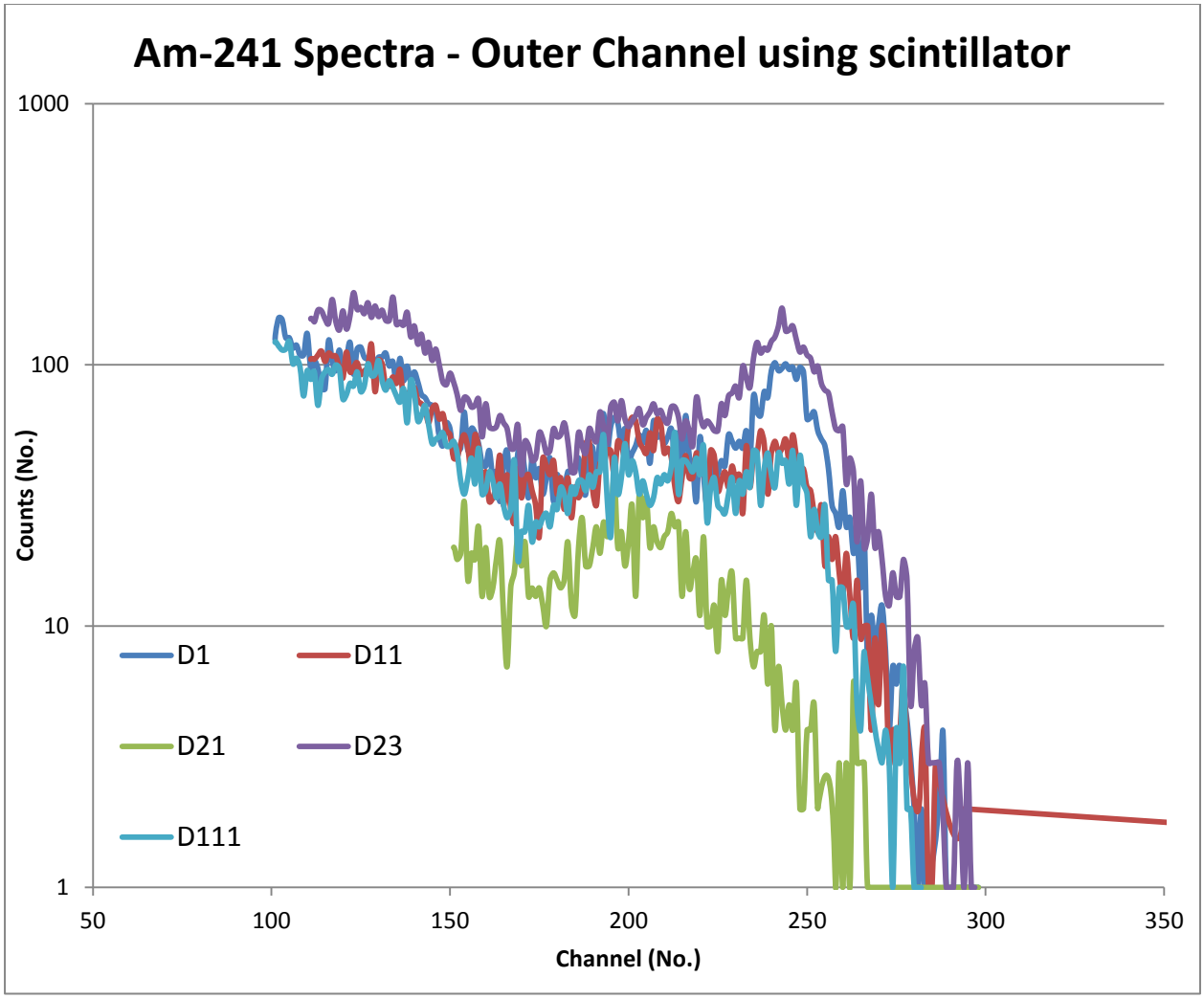


**FIG. 32:- THE SOUCE USED FOR THIS TEST WAS AM-241. THE OC'S RESPONSE IS MUCH SHARPER IN COMPARISON TO THE IC FOR RESOLVING THE AM-241 PEAKS. THE OC DATA IS ALSO A CLOSER MATCH TO THE RESULTS OBTAINED BY THE BARE DIODES FOR THE SAME EMISSION SOURCE.**

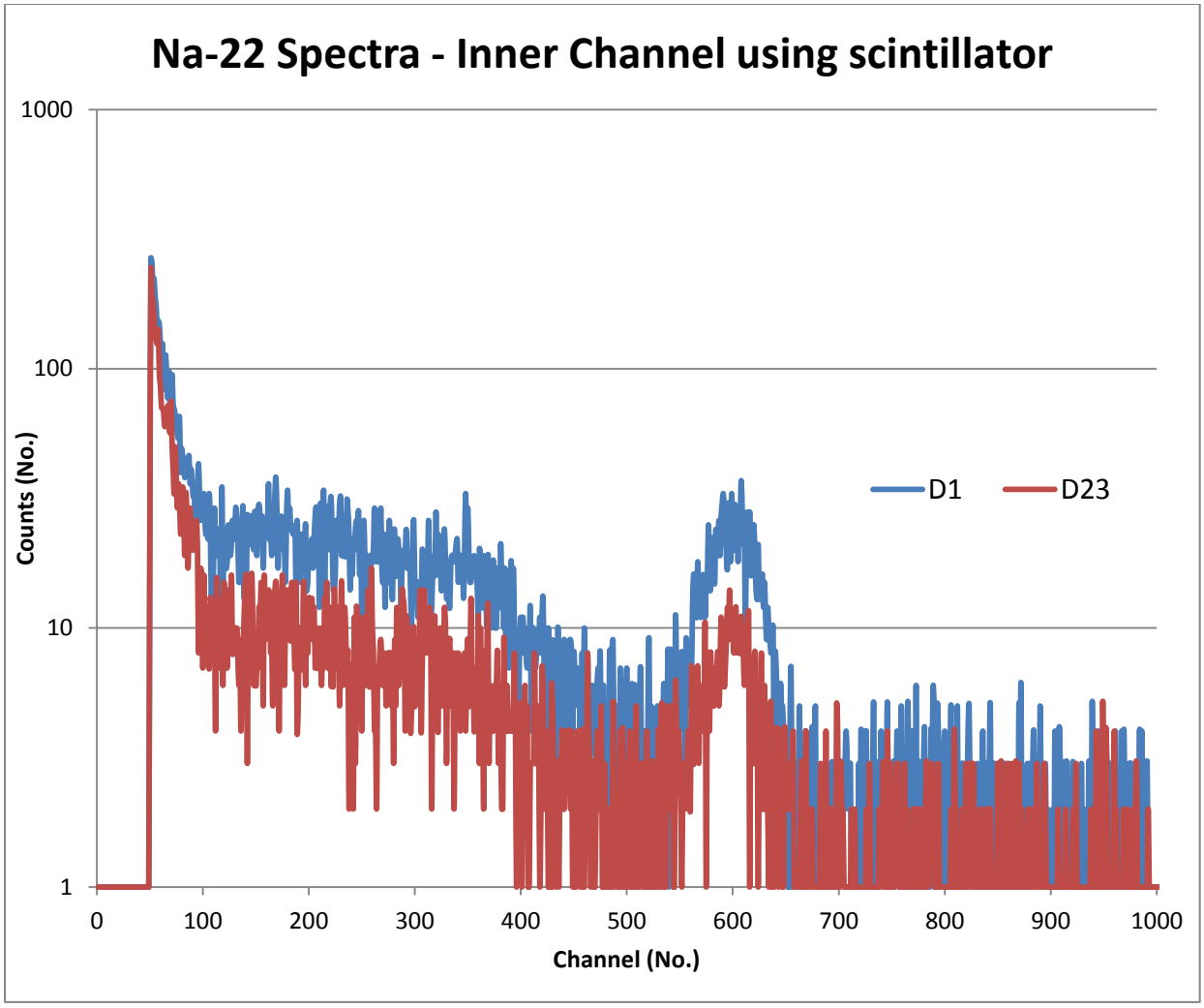


**FIG. 33:- THE SOURCE USED FOR THIS TEST WAS NA-22. ONLY TWO PROBES IC'S WERE INVESTIGATED AS ONLY TWO WERE FOUND TO BE RELIABLE FROM THE STUDY BY ULBNGALI. NOTE: - ONLY THE LOW ENERGY PEAKS ARE OF INTEREST TO THESE TESTS.**

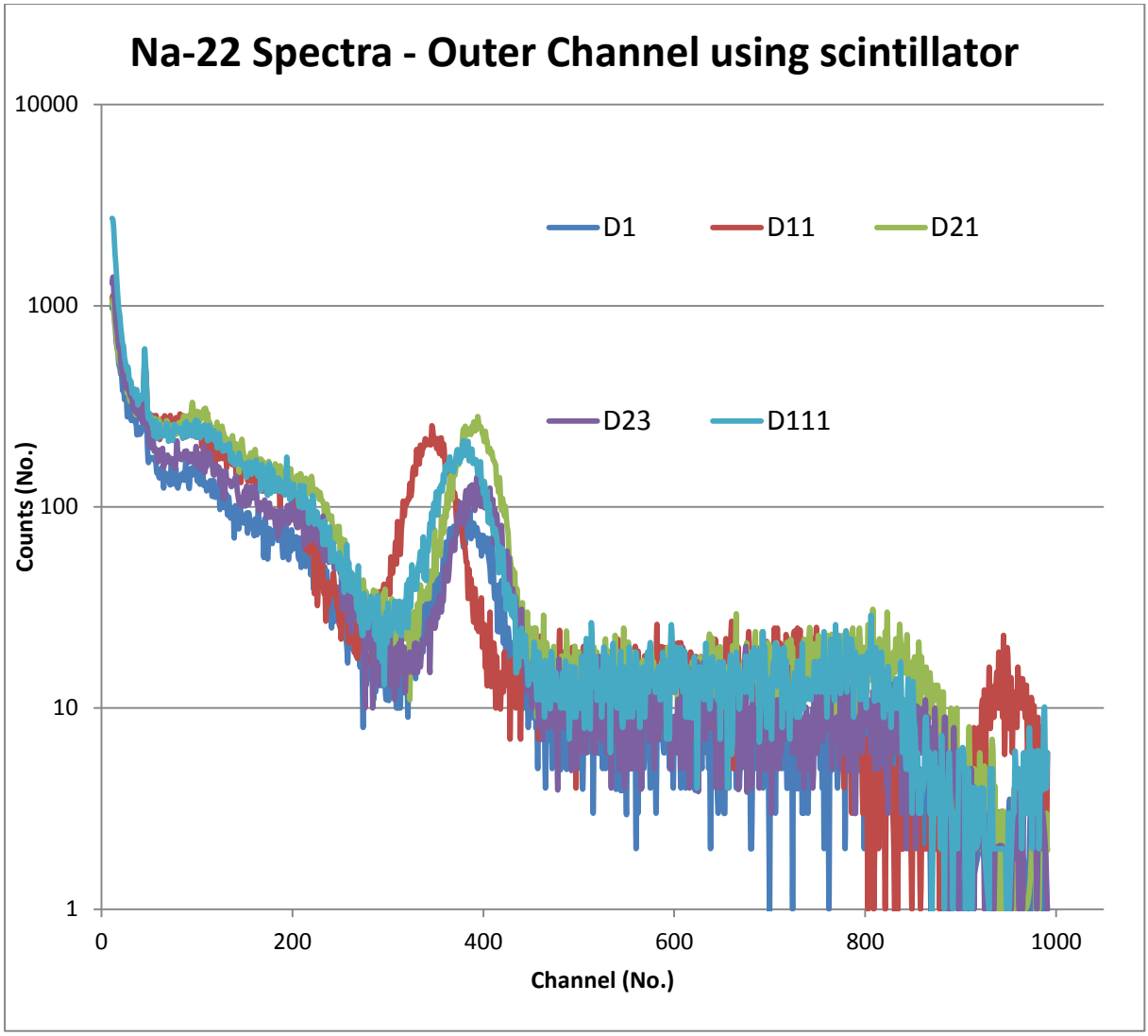


**FIG. 34:- NA-22 WAS THE EMISSION SOURCE USED FOR THIS TEST. THE OC'S FOR ALL THE PROBES WERE CONFIRMED TO BE FUNCTIONAL AS STATED BY ULBNGALI.**

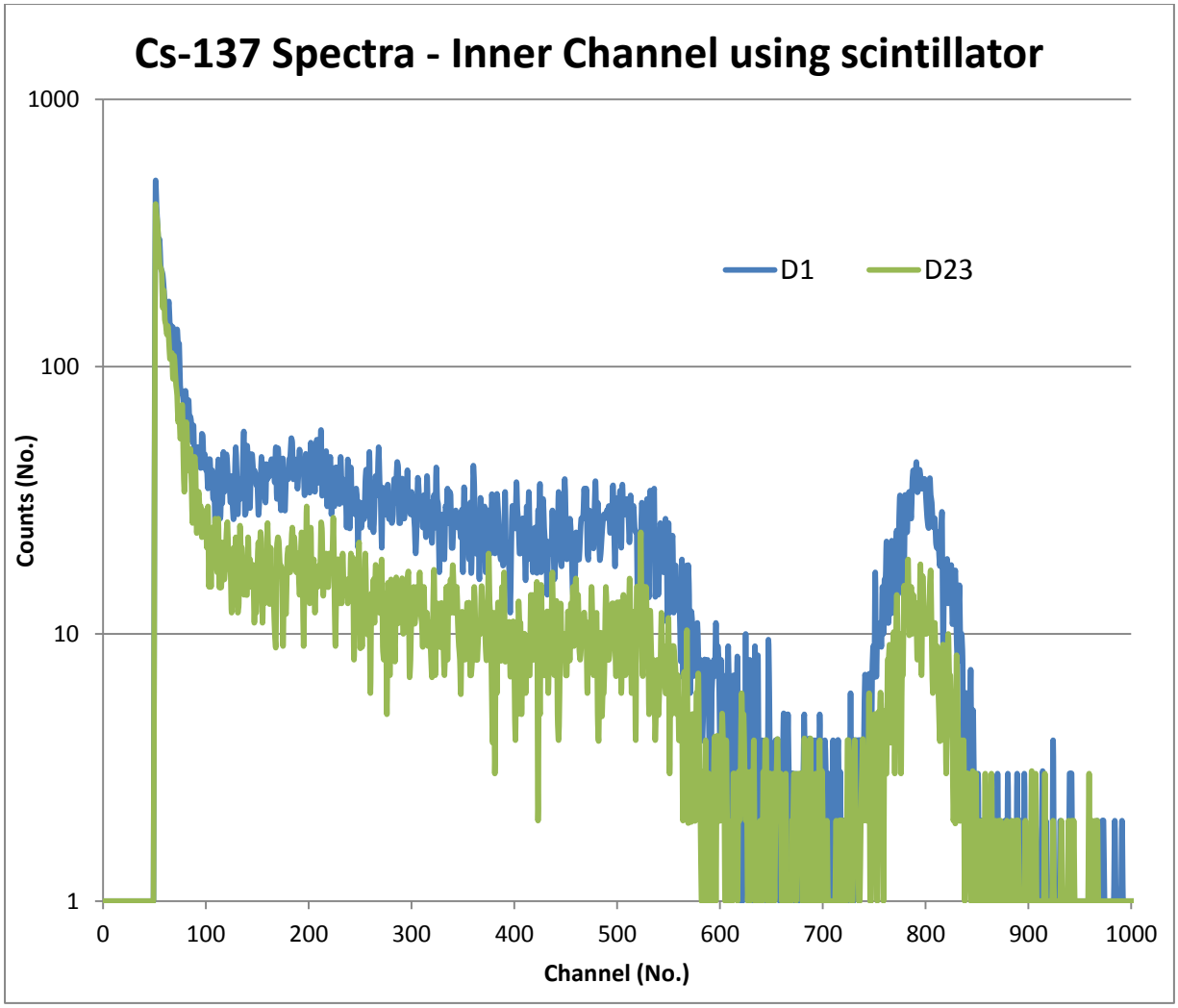


**FIG. 35:- THIS TEST USED CAESIUM-137 TO OBTAIN THE RESULTS SEEN ABOVE. ADDITIONAL SPECTRA DATA FOR THE IC WAS OF LOW RESOLUTION AND DOES NOT HAVE THE SHARPNESS OF THE BARE DIODES SPECTRA RESULTS.**

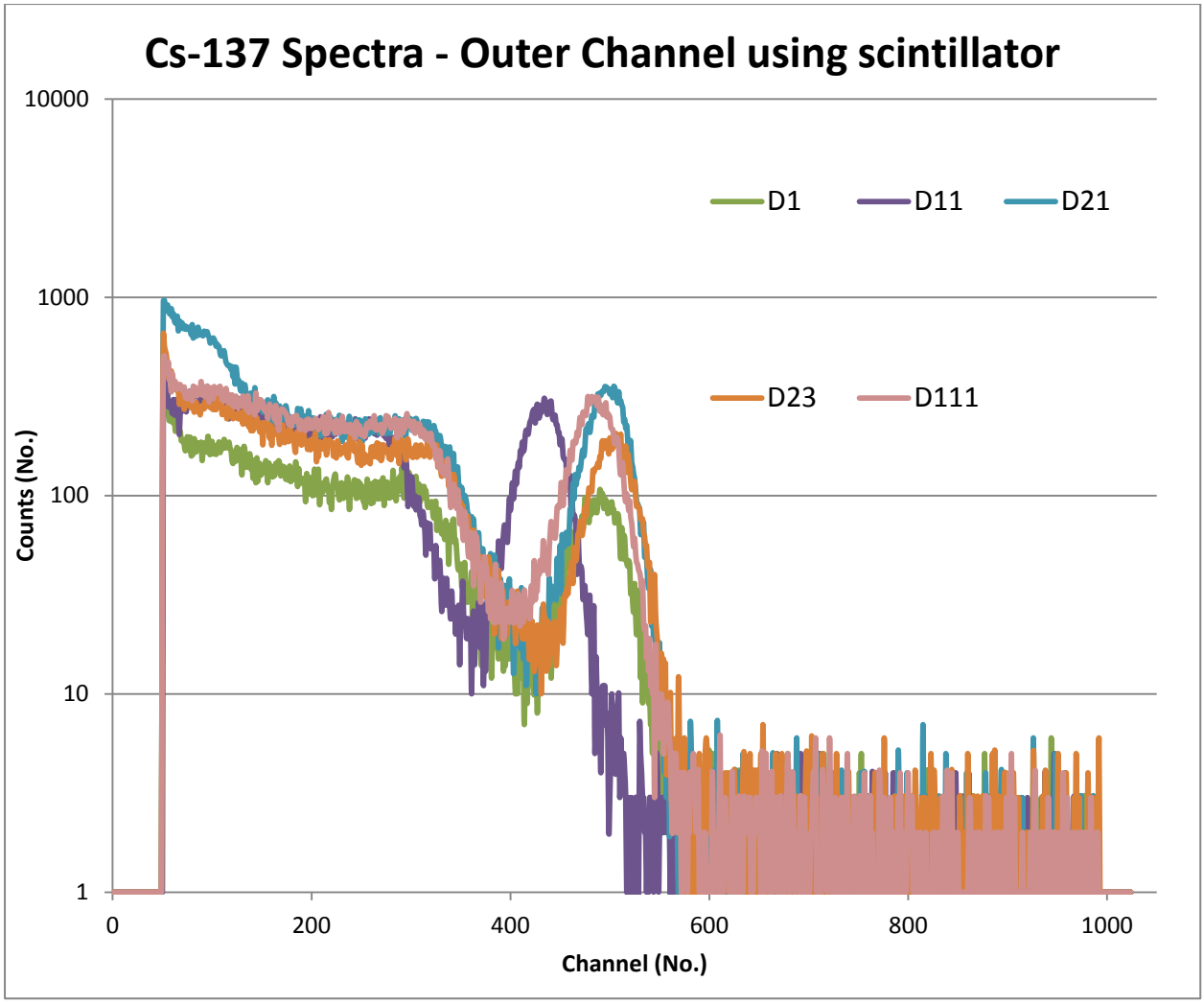


**FIG. 36:- THIS TEST USED CS-137 TO OBTAIN THE RESULTS SEEN IN THE FIGURE ABOVE. THESE RESULTS ARE CONSISTENT WITH THE RESULTS OBSERVED FOR THE NA-22 OC'S.**

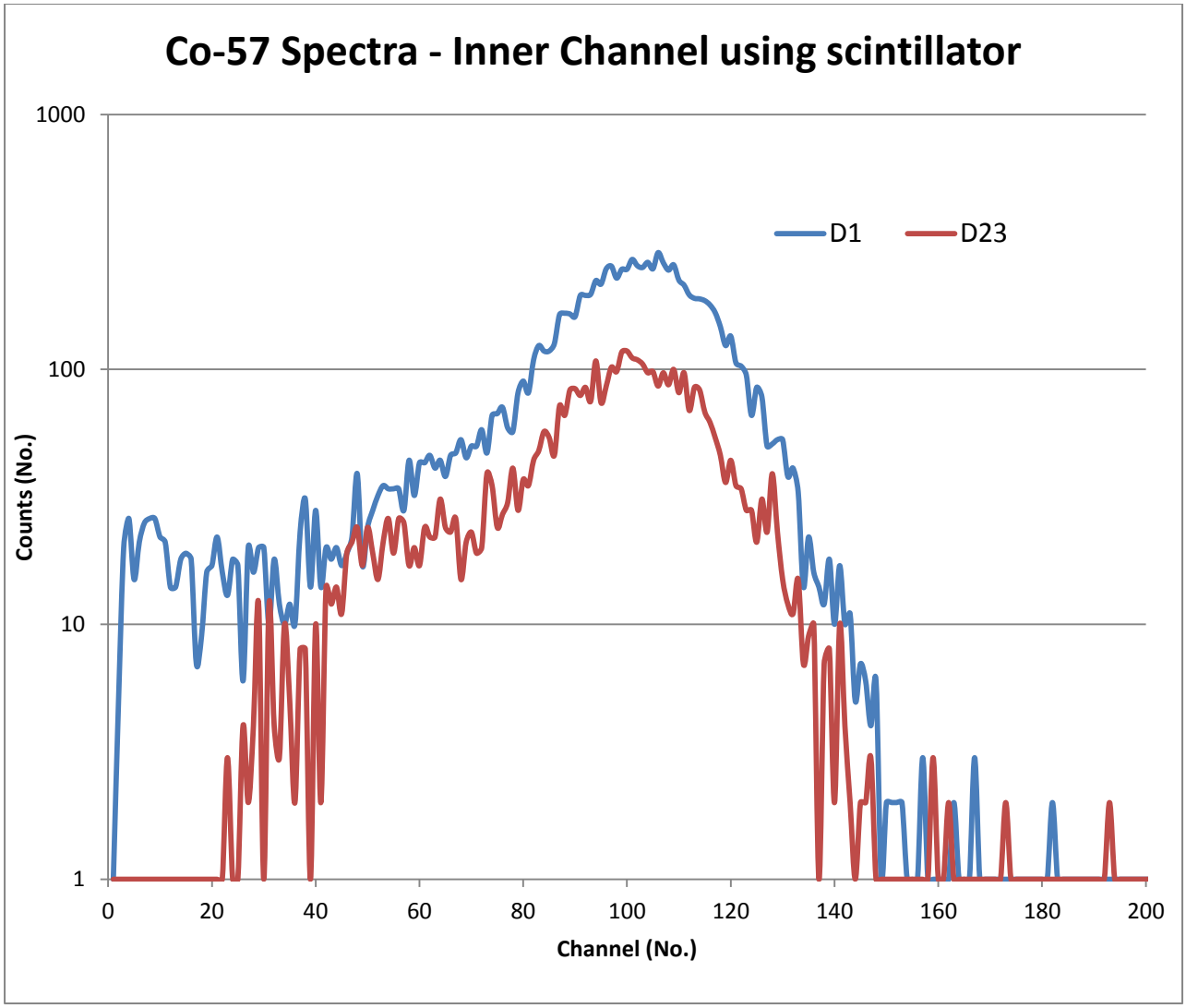


**FIG. 37:- THIS TEST USED COBALT-57 AS THE EMISSION SOURCE. THE POSITION OF THE PEAK IS LOCATED AT APPROXIMATELY CHANNEL 100.**

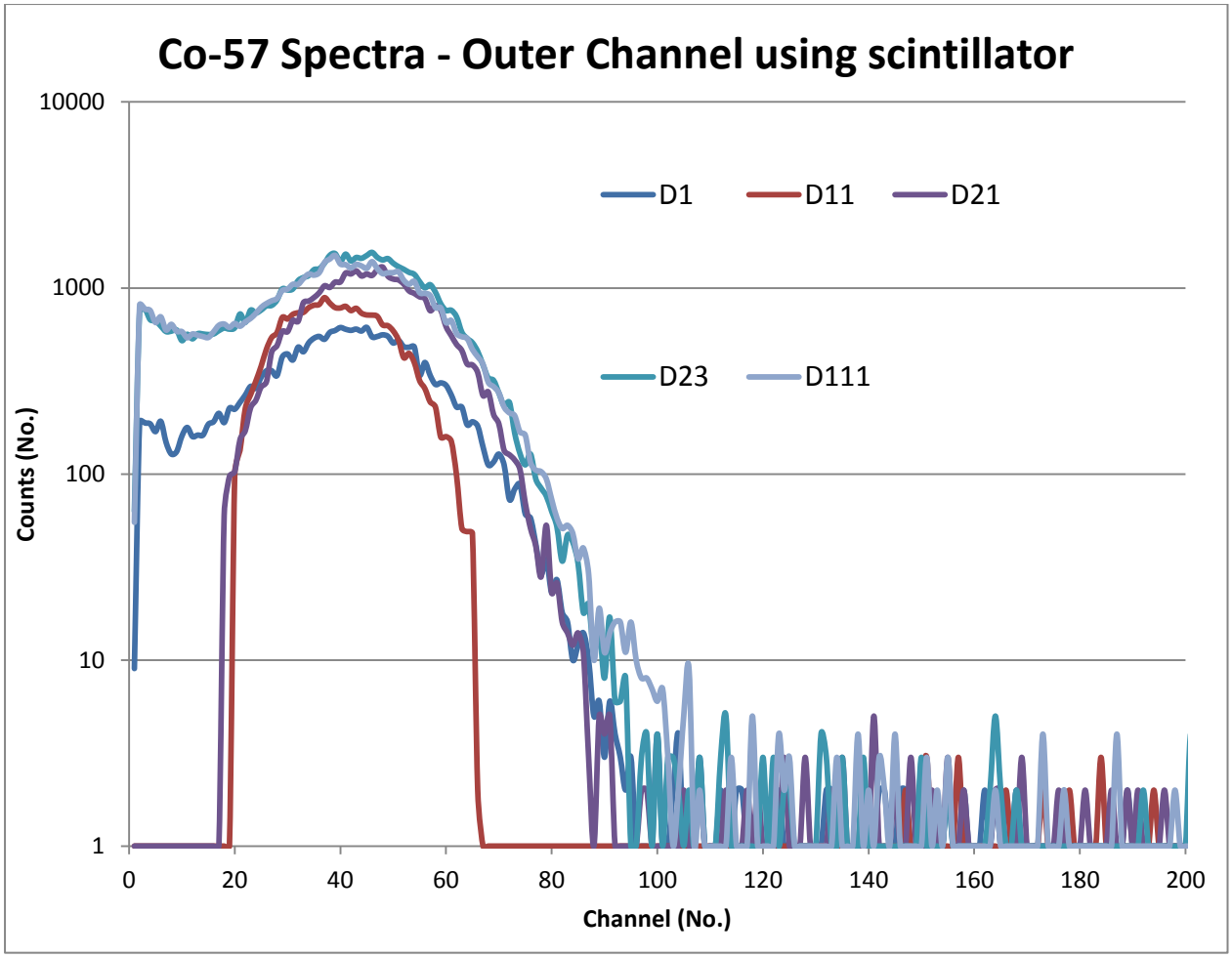


**FIG. 38:- THIS TEST USED CO-57 AS THE EMISSION SOURCE. THE GAIN OF THE IC IS GREATER THAN THAT OF THE OUTER CHANNEL. AS B3 WAS USED IT WAS EXPECTED THAT THE POSITION OF THE PEAK FOR THE IC WOULD BE FURTHER ALONG THE X-AXIS IN COMPARISON TO THE OC. IN THIS CASE THE RATIO OF THE IC TO OC GAIN IS MEASURED AS APPROXIMATELY DOUBLE.**

*SCINTILLATE SPECTRA DISCUSSION*

These tests were conducted several times as the performance of the board, scintillator and chamber was optimised to attain the highest quality spectra. The chamber required modification to ensure the correct operating environment for the probe, a dark Faraday caged chamber.

The Am-241 data was collected from ANSTO, the remaining data was acquired from the University of Wollongong. The spectra in Fig. 31 is blurred in comparison to the results observed for the bare diodes. Am-241 is a high energy alpha emitter with some low energy gamma emissions. In the presence of inorganic scintillators the conversion efficiency of alpha particles is lower than for beta and gamma emissions. Comparing the peaks obtained from the board in Fig. 31 with the characterisation in Fig. 18 suggests that more gamma peaks are observable with the scintillator attached. This is implied from the close correlation of the primary gamma peaks for ≈ 59 KeV between the IC figures for Am-241.

The primary gamma peak is not as pronounced as previously because Am-241's beta events have become more prevalent with the higher conversion efficiency provided by the scintillator. The lower energy beta and gamma events are poorly resolved with the scintillator attached as their emission energies are relatively infrequent. The energy deposition rate for these events into the detector is therefore low and resolving them requires the probe to accumulate events over a longer time period. It is noted however that the gamma peaks from Fig. 31 to Fig. 38 are blurred together despite the extended duration of the acquisition performed (15 minutes to 1 hour depending on emission source). No Passive Collimation was used in these tests. As the probe is designed for locating and resolving low energy peaks, only

these were pursued for these tests. As such the high energy peaks, although

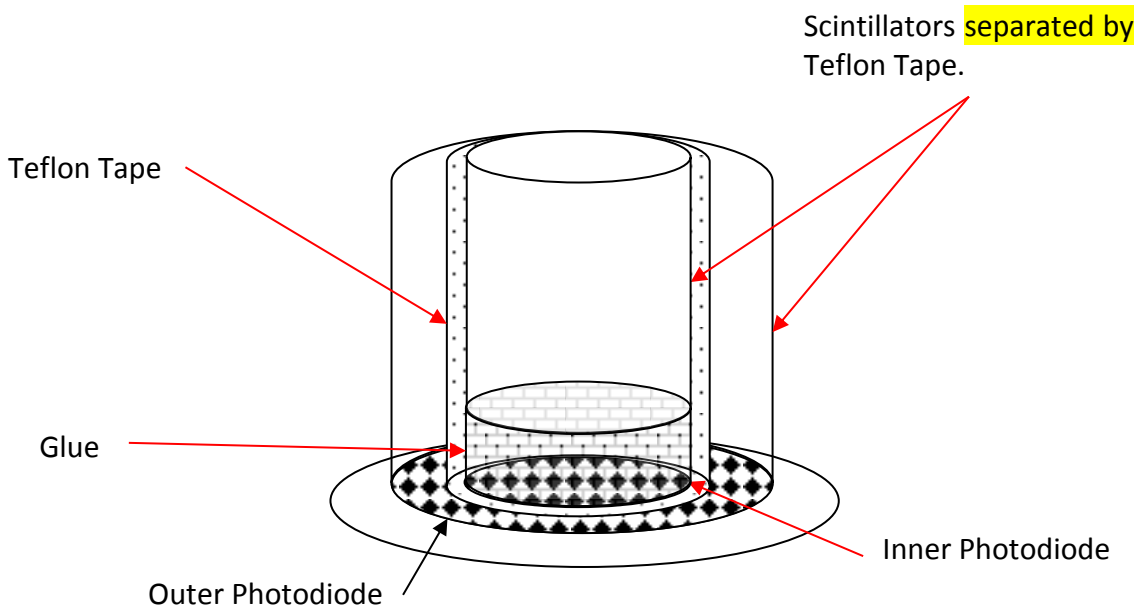


**FIG. 39:- THE SCINTILLATE SHOULD BE FLUSH WITH THE BASE OF THE PHOTODIODE. THE PRESENCE OF GLUE AND/OR THE PROTECTIVE SILICATE HINDERS LIGHT TRANSMISSION BY FRESNEL'S LAW.**

resolvable by adjusting the gain, were ignored.

Another possible contributing factor is that of the scintillate construction, a diagram is presented below.

Energy is deposited inside the scintillate material which converts to light and is collected by the photodiode. A problem is that this light may have to travel through multiple refractive media to reach the photodiode. Excluding the passivation over the photodiode, another factor is the glue used to bond the scintillator to the detector.

By Fresnel's law of refraction, the refractive index of the passivation and glue must be similar to the scintillating material the light is generated in, otherwise reflection will result. There is already a loss of signal amplitude because not all the photons emitted inside the scintillator will be collected by the photodiode.

An additional factor is the presence of air pockets or “bubbles” present inside the glue due to the bonding process. The presence of “bubbles” effectively creates an additional refractive medium. A detrimental impact on the probe energy collection efficiency is expected because of a significant difference between the refractive index of the scintillator in comparison to the air. Lastly, the scintillators bottom surface may not be parallel with the photodiode beneath it. Aside from misalignment errors, this could also mean the gap width between the scintillator and photodiode isn’t consistent.

The scintillator should ideally be coupled directly to the photodiode, but the scintillator cannot be directly fused to the photodiode without the aid of an adhesive. An additional problem is encountered if the protective film is removed as the photodiode would decay as hypothesised in the study by Franks.

The adhesive and protective film are necessary additions. Identifying a refractive index for the adhesive and protective film that is similar or equal to that of the scintillator is recommended for best performance. Equal refractive indices between layers would effectively eliminate reflection, especially if air pockets could be sufficiently removed from the adhesive process. Removing the air pockets should be possible since if the IC is adhered first the “bubbles” should displace out of the layer by compressing the scintillator to the protective films surface. Once successfully bonded and cleaned, the OC could be bonded the same way ensuring no air pockets remained between the scintillator and photodiode.

An additional problem is that the protective film is an overall passivation layer covering the entire photodiodes surface. This layer should be separated into two parts with one to cover the inner photodiode and the other to cover the outer

photodiode. The purpose of the separation is to prevent the passage of light formed in one scintillator passing through the bottom of one scintillate and reflecting into the other photodiode. A process that could cause this problem is total internal reflection. If the protective film could be internally dyed along the radius connecting the two channels but remain transparent across the area of their respective diodes. Cross talk could be prevented altogether from occurring within the probe as both channels would now be both optically and electronically isolated from each other.

The probes energy resolution could be affected by the IC composition. The IC consists of the minimum absorption volume as a trade-off between acceptable sensitivity for high energy particles and acceptable spatial resolution of the probe. The implication was that many events scatter out of this volume because of insufficient size (or depth) for complete deposition. These emitters have higher energy ranges than was intended for the Liana Probes Inner Channel.

False peaks and wide FWHM resolutions may be present because background like high energy events are passing through the secondary channel before entering the primary channel. This would result in lower energy depositions being produced and creating poorer resolution peaks. In the case of higher emissions this is more prevalent as lower energy depositions are created per the scintillators conversion factor. This results with false depositions in the low energy range and leads to increased difficulty with resolving lower energy emitters.

The Outer Channel for events would be expected to have a sharper peak since the absorption depth correlates more closely for the energies entering it. Furthermore as per the apparatus configuration the OC had a larger exposed collection volume compared to the IC's top surface being the only exposed point. This did not mean

the IC was inaccurate. This only meant that the IC would be expected to become accurate once the Passive and Active Collimation provided by the dual function was in effect.

The higher gain from B3 may have been responsible for the peak blurring since the channel binning was uneven. This would explain the rough “trace” in the spectra production.

Signal noise on the circuit board was another problem identified in spectra acquisition. Increasing the board grounding resulted in an improved spectra acquisition. The signal noise was unlikely to have impacted the higher energy spectra peaks during these tests. This was because later diagnosis showed that only the lower energy domain was affected.

Fig. 31 through to Fig. 38 demonstrated the Liana’s capacity to resolve beta and gamma emission types. This is because the primary Na-22 beta peak (511 KeV) along with the Primary Cs-137 (661 KeV) and Co-57 (122 KeV) gamma peaks were identified. The scintillate material was therefore sensitive to the medically significant emission types of beta and gamma emitters. This hypothesis is supported by the results of Ulbngali’s study.

The relevant spectra’s peak resolutions are presented below in table format. The Am-241 spectra was insufficient to produce a meaningful peak resolution in either channels case, and so was excluded from the following tables. The spectra was included only to provide a more thorough insight into the probe operation with respect to the conversion efficiency of CsI(Tl) with beta and gamma emissions.

*FIRST PROBE BATCH RESOLUTION PERCENTAGE VS EMISSION SOURCE*

| IC Resolutions (%) | | | |
|---|---|---|---|
| Detector | Na-22 | Cs-137 | Co-57 |
| 1 | 5.98 | 5.72 | 30.05 |
| 23 | 6.24 | 5.79 | 27.65 |

**TABLE IV: - DETECTOR 23 REQUIRED 2-4 TIMES THE COLLECTION TIME TO ACQUIRE A RELIABLE PEAK COMPARED TO DETECTOR 1. CO-57'S RESOLUTION IS POOR BECAUSE ITS PEAK IS CLOSE TO THE THRESHOLD RANGE, THIS WAS AMENDED IN THE NEW SCINTILLATOR TESTS DISCUSSED LATER.**

| OC Resolutions (%) | | | |
|---|---|---|---|
| Detector | Na-22 | Cs-137 | Co-57 |
| 1 | 9.89 | 9.03 | 62.29 |
| 11 | 12.09 | 9.97 | 80.47 |
| 21 | 10.47 | 8.60 | 63.35 |
| 23 | 9.88 | 8.49 | 63.28 |
| 111 | 11.86 | 9.67 | 65.20 |

**TABLE V: - A COMPARISON WITH FRANKS AND ULBNGALI'S DATA FOLLOWS.**

The resolutions presented were the result of averaging across 20+ tests, the average also accounted for differing acquisition times. The results presented should depict the resolution capacity of the detector across any acquisition duration from 5 minutes to 3 hours. The statistical uncertainty was calculated to be 2.63% for the OC, this was based on the average peak deviation between tests when conditions such as the displacement and emission source were unchanged. This means the results were consistent with a 97.4% accuracy across the relevant time durations.

The IC results could vary by 12% however, this means the resolution of higher energies was only 88% accurate under the same conditions as the OC. In terms of medical application this is not severe and is resolved in the 2$^{nd}$ probe batch where it was found not to be a prevalent issue. Excluding the resolution obtained from Co-57,

each probes results for Na-22 and Cs-137 were placed in a table for comparison with those obtained by Franks study.

This data was significant because the results obtained from the project used the Scintillators from Franks study. The only difference in the experimental setup between these two studies was the electronics used for processing the signal. An assessment regarding the impact of a different signal processing unit was made with respect to the overall detector performance and functionality.

## *RESOLUTION TABLES*

| Na-22 IC Resolutions | | |
|---|---|---|
| Detector | Res (%) –This Study | Res (%) - Franks |
| 1 | 5.98 | 6.9 |
| 23 | 6.24 | 9.5 |

**TABLE VI: - IC RESOLUTION RESULT COMPARISON FOR NA-22.**

| Cs-137 IC Resolutions | | |
|---|---|---|
| Detector | Res (%) –This Study | Res (%) - Franks |
| 1 | 5.72 | 6.8 |
| 23 | 5.79 | 7.3 |

**TABLE VII: - IC RESOLUTION RESULT COMPARISON FOR CS-137.**

| Na-22 OC Resolutions | | |
|---|---|---|
| Detector | Res (%) –This Study | Res (%) - Franks |
| 1 | 9.9 | 13.9 |
| 11 | 12.1 | 15.7 |
| 21 | 10.5 | 14.1 |
| 23 | 9.9 | 15.1 |
| 111 | 11.9 | 16.7 |

**TABLE VIII: - ULBNGALI'S STUDY DID NOT INCLUDE A RESOLUTION FOR NA-22.**

| Cs-137 OC Resolutions | | | |
|---|---|---|---|
| Detector | Res (%) –This Study | Res(%) - Ulbngali | Res (%) - Franks |
| 1 | 9.03 | 9 | 13.9 |
| 11 | 9.97 | 7.8 | 15.7 |
| 21 | 8.60 | 5.4 | 14.1 |
| 23 | 8.49 | 9.6 | 15.1 |
| 111 | 9.67 | 7.3 | 16.7 |

**TABLE IX: - THIS IS THE ONLY RESOLUTION DONE BY ULBNGALI'S STUDY.**

| Average IC Resolutions Comparison | | |
|---|---|---|
| Detector | Res (%) –This Study | Res (%) - Franks |
| 1 | 5.85 | 6.85 |
| 23 | 6.01 | 8.4 |

**TABLE X: - COMPARISON OF THE AVERAGE SPECTRA RESOLUTION ACROSS EMISSION TYPES.**

| Average OC Comparison | | |
|---|---|---|
| Detector | Res (%) –This Study | Res (%) - Franks |
| 1 | 9.46 | 13.25 |
| 11 | 11.03 | 14.7 |
| 21 | 9.54 | 13.25 |
| 23 | 9.19 | 13.8 |
| 111 | 10.76 | 14.6 |

**TABLE XI: - COMPARISON OF THE AVERAGE SPECTRA RESOLUTION ACROSS EMISSION TYPES.**

## *RESOLUTION TABLE DISCUSSION*

Comparison of TABLE VI to TABLE XI presents the scintillator converting certain emission types more favourably as demonstrated by the averages differing resolutions across emission sources. The difference was minor but with respect to the conversion efficiency expected from CsI(Tl) the results correlated with the known physics.

Comparing the results across the 3 studies for the same set of probes indicated a deviation. Though the Scintillators were the same ones used by Franks, the boards used to process signal from the Scintillators were different. The electronics discussed in Franks study produced statistically significant amounts of noise impeding precise signal processing for event binning. This factor was identified as the cause of the poorer quality resolution in Franks study, and was amended prior to this investigation. The probes total resolution was found to have improved by ≈ 15-

25%. The result was significant but electronic noise was still noticeable in the circuit, removal of the noise would be expected to improve the resolution further and is suggested for later studies.

## *Conclusion of Data from first probe set characterisation*

Across the 3 studies it was observed that the overall performance of the probes did not change significantly. Data was acquired allowing for diagnosing the changes in both the probe and the boards responses should an event occur that may impact their function. This was achieved while exploring the various physical fundamentals of these probes, simultaneously explaining the advantages of the probe design.

The most significant information acquired from these tests was the 15-25% improvement in the energy resolution obtained for each probe using the new board electronics.

# 2ND SCINTILLATOR BATCH CHARACTERISTICS

As experiments were conducted on the 1st probe batch the two remaining dual functioning diodes eventually deteriorated to the point of non-operation. The first failed due to mishandling and was not attributed to any factor of the probe design. The second detector (D1) never indicated performance decline and ceased producing spectra during testing. No observable transition period from functional to inactive was found in any of the recorded results from earlier testing. It was conjectured that a connection within the photodiode itself was severed.

A new batch of probes was acquired. The CV and IV Characteristics including the Spectra for the substances of Co-57, Na-22 and Cs-137 for energy characterisation was produced and presented below. Board 3 after experiencing numerous failures was replaced as the primary testing circuit with Board 6. This was because of its impact on the time period for the research cycle. Board 3's results during the 1st scintillate batch characterisation are considered reliable as the results were only recorded if Board 3 passed the diagnostics provided by earlier testing. This ensured that Board 3 was consistent across the numerous tests it underwent and that the results are reproducible under the same operating conditions.

Board 3's factor for increasing the signal gain was still an unknown factor, it was not reproducible by any of the Liana boards after numerous modifications.

Assessment of the probes dual function operating modes was easier if the gain from each channel was identical. The processed data would more accurately align with its counterpart channel and allow for direct comparison of the IC and OC spectra's. The A+B and A-B modalities would then be directly assessable.

Comparing the results of these scintillate trials with those by Franks implies that the gain of the IC may not directly attribute to improving the energy resolution of the spectra. The OC results in TABLE VI to TABLE XI showed that the resolution was improved by superior design in the circuit electronics between the two studies. The same factor was attributed to the IC as a 15-25% improvement in resolution was also observed for the IC across the two studies.

In summary, the gain produced by B3's IC was only useful if it was reproducible across all Liana boards and channels. Due to the above factors Board 6 was selected as the results would be more realistic and the circuit less failure prone when it was operating.

Board 6 (B6) lacked the gain of B3 but never experienced technical difficulty during the course of the project. This was attributed to B6 experiencing fewer manufacturing errors. For the purpose of batch comparison, the gain difference of the IC from B3 to B6 could be factored. This allowed for the differences in probe structure to be assessed across the batches and provide greater insight into the detector fundamentals should it be necessary.

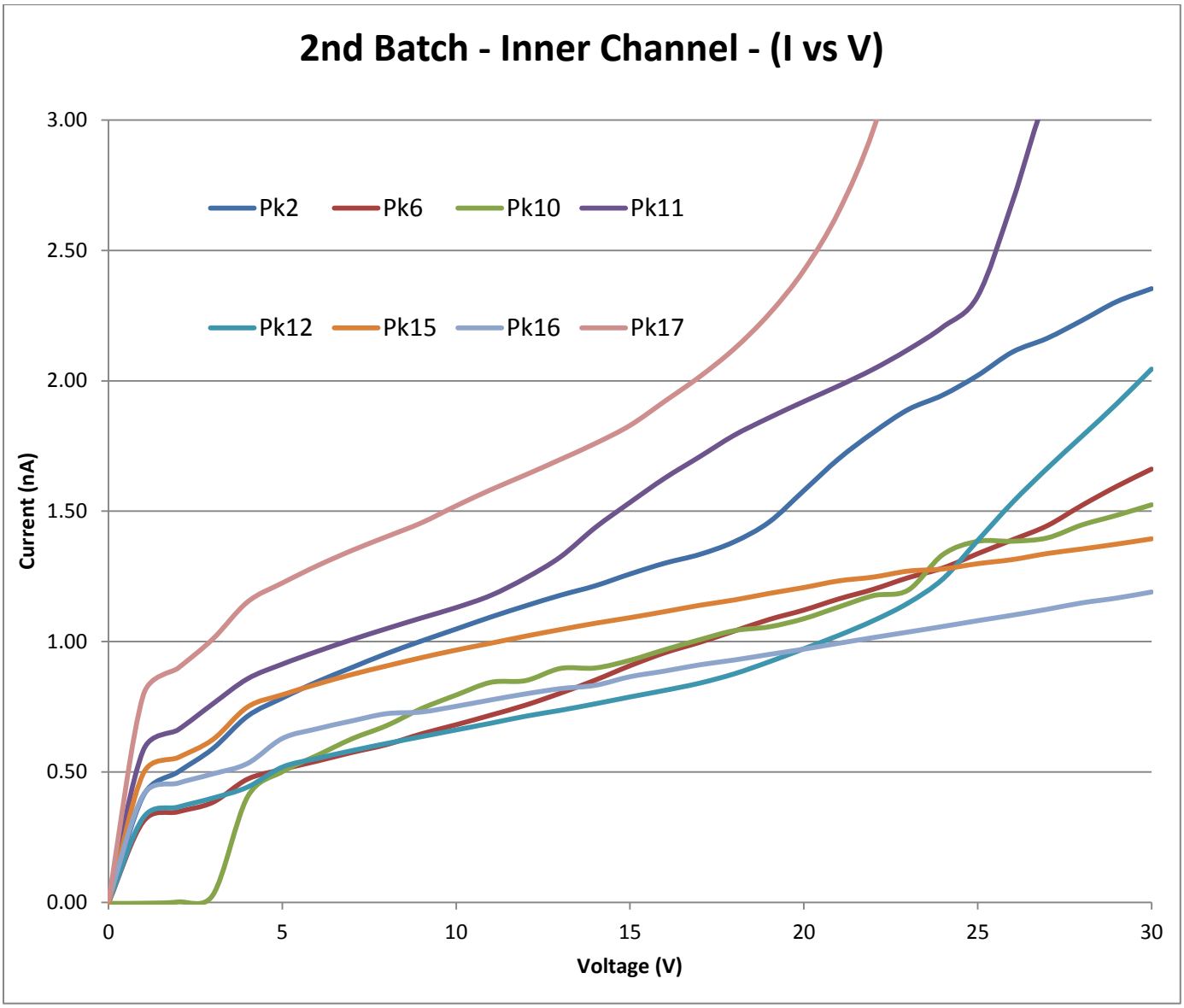


**FIG. 40:- COMPARED TO THE 1ST SET OF PROBES THE REVERSE BIAS GRADIENT ACROSS THE REGION OF INTEREST IS LARGER. THIS IMPLIES A LESS IDEAL PHOTODIODE. THE NOISE CONTRIBUTION FROM THE PROBE MAY BE LARGER FROM INCREASED DARK CURRENT CAUSED BY IMPURITIES. (PK6 GRADIENT = 0.037 NANOAMPERES/VOLT FOR THE IC)**

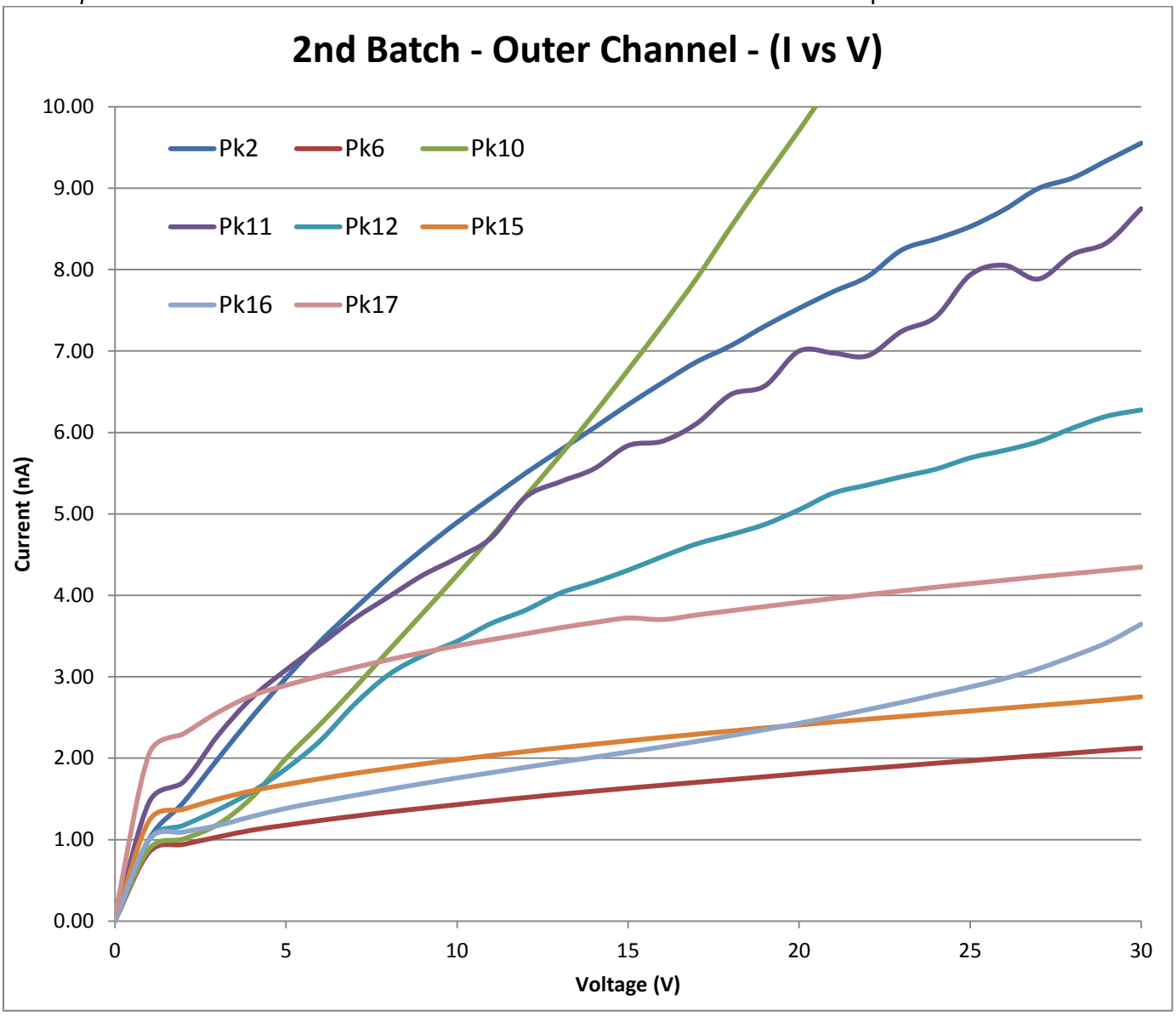


**FIG. 41:- AS OBSERVED IN FIG. 40 THE GRADIENT IN THE VOLTAGE RANGE OF INTEREST IS GREATER THAN IN THE 1ST PROBE SET. (PK6 GRADIENT = 0.04 NANOAMPERES/VOLT FOR THE OC)**

## 2ND PROBE SET CV RESULTS

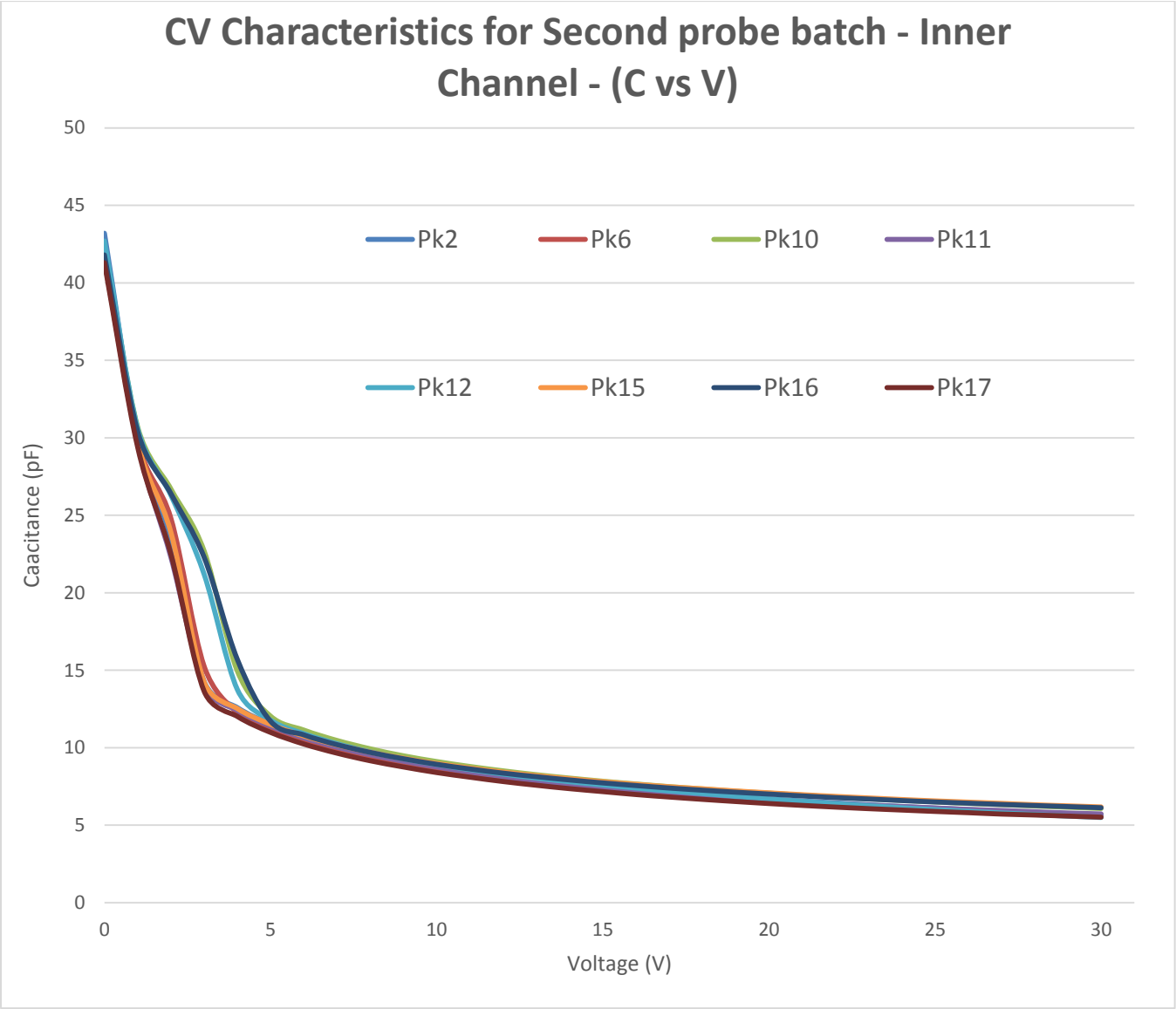


**FIG. 42:- THIS CAPACITANCE RESULT IS SIMILAR TO THE INNER CHANNEL RESULT FOR 1ST SET OF PROBES.**

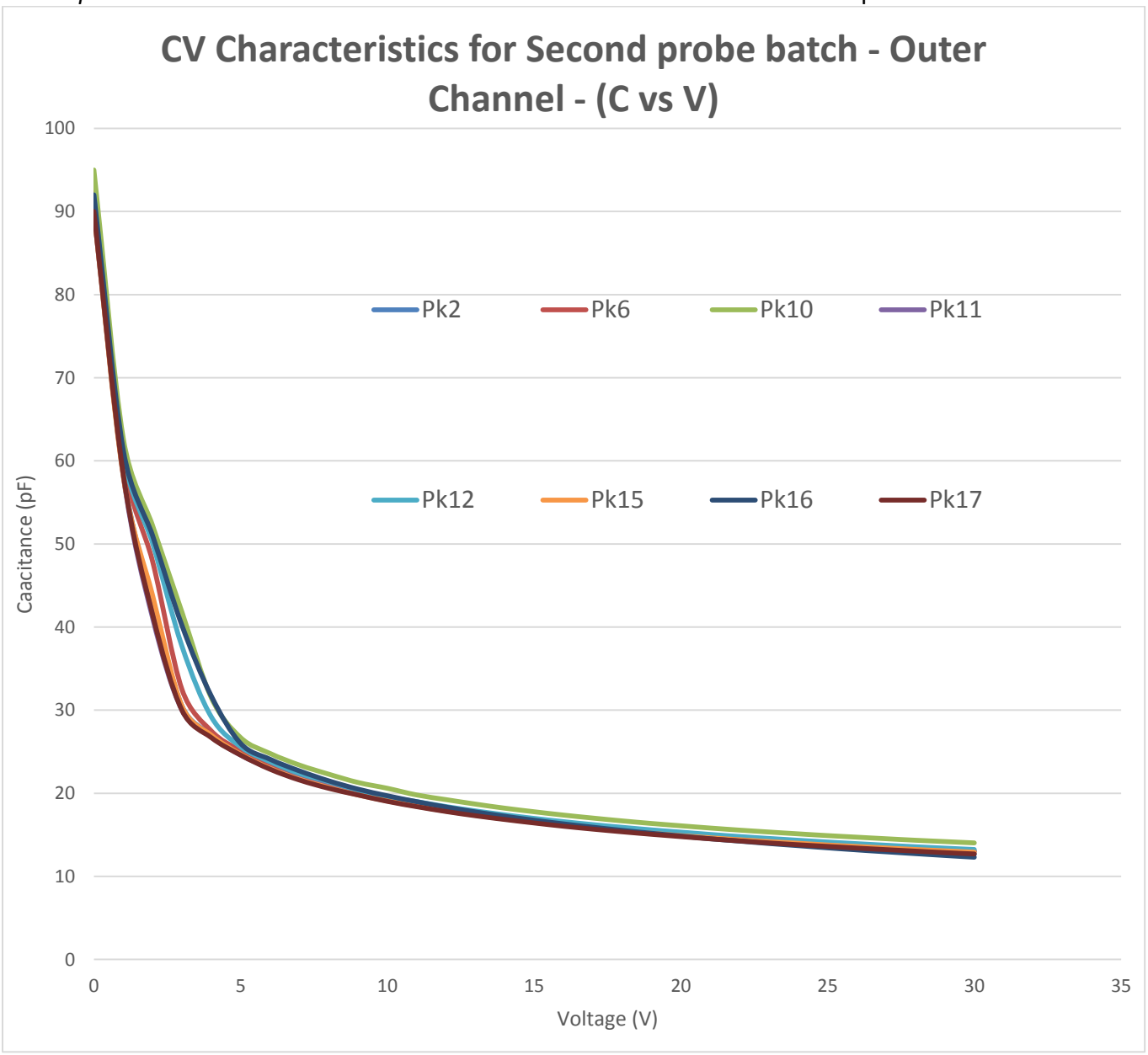


**FIG. 43:- THIS CAPACITANCE RESULT IS SIMILAR TO THE OUTER CHANNEL RESULT FOR THE 1ST SET OF PROBES.**

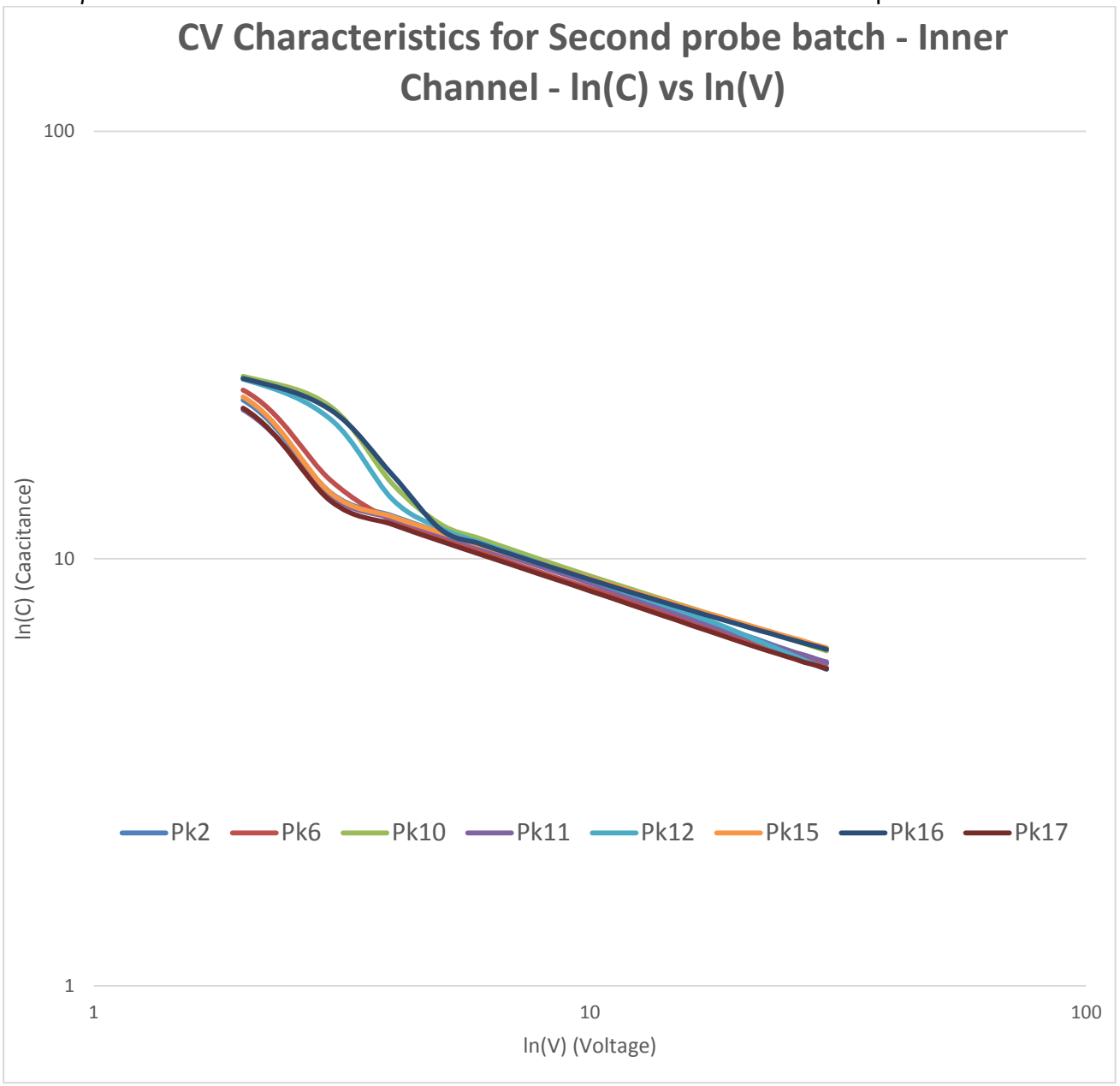


**FIG. 44:- C-V CHARACTERISTICS IN LOGARATHMIC SCALE (LINEAR SCALE IS PRESENTED ON FIG. 42.)**

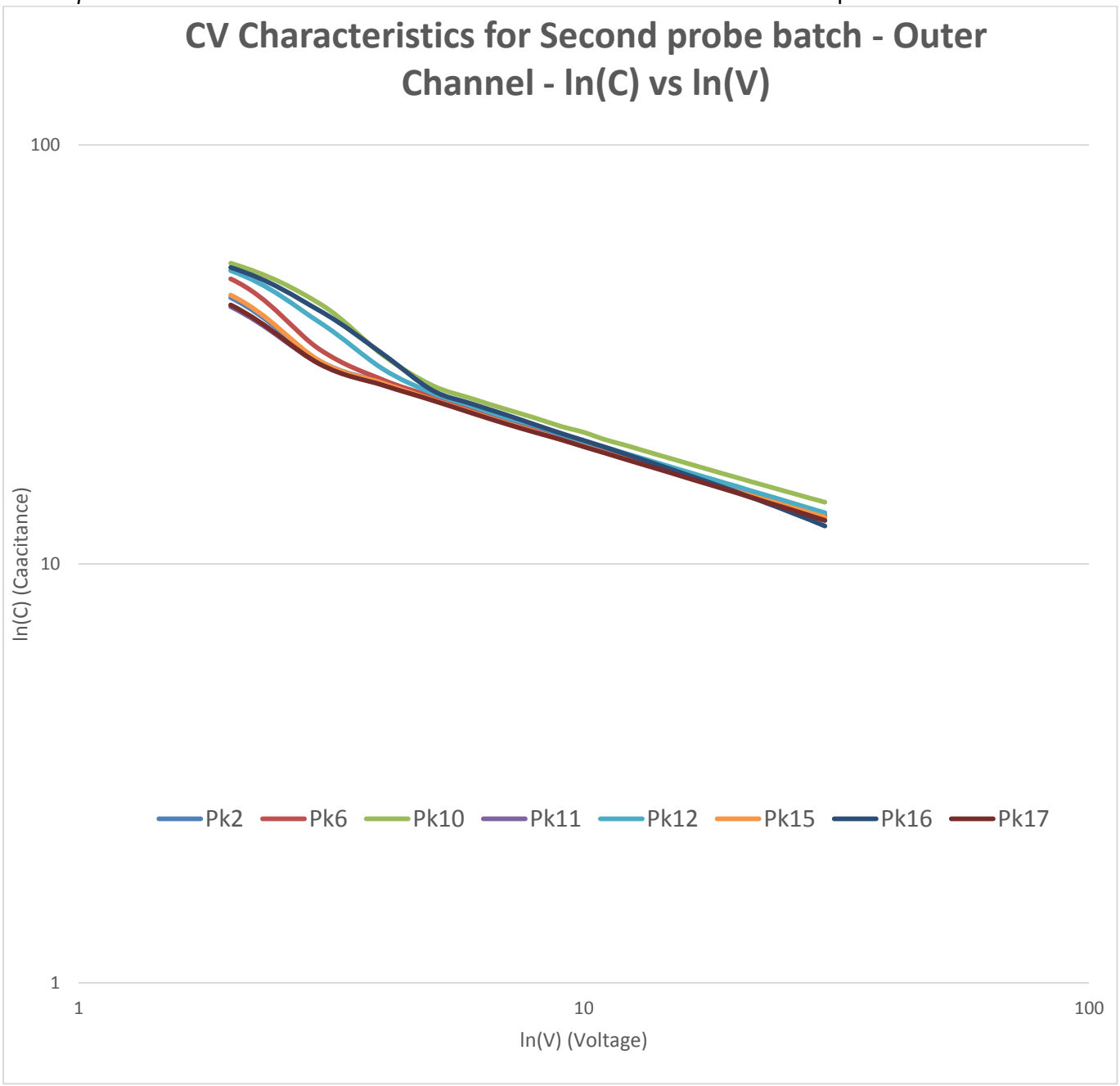


**FIG. 45:- C-V CHARACTERISTICS IN LOGARATHMIC SCALE (LINEAR SCALE IS PRESENTED ON FIG. 56.)**

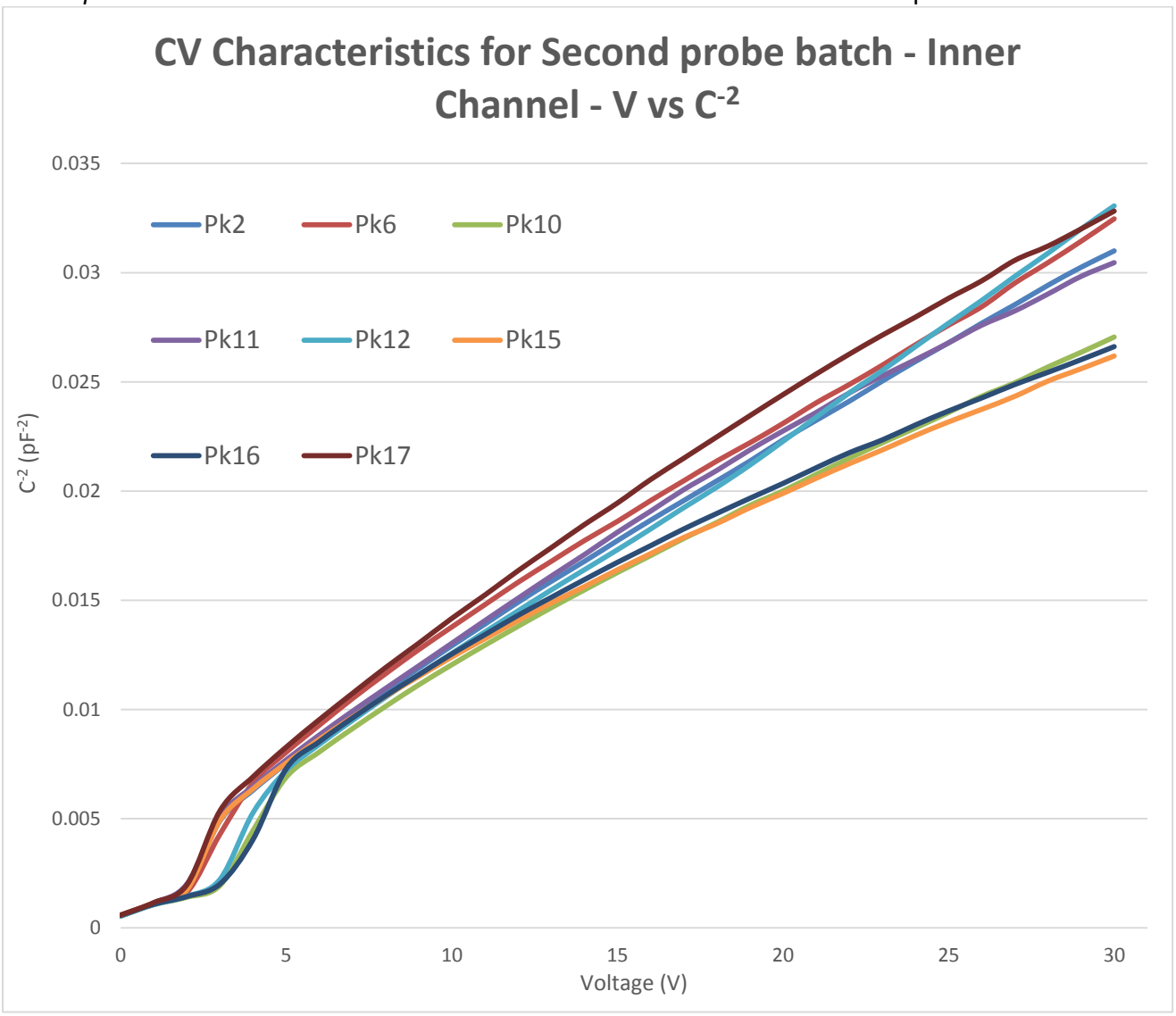


**FIG. 46:- THIS IS THE INVERSE SQUARED CAPACITANCE ACROSS THE SAME VOLTAGE AS FOR FIG. 42.**

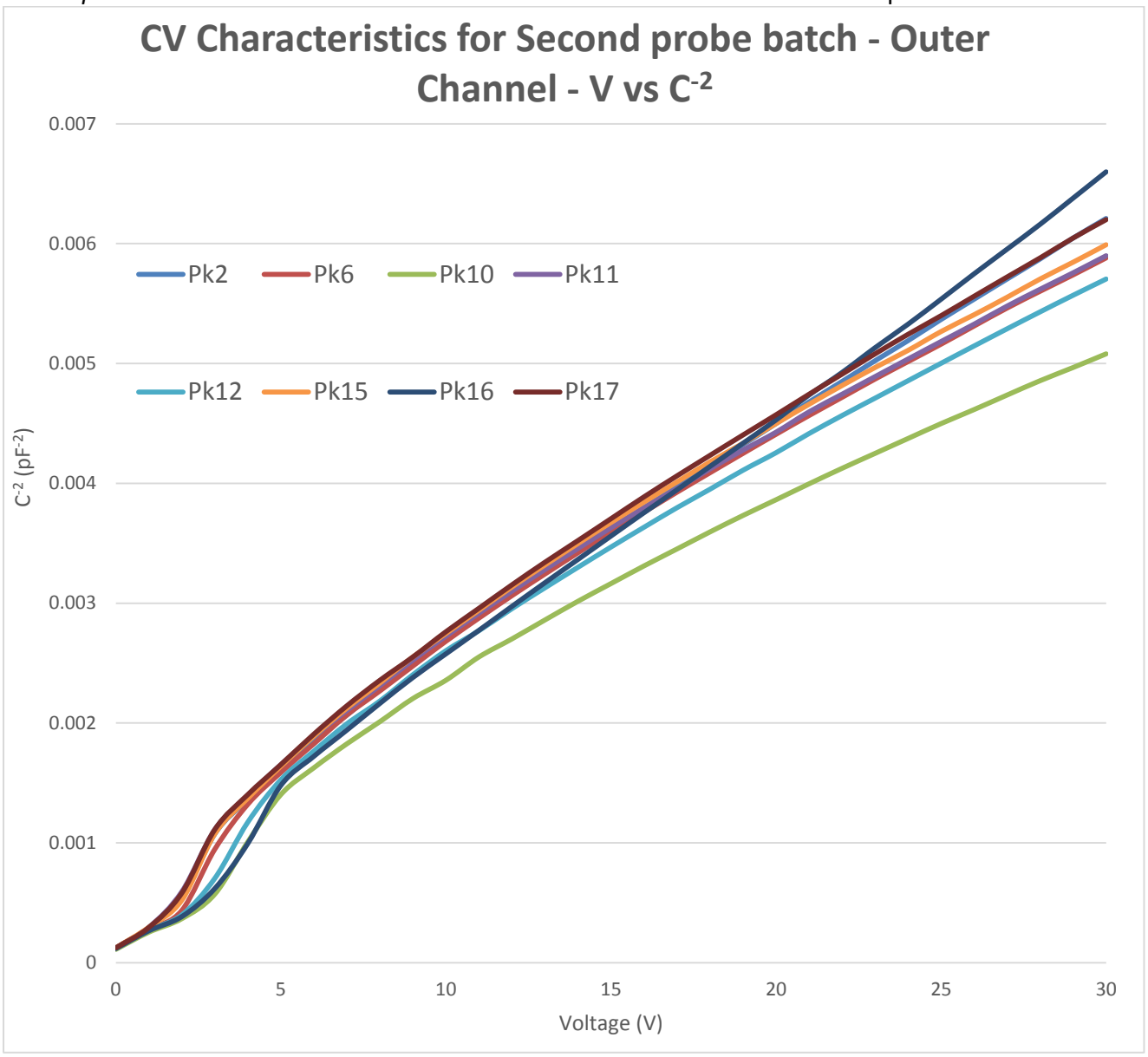


**FIG. 47:- THIS IS THE INVERSE SQUARED CAPACITANCE ACROSS THE SAME VOLTAGE FOR FIG. 43**

| *INNER CHANNEL IV CHARACTERISTICS COMPARISON* | | |
|---|---|---|
| Batch No. | Current at 15V (nA) | Gradient (nA/V) |
| First Batch | 0.25 | 0.016 |
| Second Batch | 0.8 | 0.135 |
| Franks First Batch | 1 | 0.081 |

**TABLE XII: - RESULTS ARE THE AVERAGE OF EACH SET TO ALLOW FOR BETTER COMPARISON. UNCERTAINTIES ARE OMITTED**

| *OUTER CHANNEL IV CHARACTERISTICS COMPARISON* | | |
|---|---|---|
| Batch No. | Current at 15V (nA) | Gradient (nA/V) |
| First Batch | 0.7 | 0.105 |
| Second Batch | 0.8 | 0.187 |
| Franks First Batch | 0.6 | 0.056 |

**TABLE XIII: - GRADIENT AND CURRENT AT 15V BIAS ALIGN MORE CLOSELY ON AVERAGE. UNCERTAINTIES ARE OMITTED.**

### *DISCUSSION OF IV AND CV IN COMPARISON TO THE 1ST SET OF PROBES*

An event was observed to occur in the C-V characteristics within the voltage domain of -1 to -5V, this event was not observed in the 1st probe batch. The nature of this event was unclear but correlates directly with the operating voltage domain and was noted for later tests. This aspect was found to be the only significant deviation from the First probe batch CV characteristics conducted by both studies.

IV Characteristics demonstrated a large difference between the reverse bias IV gradient between the IC of both probe batches. The gradient of the Second probe batch IC was approximately ten times the First probe batch result obtained by this study on average. Comparison of the OC depicts a similar though slightly higher IV gradient in the Second probe batch vs. the First probe batch. This difference

between each channels IV gradient across both probe batches implied that the First probe batch IC composition was different to the First probe batch OC, Second probe batch IC and the Second probe batch OC.

It is anticipated that the First probe batch's IC photodiode comprises of a lower ion impurity percentage that results in less dark current due to less surface current. More doping would reduce the noise factor by producing a flatter response in the photodiode regardless of voltage applied. It is clear that this factor was changed for the Second probe batch. It is expected that the reason for the change in IC composition was to make the IC response to emissions similar to the OC. Similar channel composition would make the event processing for the A-B/A+B functions more linear and thus a simpler process for the circuit logic to perform.

The IV gradients in Franks study for the First probe batch were for the IC 0.081 nA/V and for the OC 0.056 nA/V. Comparison with the characteristics obtained by this study (IC = 0.016 nA/V and OC = 0.105 nA/V) illustrates a difference in the I-V characteristics. A clearer picture is given from the current at 15V. In Franks' investigation the current at 15V for each channel was 1 nA for the IC and 0.6 nA for the OC with an uncertainty of $\pm$ 0.4 nA. This study found that the current at 15V for each channel was 0.25 nA for the IC and 0.7 nA for the OC with a statistical certainty of $\pm$ 0.1 nA.

The OC results are therefore in reasonable agreement as their differences can be reconciled by the difference in the equipment used to obtain their characteristics. The IC results are more difficult to understand and require greater scrutiny. The ratio of Franks results for the IV characteristics are approximately four times higher than those acquired by this study. It is suggested from internal comparison of the results

by Franks that the measurement technique used for the IC may not have been as precise as those used for the OC in Frank's study.

The First probe batch's IV and CV characteristics in this study were obtained using equipment from ANSTO's Detector Radiation Group (DRG). The DRG equipment comprised of a top of the line Keithley 2224 electrometer, Boonton capacitance modulator and a dedicated vacuum chamber which was regularly maintained and configured for characterising detector photodiodes. The UOW equipment comprised of a Keithley 614 electrometer and a lockable tin alloy box which couldn't be "light-tight" sealed. The ANSTO equipment was therefore anticipated to produce higher accuracy results than with the apparatus used at UOW for the second batch characterisation.

Franks study measured the IV and CV using the same apparatus as was used for the Second probe batch set in this study. Comparing the CV characteristics of Franks First probe batch with the Second probe batch from this study highlights the same deviation present in the -1 to -5 Volt operating range. This deviation was found in both studies and was reproducible under the same conditions. It was determined that all minor deviations from the First probe batch's I-V and C-V characteristics in Franks study were accounted for by the differences in apparatus used to acquire the results. This conclusion did not explain the higher I-V gradients found in the Second probe batch IC batch however and still required further investigation.

The results of the OC I-V implies that decay is occurring within the probe but at present is minimal and can be considered negligible. The performance lifetime of these probes excluding the impact of mishandling is therefore considered to be high and at least 3 years which is the first batch's current age. A qualitative estimate for

the scintillators performance lifetime when they are placed within the probes sealed container is approximately 5 – 10 years.

The Second probe batch results for the IV implies that the photodiodes have fewer imperfections throughout their structure causing a higher development of holes and electrons to conduct. This was noted when the spectra results were interpreted for the second batch of scintillators. It was expected that because of increased dark current, the noise coming from the photodiodes would increase. The noise in previous tests was shown to impact resolving lower energy events. It was anticipated that lower energy events would have lower resolution because of the greater noise from the photodiode in the second probe batch.

Based on the results of the IV and CV the best operating Scintillators were identified as Pk 6, 15 and 16 for the second probe batch. These probes were considered the best operating for the same reasons applied to the First probe batch, they demonstrated the flattest reverse bias IV of their batch and were consistent across both channels.

## *2ND BATCH TABLED RESOLUTIONS*

The spectra for each emission source has been shown in previous tests before the peak resolution was reported. To appreciate the energy to channel conversion occurring in the signal processing, the probe with the best resolution across both channels was identified from the tabled resolutions of the batch. An additional criteria for selecting the probe spectra is the close alignment of its channel to energy function for the IC with the OC. This would allow assessment of the “A+B” and “A-B” functions to be more accurate and performed with greater ease. A fully calibrated spectra chart of both channels is then provided giving a thorough analysis of the

scintillators composition and signal processing. This data is presented over the next page.

| Inner Resolution Second probe batch (%) | | | |
|---|---|---|---|
| Sample | Co-57 | Na-22 | Cs-137 |
| 2 | N/A | N/A | N/A |
| 6 | N/A | 10.7 | 9.8 |
| 10 | 28.9 | 9.5 | 7.3 |
| 11 | 31.0 | 9.6 | 9.4 |
| 12 | 25.3 | 12.4 | 1.9 |
| 15 | 37.3 | 11.6 | 12.1 |
| 16 | 37.4 | 8.5 | 8.5 |
| 17 | 29.9 | 2.7 | 8.6 |

**TABLE XIV: - CELLS MARKED RED INDICATE FALSE READINGS DESPITE SIGNIFICANTLY LONGER ACQUISITION INTERVALS. N/A AS STANDARD MEANS NOT-APPLICABLE AND IS CLASSIFIED DUE TO THE CHANNEL PRODUCING UNUSUABLE RESULTS. N/A PROBES ARE NOT OMITTED BECAUSE THEIR FAILURE MUST BE CLEARLY IDENTIFIED.**

| Outer Resolution Second probe batch (%) | | | |
|---|---|---|---|
| Sample | Co-57 | Na-22 | Cs-137 |
| 2 | N/A | 7.1 | 8.2 |
| 6 | 26.4 | 9.9 | 9.1 |
| 10 | 30.9 | 10.4 | 9.0 |
| 11 | N/A | 12.5 | 9.0 |
| 12 | 24.5 | 9.5 | 8.5 |
| 15 | 38.9 | 9.3 | 8.9 |
| 16 | 29.2 | 13.1 | 8.5 |
| 17 | N/A | 10.5 | 9.5 |

**TABLE XV: - PROBES 2, 11 AND 17 EXPERIENCED DIFFICULTIES RESOLVING THE CO-57 PEAK AS IT WAS LOCATED WITHIN THE THRESHOLD RANGE.**

| Channel | Co-57 | Na-22 | Cs-137 | Ch. Avg. |
|---|---|---|---|---|
| Inner | 31.6 | 10.4 | 9.3 | 17.1 |
| Outer | 30.0 | 10.3 | 8.8 | 16.4 |
| Sam. Avg. | 30.8 | 10.3 | 9.1 | 16.7 |

**TABLE XVI: - THE SCINTILLATOR AVERAGE RESOLUTION IN % FOR EACH CHANNEL. UNLIKE FIRST PROBE BATCH THE CH. AVG. DOES NOT EXCLUDE THE CO-57. THE COMPARATIVE RESULT FOR THIS IS 9.85 FOR THE IC AND 9.55 FOR THE OC.**

*RESOLUTION TABLE COMPARISON*

The results for Cs-137 using the first batch gave an energy resolution of 5.9% for the IC and 9.9% for the OC. A rough comparison between the first and second batch energy resolution percentage was made using each probe batch's average results. The OC in both batches was similar, the IC in both probe batches however was different.

An expected result was the similarity of the IC resolution to the OC as is depicted for the whole batch of Second probe batch. This result cannot be due to the gain difference between B3 and B6's IC. This is because the signal improvement had already been identified as a factor of the improved electronics used between the two studies. This is supported by Franks' study not having the electronics capable of producing the gain used by this study. Furthermore results produced from other boards in this study produced a similar resolution for the IC using the First probe batch probes.

The factor responsible for the reduced resolution accuracy of the IC was isolated to two factors. The first was due to the observed increase in the IC's dark current producing noise, the second is discussed shortly.

## *2ND PROBE BATCH CALIBRATED SPECTRA*

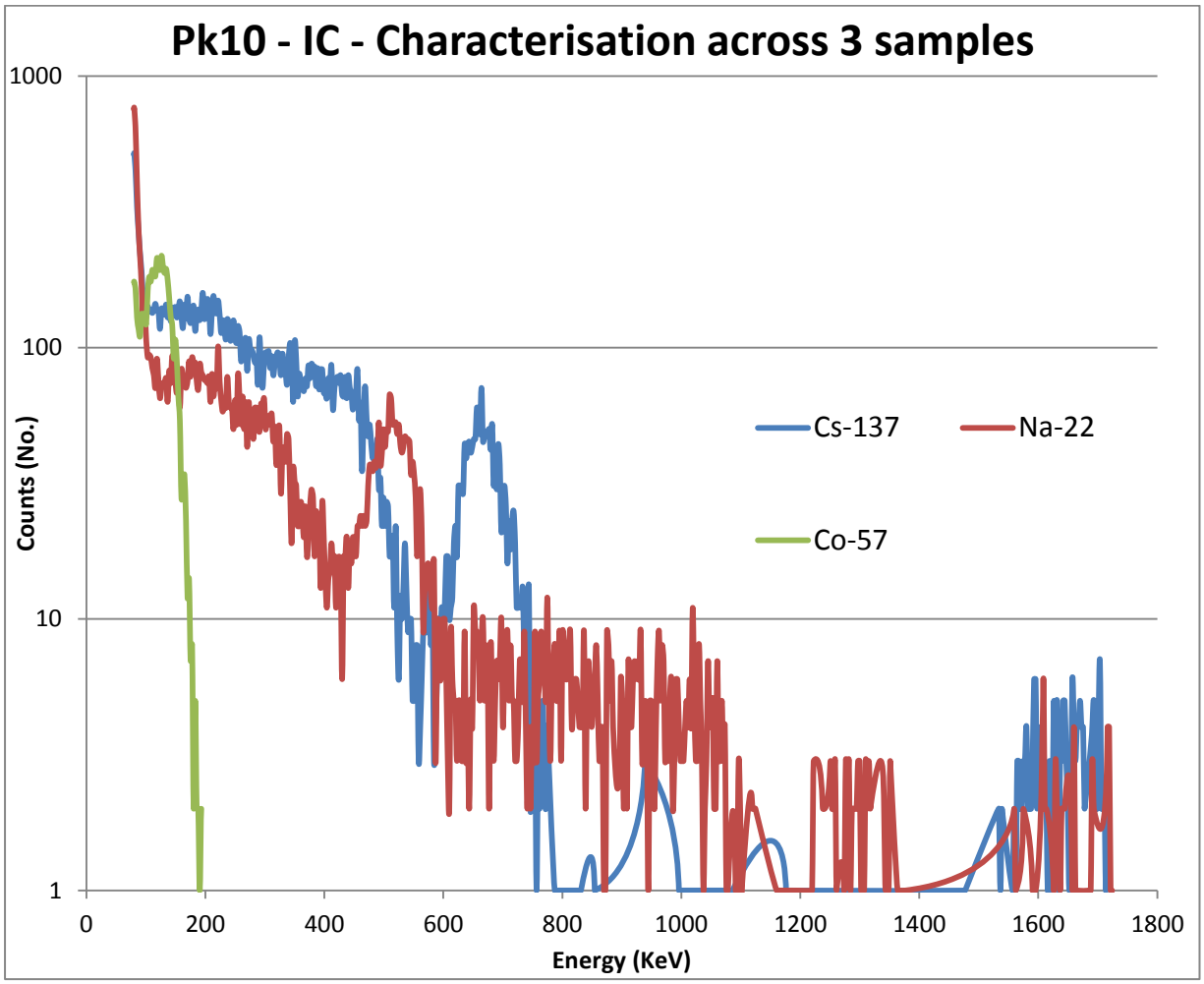


**FIG. 48:- THE CO-57 PEAK IS LOCATED AT 122 KEV, NA-22 AT 511 KEV AND THE CS-137 PEAK AT 662 KEV. THERE IS SOME OVERLAP IN THE LATER CHANNELS.**

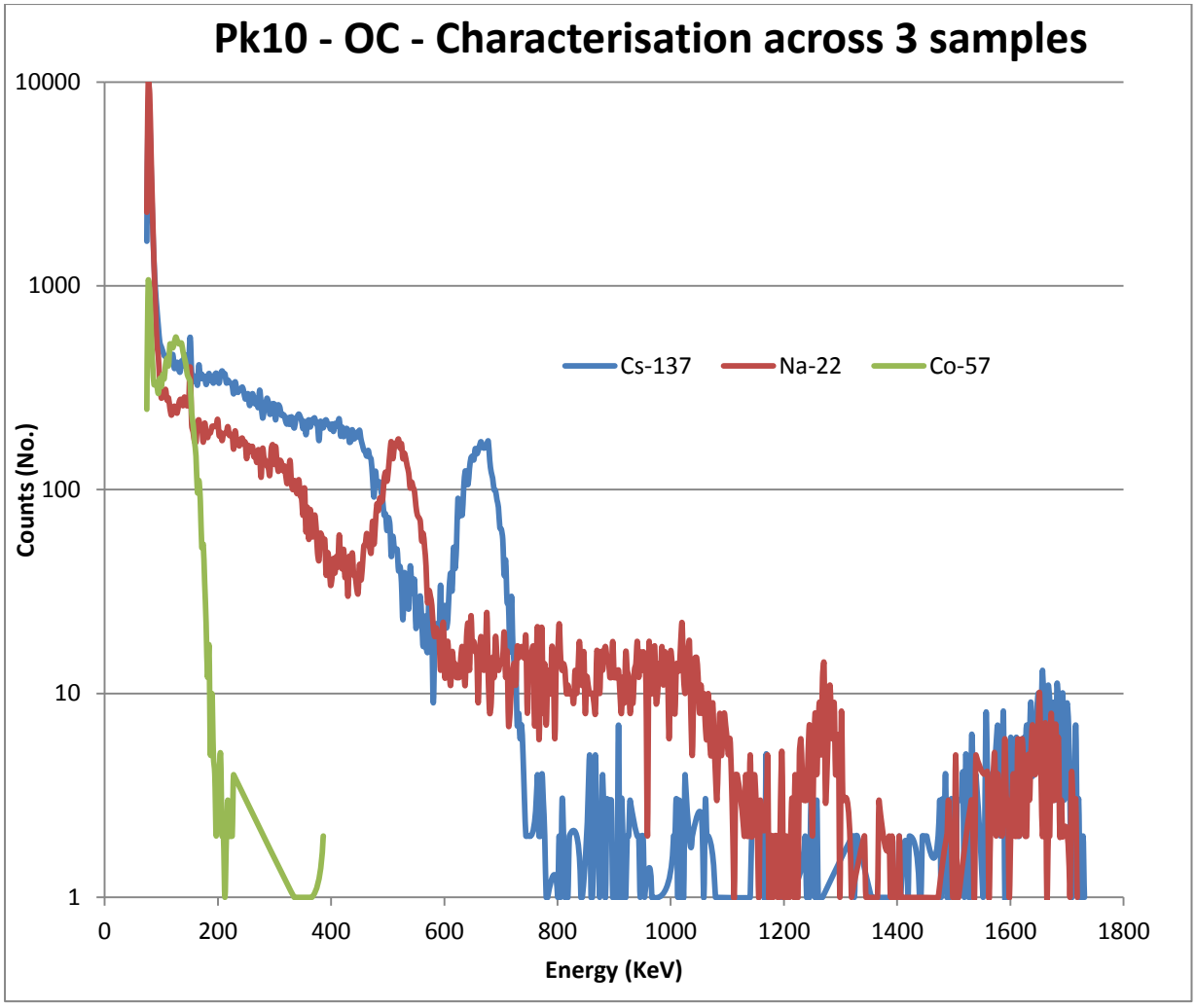


**FIG. 49:- THE INCREASED VOLUME OF THE CSI(TL) LOCATED IN THE OC WAS ABLE TO ADEQUATELY RESOLVE NA-22'S 1275 KEV GAMMA PEAK. IN FIG. 48 THE 1275 KEV PEAK IS PRESENT BUT NOT AS CLEARLY DEFINED AS PRESENTED HERE IN THIS CHART.**

### *2ND PROBE SET SPECTRA DISCUSSION*

The calibration of the probes was performed using Co-57's 122.1 KeV peak, Na-22's 511 KeV peak and Cs-137's 661.6 KeV peak. The presence of Na-22's 1275 KeV peak in the OC is useful information for two reasons:-

1. The energy to channel calibration did not include the 1275 KeV peak. The fact this peak aligns correctly with the calibrated channel for its energy anyway is a credit to both the linearity of the signal processing and the calibrations accuracy used for that energy. The channel to energy function was recorded.
2. The presence of the peak being more outstanding for the OC than for the IC is what would be expected when considering that the 1275 KeV peak is of higher energy. This is explained by the OC larger scintillator volume having a better efficiency than when the IC is used alone.

When the results for the other probes was collected it was determined that the spectra produced was consistent across all of the probes in the Second probe batch. The energy to channel conversion going to the MCA differed slightly for each probe. This was due to minor and unintended slight differences in each probes construction by the manufacturer in developing the second batch.

## *2ND PROBE BATCH CHARACTERISATION DISCUSSION*

The resolution capacity of both channels was not only similar but found to favour the OC as more accurate. Considering two of the emitters used for the tests were higher energy emitters and that the IC was supposed to function in complement with the OC. It was expected that the OC would perform more suitably under these conditions than the IC. The IC's performance would improve by working co-operatively with the OC.

The IV gradient for the OC in second probe batch is greater than its IC equivalent. Each channels IV results depicted more consistent gradients across the second batch than what was observed for the first batch. This information would purport that dark current was creating more noise for the second batch than what was generated for the first batch. This hypothesis would explain the relatively lower accuracy results of the second probe batch as due to the greater presence of defects in the photodiode.

The difference in the signal processing electronics could not have been a factor for the lower accuracy of the IC. This would not explain why the results obtained by Franks for the first probe batch IC scintillator were similar to those acquired by this study. The cause of the lower IC accuracy was attributed to a factor of the second probe batch probes. This result is supported by the IV characteristic which is indicative of a structure difference in the probes in the form of increased impurity conductivity.

The OC of second probe batch was higher functioning in comparison to the first probe batch, whereas the IC of second probe batch was theoretically found to be of poorer function by the IV characteristics but experimentally was found to function satisfactorily. A lower quality reverse bias for the IC photodiodes when comparing the first to the second probe batch signifies a difference in the second batch's IC construction. The problem was determined to be in the photodiode for the inner channel across the entire second probe batch.

The above information is indicative of a differing manufacture technique between both sets of probes as it applies to all ICs across the entire second probe batch. This reduction in accuracy was not found to interfere with the dual probe functionality. The

factor was merely an inconvenience when compared to the superior function of the first probe batch ICs.

The change in the probe may have been intended by the manufacturer to improve absorption of lower energy optical photon wavelengths for the IC as it was the only difference in resolution between the two results. Comparing the data found in TABLE X and TABLE XI with TABLE XVI for Co-57 implied a twofold improvement of resolution which supported this hypothesis. Extrapolation of the result consistency across the second probe batch also implied the change to be intentional and thus supported this hypothesis. The improvement of spectral sharpness for the spectra observed from first to second probe batch further supported this hypothesis. If this was the manufacturers intention (which is unlikely), the change has resulted in reducing the energy resolution of the IC's in the higher energy domain. This change does however make the probes more useful for intraoperative application.

## *2ND PROBE BATCH CHARACTERISATION CONCLUSION*

The lower quality resolution for the IC of the Second probe batch compared to the First probe batch was not found to significantly affect later tests. The test results support the manufacturer as responsible for changing the photodiode of the second probe batch ICs. It was anticipated that this design change would offer a different spatial resolution compared to the first probe batch. This factor was not able to be assessed due to the IC failure of the First probe batch.

# PROBE SENSITIVITY AND SPATIAL RESOLUTION INVESTIGATION

The Liana board and Scintillators for both the first and second probe batches were characterised. Diagnosing the components in the event of mishandling or malfunction was now available and ensured the components operated consistently for all tests. The next stage of the intraoperative probes assessment was the spatial resolution capacity for Liana's medical based application. A Lead collimator is used for all these tests to make the radioactive substance simulate a point like source. This is important in surgery for finding any smaller trace amounts of radioactive isotope left once the bulk of the material has been removed from the patient.

Initial tests using the first batch illustrated a fluctuation in sensitivity with respect to time when placed in the module presented in Fig. 50. It was identified that the fluctuation affected only lower energy channels. Providing more grounding to the electronics did rectify the issue slightly, however noise was still observable in the pulse presented by the oscilloscope. The magnitude of this noise with respect to the signal produced was determined to be insignificant for the coming tests.

The need for lower energy peak resolution is critical for the medical applications of this device, lower energy emission isotopes are preferred because of the greater localisation capacity they offer. Co-57 collimated by lead of 8mm thickness ensured 99.9% of emissions could only pass through the aperture and was used in the following tests. Na-22 would require 29.6cm of Lead for 99.9% collimation. This amount of lead was unavailable during the study. It was calculated that 78% of Na-22 photons would pass through 8 mm of lead. I.e. Only 22% of the emissions will be blocked by 8 mm of lead.

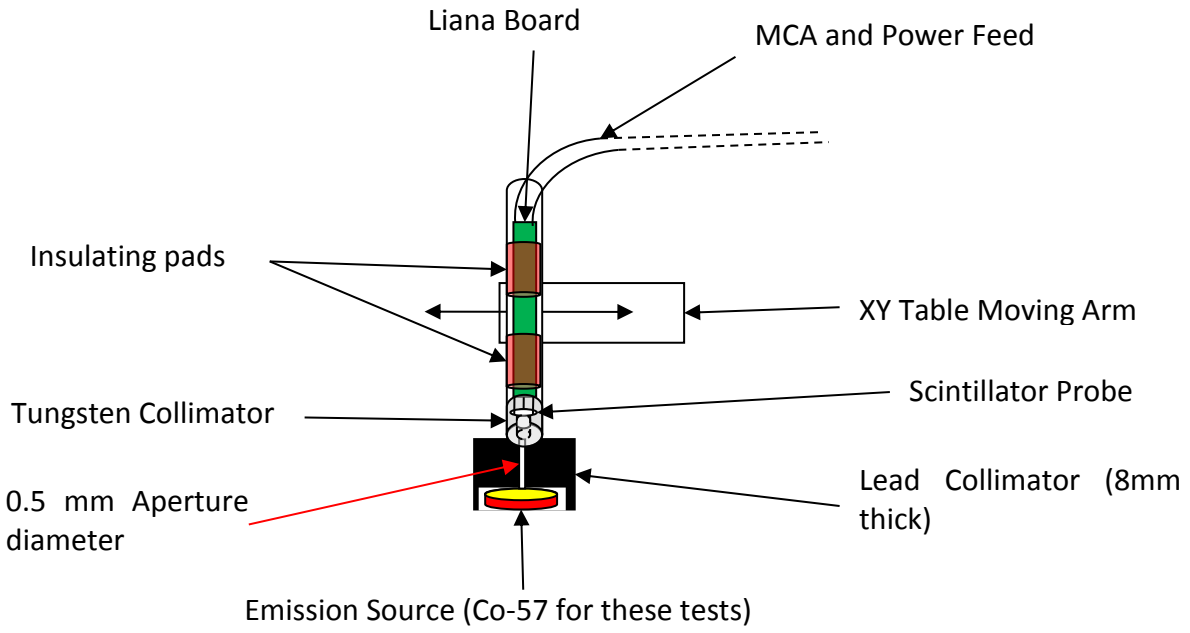


**FIG. 50:- NOT TO SCALE. THE SCINTILATOR IS POSITIONED IN AN EM SHIELDED TUBE DIRECTLY OVER THE SOURCE. LEAD COLLIMATION THICKNESS WAS SUFFICIENT TO ENSURE ABOUT 99.9% OF PHOTONS WITH ENERGY 122 KEV PASSED ONLY THROUGH THE APERTURE. THIS MEANT THE SOURCE WOULD SIMULATE POINT LIKE EMISSIONS FOR THE CO-57 SAMPLE.**

It should be noted that in Fig. 50 above the probe casing and collimator were 'grounded' to the PCB, but electronically isolated from the XY Table moving arm.

The initial tests were not able to identify the cause of this fluctuation. Two factors recognised as possible sources for this error were: The discharge of the Li-Ion 4.21 V battery; and the electronics warm up period.

A sensitivity test was conducted over a course of 2+ hours to observe the change in collection consistency with respect to time. If the fluctuation was because of a warm up period, a rise and fall in the collection rate across the first few minutes of operation would be observed. If the fluctuation was due to the decline in battery charge supplying voltage to the circuitry, then a decline would be observed as the

time period increased. Depending on the data acquired other diagnostic information could be ascertained.

The probes position was fixed for the sensitivity test. The Lead collimator combined with Co-57 used in this test simulated the presence of a low energy point like gamma source (0.5mm diameter). This test would simulate the localisation of Tc-99m which was the intended radionuclide to be used in surgical conditions.

The acquisitions for the sensitivity test were performed over 5 minute intervals, the results were collected from the pre-defined region of interest, and then placed into a chart (Fig. 51).

In surgical conditions the probe would be expected to locally resolve the position of an isotope spread throughout an entire persons' body. The amount of isotope located in a particular area could be as small as a few atoms worth of emitter. The capacity of the probe to resolve emissions from point like emitters is therefore a useful property. Realistically the amount absorbed by any node is likely to be greater than this amount and so this test would provide an assessment of the probes finest localisation detection capacity.

More thorough testing would utilise medically preferred radioisotopes like Tc-99m, however this substance was unavailable during the course of the research. As Tc-99m's 141 KeV peak is higher than Co-57's 122 KeV peak, both energy and spatial resolution were expected to improve if Tc-99m was used in place of Co-57.

The spatial resolution tests utilised the same configuration as the sensitivity tests. The spatial resolution tests however involve the probe moving set displacements from physical centre. This was to assess the drop in sensitivity as the probe moved

away from the point like source. Earlier tests identified the sensitivity reducing exponentially with increased distance from the emission source. It was also identified empirically that the probes farthest reliable detection capacity for a point like source was approximately 2cm.

The sensitivity and spatial resolution test results were collected by defining a region of interest (ROI) around Co-57's primary gamma peak. The ROI was pre-calibrated based on the probes earlier spectra characteristic assessment result. This reduced the impact of noise in the lower energy domain and ensured both channels were assessed equally.

To further illustrate the impact of noise generated within the Liana boards' electronics and the impact of background counts. Na-22's peak was also collected to assess the change in its collection rate across the same time frame but for a higher energy emission. It was expected that the collection rate would be more consistent and have lower error for the higher energy emissions than the lower energy emissions of Co-57. The Co-57 sample used for these tests was fresher than the emission source of Na-22. The number of events collected for the Co-57 was expected to be higher than the number collected for Na-22, but not as consistent across both channels.

If the information collected during this project was accurate up to this point a hypothesis could be made on the outcome of the test. Na-22's 511 KeV emission rate is significantly lower than that of Co-57's 122 KeV emission rate. It was expected then that the number of counts recorded for Co-57 would be significantly higher than that observed for Na-22. As the emission source is limited to the aperture opening of the collimator, emissions should only enter the OC if the

aperture is placed above it. As the aperture size was 0.5 mm and the collimation thickness was 8mm the emission penumbra approaching the 1.5 mm radius IC was not expected to enter the OC.

The OC was therefore expected to collect fewer emissions than the IC for the sensitivity test with both emission sources, and ideally shouldn't collect any emissions for Co-57. For Na-22 it was expected that the OC would be exposed to 78% of photons emitted by the source compared to the recorded by the IC. The sensitivity and spatial resolution tests therefore provide a means for assessing the Liana Probes dual feature operation effectiveness.

The results illustrating the change of sensitivity are presented first.

## *SENSITIVITY TEST RESULTS*

For the IC the statistical deviation of results with respect to the average was 1.36% for Co-57 and 2.3% for Na-22 across the whole 2 hour period. These results were

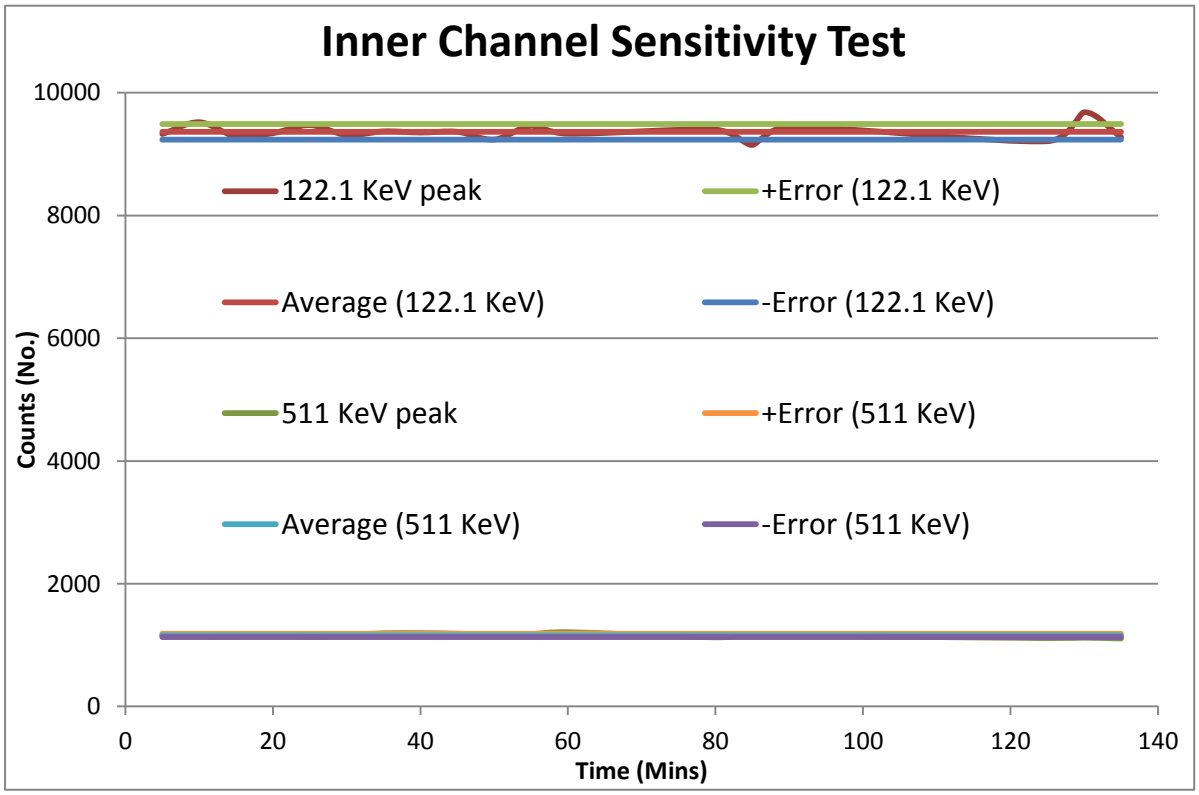


**FIG. 51:- THE UPPER LINE REPRESENTS THE CHANGE IN COUNTS WITH RESPECT TO THE LOWER ENERGY CO-57. THE LOWER LINE REPRESENTS THE COLLECTION WITHIN THE REGION OF INTEREST FOR THE HIGHER ENERGY NA-22 511 KEV. ACROSS 2 HOURS THE CHANGE IN SENSITIVITY WAS MINIMAL FOR BOTH CASES.**

mostly found to be within standard error.

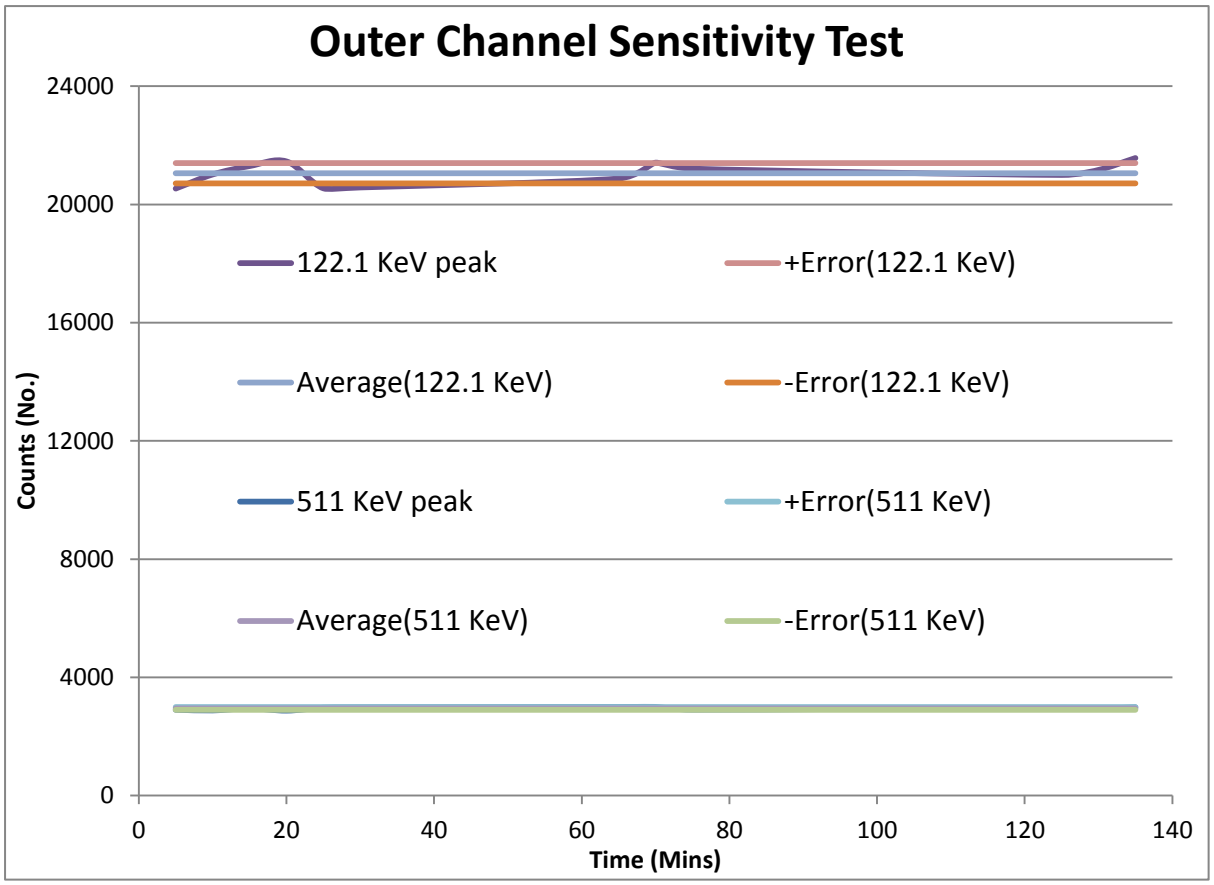


**Fig. 52:- Results are mostly within one Standard Error of the average. The deviation of the results from their calculated average for both channels was 1.6%**

*SENSITIVITY TEST DISCUSSION*

The results percentage deviation from the calculated average across both channels was less than 3% for the 2 hour period. The result implied that under the same conditions the peak could be reproduced with a consistency of 97-99% across any point within at least a 2 hour timeframe.

The results of this test are the product of multiple chamber adjustments. Previously the errors encountered were the ones introduced for this test:

1. A rise then decline in results for the first 15 min collection period
2. A slow decline in counts over extended time durations.

Insufficient grounding and EM shielding was identified as the cause of the problem. The insufficient shielding was due to inconsistent contact with the uppermost contact plate sealing the probe inside the chamber. (See Fig. 50) The Liana board's grounding was amended by connecting the spare grounding points available in the circuit to ground. The main star point was not directly grounded due to a physical alteration required for the probe to operate in the vertical orientation during these tests. It may be possible to improve the board performance by sufficiently grounding this point in future studies.

Across the 2hrs and 15min time period, data was collected as the battery charge lowered from 4.21V to 3.91V. The result is that the charge depletes by $0.1\dot{3}V/hr$. Results of this test show the probes operation is >97% consistent for repeat tests across this extended duration.

Na-22 had a lower collection rate in comparison to the Co-57 as suggested by the hypothesis. An unexpected result for this test was the number of counts collected by

the OC. For Co-57 the number of emissions collected in the OC should have approached zero. For Na-22 the number of emissions collected by the OC should have been 78% of the IC. The result observed for the OC in both cases showed that the OC registered more photons than the IC.

The software used for collecting and recording the results for each 5 minute interval of the 2 hour sensitivity trial had been configured for this test. It was configured to identify the emissions within the FWHM resolution of each sources independent spectra as recorded during the Second probe batch spectra test. The amount of collimation had been carefully considered prior to the investigation and was specifically constructed to block about 99.9% of Co-57. In addition this thickness was supposed to block about 22% of Na-22. Lastly, the positioning of the probe and source was specifically and carefully calibrated to be directly on top of the IC using a digital XY table moving arm. It had been calibrated by performing initial spatial tests specifically for the IC to determine the point of maximum emission collection.

This result leaves 3 possible conclusions excluding an error in the experimental technique:-

1. The penumbra of the emissions passing through the aperture is wider than originally conceived.
2. Cross talk between the channels is present within the probe.
3. The OC extends itself as a layer either above or below the IC.

The point like source under these conditions should not have a very wide Penumbra as the aperture depth was 8mm and the source was flush against the Lead. Additionally the probe was also flush against the opposing side of the collimation material. A calculation was performed using MATHCAD to determine the impact of a

Penumbra if it were present. A Penumbra was determined to be possible as closer inspection of the collimation length showed that events passing at an angle inside the aperture may avoid the significant part of the collimation material as presented below.

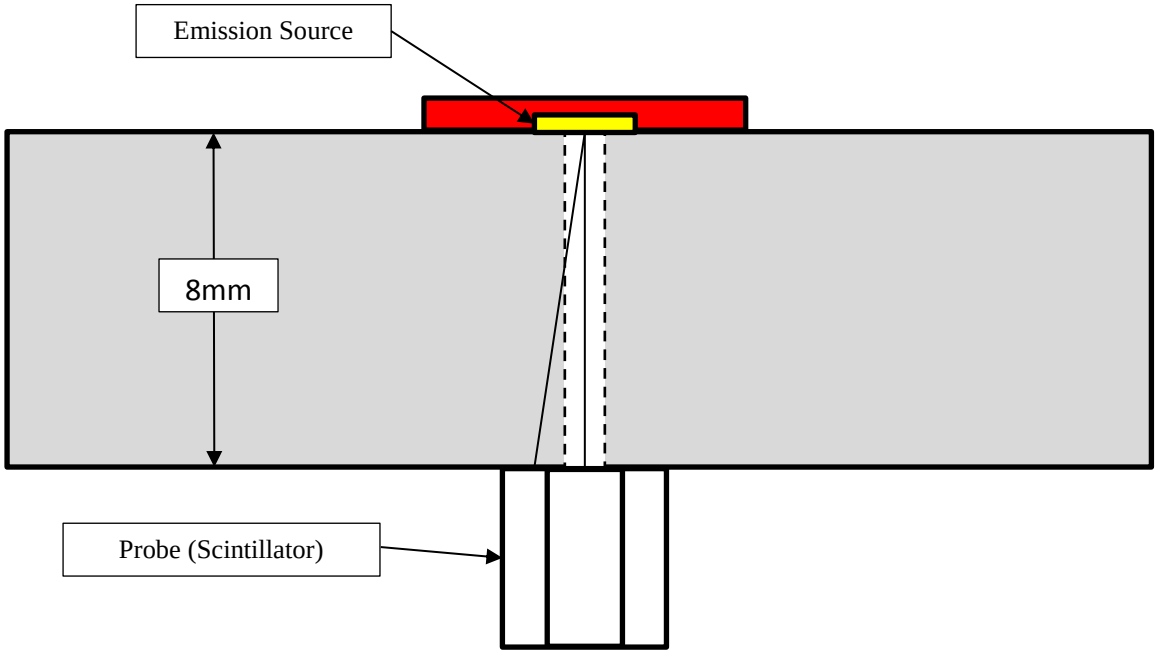


**FIG. 53:- ILLUSTRATED ABOVE IS AN EXAMPLE OF PHOTONS PASSING THROUGH ONLY PART OF THE LEAD MATERIAL REQUIRED FOR COMPLETE COLLIMATION.**

A calculation was independently derived then performed using the intensity formula to approximate the number of emissions able to pass through the collimator.

$$\left(\frac{I}{I_0}\right) = e^{-\mu \cdot L}$$

Where "I" is the final intensity and "$I_0$" the original intensity. μ is the collimation co-efficient and is dependent on the emissions energy and the collimation substance. "*L*" is the amount of collimation material the emissions have passed through.

At $L$ = 8mm, ($I/I_0$) equalled zero. The remaining emission percentage for every possible path through the collimator could therefore be determined numerically. Hypotenuse lengths less than 8mm between the base of the emission source and the top of the probe were recorded. The intensity for each of these hypotenuse distances was then calculated for every possible combination of $X_s$ and $X_a$.

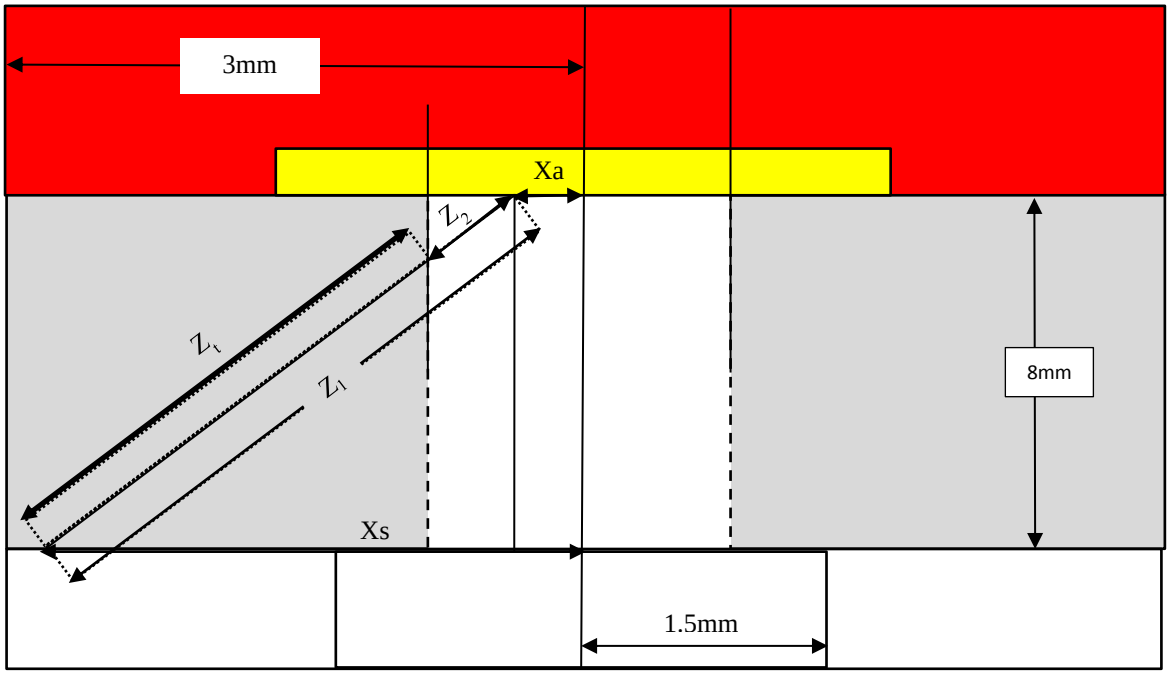


**FIG. 54:- THIS FIGURE ILLUSTRATES THE RELATIVE DIMENSIONS OF EACH COMPONENT FROM FIG. 53. THE APERTURE DIAMETER IS 0.5 MM. THE TOP SECTION IN RED DESIGNATES THE EMISSION SOURCE. THE MIDDLE GREY SECTION REPRESENTS THE COLLIMATOR. THE BOTTOM WHITE SECTION REPRESNTS THE SCINTILLATOR. THE SCINTILLATORS TWO PROBE SECTIONS HAVE BEEN DESIGNATED BY A DIVIDING LINE OUTSIDE OF 1.5 MM FROM THE CENTRE OF DIAGRAM.**

Collinear trigonometry was used for determining these lengths along with Pythagoras's Theorem where 8 mm was the set height.

$$Z_1 = \sqrt{(Xs - Xa)^2 + (8mm)^2}$$

$Z_1$ is the total hypotenuse length.

$X_s$ is the scintillator acceptance point for the emission and is confined to between 1.5mm and 3mm.

$X_a$ defines the starting point for the emission, where $X_a$ is confined between -0.25 mm and 0.25 mm for this example.

The amount of distance travelled in the air must be subtracted from this amount. $Z_2$ was the length of the hypotenuse travelled in air.

By trigonometry $Z_2$ was found to be,

$$Z_2 = \frac{(0.25mm - Xa)}{\sin\theta}$$

Where,

$$\sin\theta = \left(\frac{Xs - Xa}{Z_1}\right)$$

This meant the total distance travelled by an emission through the collimate material is definable by,

$$Z_t = Z_1 - Z_2$$

If $Z_t$ was less than 8mm MATHCAD would iteratively substitute the depth value into the intensity formula for the specific point $X_s$. Each emission point $X_a$ was assigned a percentage of the total source emission rate. This was for simulating an emission sources spreading rate as it is not in reality point like. The percentage assigned was based on the area for a step size $X_a$ (in this case $\pi(0.001mm)^2$) with respect to the total emission area. ($\pi(0.5mm)^2$) and was defined as $I_0$.

$$\left(\frac{I}{I_0}\right)\% = I_0 \cdot e^{-\mu \cdot Z_t}$$

As MATHCAD iteratively inserted the depth information into the intensity formula, it recorded the intensity received at point $X_s$ from each point $X_a$. MATHCAD then repeated this process for every point $X_s$, where it eventually added up the total amount of energy deposited into the OC. This process was then repeated for finding the amount of energy deposited into the IC.

The IC and OC data were then added together to find the hypothetical emission total, which was then compared to the OC data to find the percentage of these events entering the OC. The solution is therefore found numerically by finding the energy deposited into each point of the scintillator, then adding and comparing the total energy deposited into each channel.

Although *showing* the calculation steps for one combination of $X_s$ and $X_a$ isn't difficult to provide and explain. Showing the calculation steps for *all* combinations of $X_s$ with $X_a$ is obviously far too large to be included in this paper. The steps explained above should be sufficient for replicating the process using most mathematics software packages such as MATHCAD or MATLAB.

To simplify this calculation emissions were considered to fully deposit themselves from the moment they made contact with the OC surface. This calculation was only performed along the top of the OC and on its innermost surface along the interface with the IC. The greatest contribution of emissions was expected to come from emissions passing through the IC to OC interface. This is because the paths that travel through the least amount of Lead pass through the IC. The IC to OC

contribution would require a modified form of the above equations and includes the small contribution from the source between -0.25 and -0.5 mm radius.

The results of this calculation concluded that a Background Penumbra caused by the lead collimator can exist. In this configuration the Penumbra would be expected to contribute approximately 68.6% of the total Co-57 emissions into the OC. As anticipated the significant percentage of the Penumbra was from emissions passing through the IC to OC interface. TABLE XVII contains the experimental results of each channels total event collection for each emission substance.

| | Co-57 | Na-22 | Total Counts |
|---|---|---|---|
| Inner | 9362.89 | 1158.11 | 98744.00 |
| Outer | 21053.50 | 2949.25 | 286470.00 |
| Total | 30416.39 | 4107.36 | 385214 |
| Fraction of OC to Total | 0.692176 | 0.71804 | 0.743665 |

**TABLE XVII: - THE FRACTION OF EVENTS IN THE IC TO OC IS APPROXIMATELY 40%.**

For Co-57, the IC was found to have collected 30.8% of the total Co-57 events emitted. The remaining 69.2% $\pm$ 0.6% of the emissions was collected by the OC. A theoretical calculation was completed for the Penumbra caused by the Lead collimators interaction with the Co-57 emissions. It was determined that 68.6% $\pm$ 0.01% of the total Co-57 emissions directed at the probe would deposit into the OC. This theoretical result is within one standard error of the experimental results uncertainty range.

Though it was unintentional, the penumbra simulated the impact of background events caused by emissions interacting with a material. The Penumbra was found to make such a large contribution to the OC simply because of its much larger acceptance volume. A larger percentage of the possible emission paths passed

through the OC and this percentage could only be reduced by adding more collimation material.

The results of this experiment justify and support the need for background suppression probes in radio guided surgical procedures. The dual detection system therefore excludes background events from detection and produces a non-diverging physical acceptance window. The physical acceptance area is therefore limited to directly in front of the probe. The physical acceptance area will be discussed shortly.

Each channels accuracy was found to be consistent across a minimum timeframe of 2 hours. Spatial Resolution tests could now be precisely acquired. To ensure the results collected by the probe were accurate, the acquisition time was confined to within a 2hr time period from the point the battery was considered fully charged. If tests required longer durations the experiment would cease and the battery would be replaced with another that was fully charged.

### *SENSITIVITY TEST CONCLUSION*

All of the Spatial Resolution results acquired below would be accurate and reproducible as they would be all taken within a 2 hour time period. The sensitivity test has unintentionally illustrated the need for the background suppression capability in the Liana Probe. Despite such high collimation from the lead, events from outside of the testing area have deposited into the OC. This result implied that the Active Collimation configuration for the Liana probe would be effective. This is because the energy reading across channels align accurately. Assuming the timing function worked accurately events could be precisely vetoed from the IC ensuring fine localisation of an emission source. This conclusion cannot be confirmed without first performing a spatial resolution that illustrates the probe performance with and without the A-B function in effect.

## *SPATIAL RESOLUTION TESTS*

The spatial resolution tests were initially conducted in the study by Franks using just an x-axis slice of the probes IC and OC. Since the probes were cylindrical it could be assumed that the sensitivity was uniform or all angles around axial axis of the probe. The spatial resolution study performed a test to assess this assumption. A formula was developed to predict the probes sensitivity to a point source with respect to its X and Y axes. The depth sensitivity was not performed because of both time constraints and the known factor that the depth sensitivity drops exponentially as identified in earlier tests.

Data was collected for each displacement point 12 times for 30 second iterations. The average result of these iterations was then declared as the “sensitivity” for the probe at the specified displacement point. The spatial resolution peak was then normalised with respect to the displacement point identified as having the largest

number of counts. This is the most sensitive point on the probe. This shorter acquisition time frame was chosen to be more realistic of the requirements for this probe in the surgical environment. The test results would also explore the possibility of other applications for the probe.

The IC due to requiring a higher accuracy was more rigorously tested than the OC. Data was provided for the X-axis, Y-axis and 3D spatial of the IC. The same data was not collected for the OC because its function was primarily for collecting Background events for subtraction when localising the position of a radionuclide. This data may have been useful for confirming and illustrating the interface area between the two channels but time constraints were an impinging factor. The X-axis spatial resolution for the OC was acquired in an attempt to address this point regardless.

The X-axis resolution was performed for the OC to assess the effectiveness of the active collimation mode. It was possible that two high sensitivity spikes approx. $\pm$ 1.5 mm along the x-axis may appear correlating to the position of the OC. The reason for this is because the OC scintillator starts at a radius of > 1.5 mm from the probes physical centre. Sufficient Tungsten Collimation however should result in the OC having a singular peak correlating to the position of the IC. This is because the function of the Probes Passive Tungsten Collimation is to prevent emissions entering the OC through anywhere except the IC. This test would therefore assess the scintillators capacity to operate with the background suppression circuit in the Liana Probe.

The experimental setup was nearly identical to the configuration used in the study by Franks. The setup was similar to the one used for the sensitivity test in Fig. 50, which

involved simulating a point source to determine the probes sensitivity to trace amounts of radionuclide confined within a patients body. In this case, the test will be to determine the probes capacity to spatially resolve events coming from a simulated Co-57 point source in the patients body. Results of this spatial resolution test should be comparable to those performed by Franks.

## *IC SPATIAL RESOLUTION RESULTS*

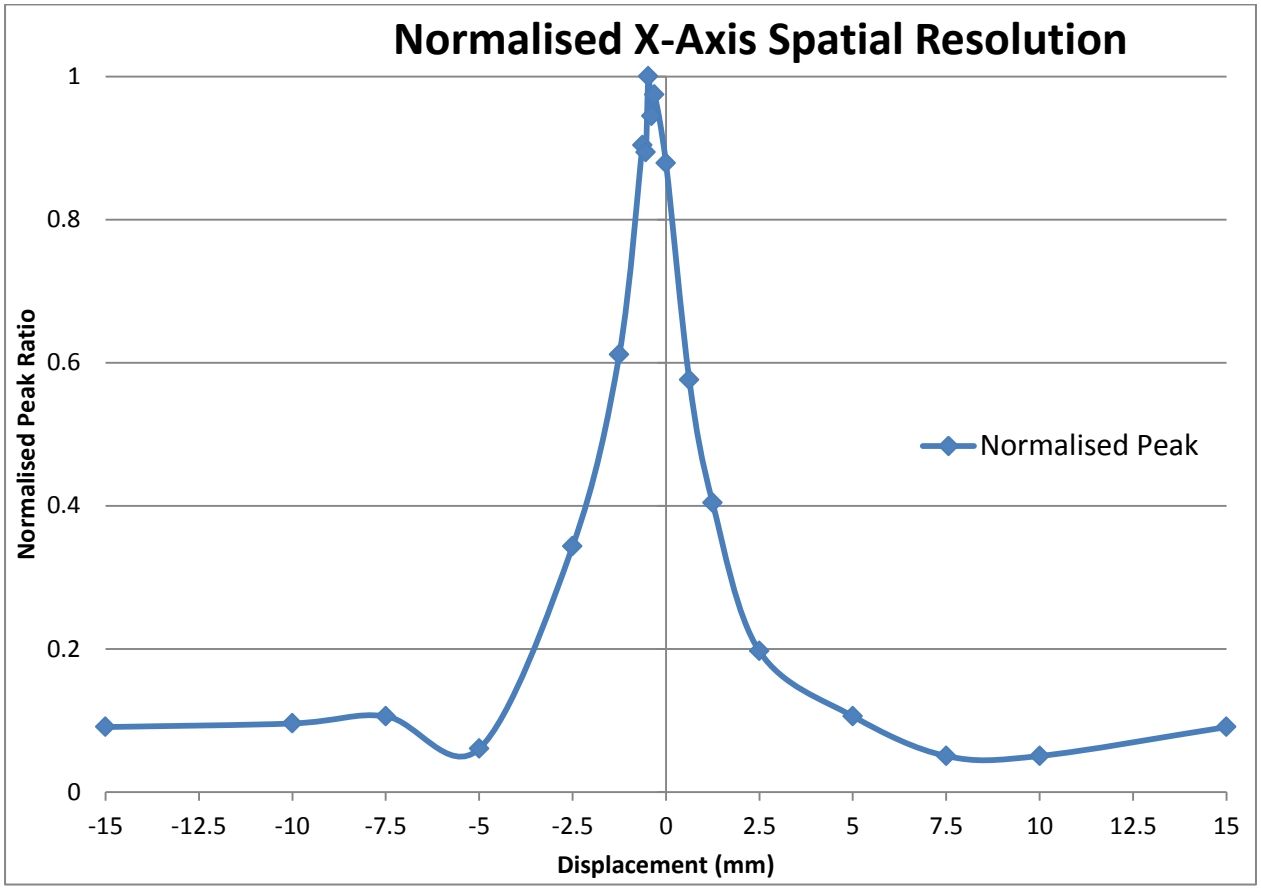


**FIG. 55:- NORMALIZED RESPONSE OF THE LIANA PROBE SCANED THORUGH THE POINT SOURCE IN X-DIRECTION.**

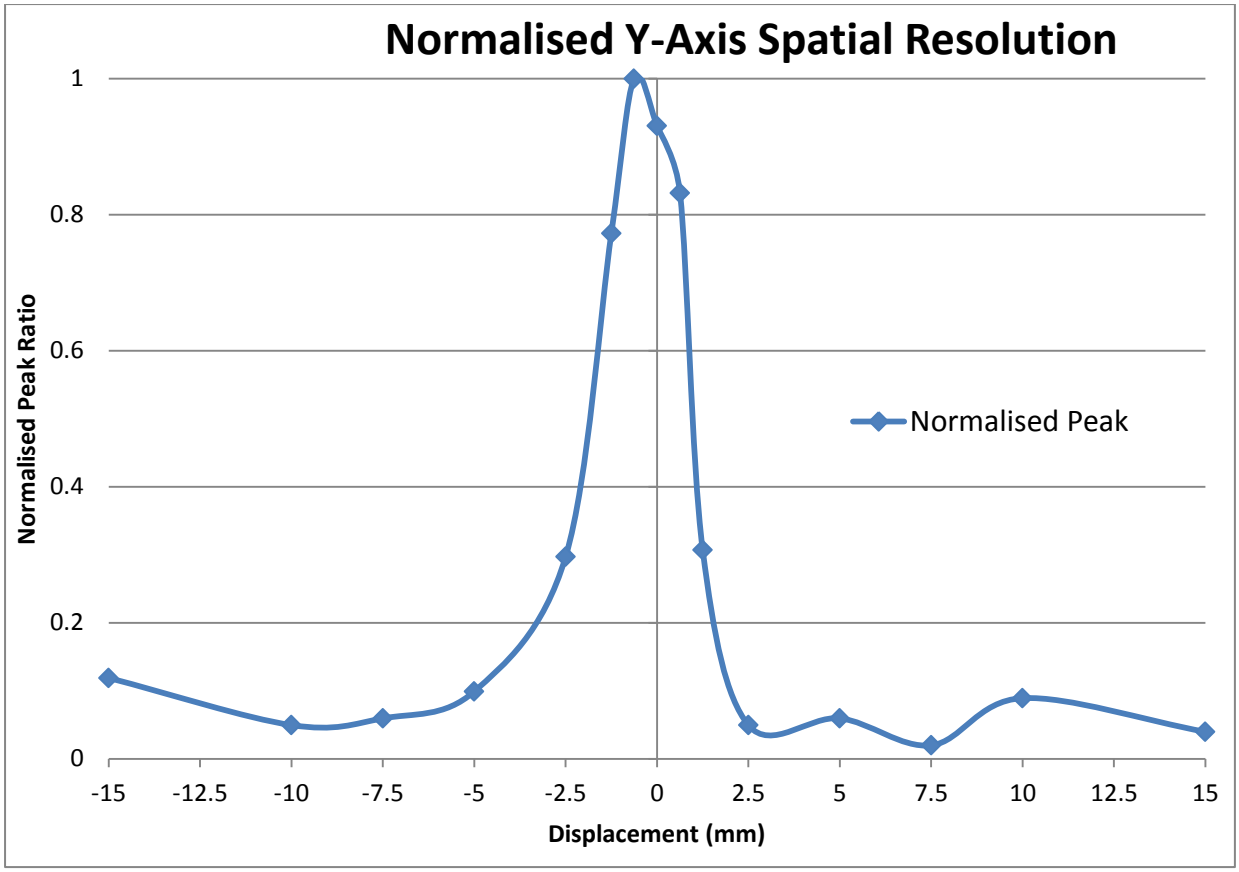


**FIG. 56:- NORMALIZED RESPONSE OF THE LIANA PROBE SCANED THORUGH THE POINT SOURCE IN Y-DIRECTION.**

## *IC RESULT DISCUSSION*

This investigation found that the Liana probe produced a much better spatial resolution than was found in the study performed by Franks. This implied that the probe was ideal for the precise localisation of radiopharmaceuticals. The most sensitive point of the probe corresponded to the axial axis of the collimator. The height of the emission peaks was distinctive and well above background counts as was demonstrated in the spatial resolution test. This information was useful because a comparison could be made between the recorded centre peak and the background counts. The results therefore identified that background events comprised of approximately 10% of the counts in the resolvable peak.

It was observed that the sensitivity did not decay instantly like a $\delta$-function, this result was expected because the area of the IC crystal was not point like. A 3D spatial resolution was obtained during the above mentioned experiments and is demonstrated in Fig. 57

The XY-spatial resolution was acquired under the same conditions as the sensitivity measurement tests. The function used to extrapolate this curve was,

$$\frac{I}{I_{Max}} = \exp\left( -0.3\left[ \left( x_2 + 0.39 \right)^{\frac{8}{5}} + \left( y_2 + 0.63 \right)^{\frac{8}{5}} \right] \right)$$

The maximum counts were found at a displacement x = -0.39 mm and y = -0.63 mm which corresponded to the locations of the peak maximum presented in Fig. 55 and Fig. 56. These points are most likely not located at x = 0, y = 0 because of a difficulty in precisely aligning the probe over the collimation hole. The results of the XY 3D spatial resolution are presented below. The background counts were not modelled in

this figure. This is because they were already observed in the spatial resolution studies in Fig. 55 and Fig. 56.

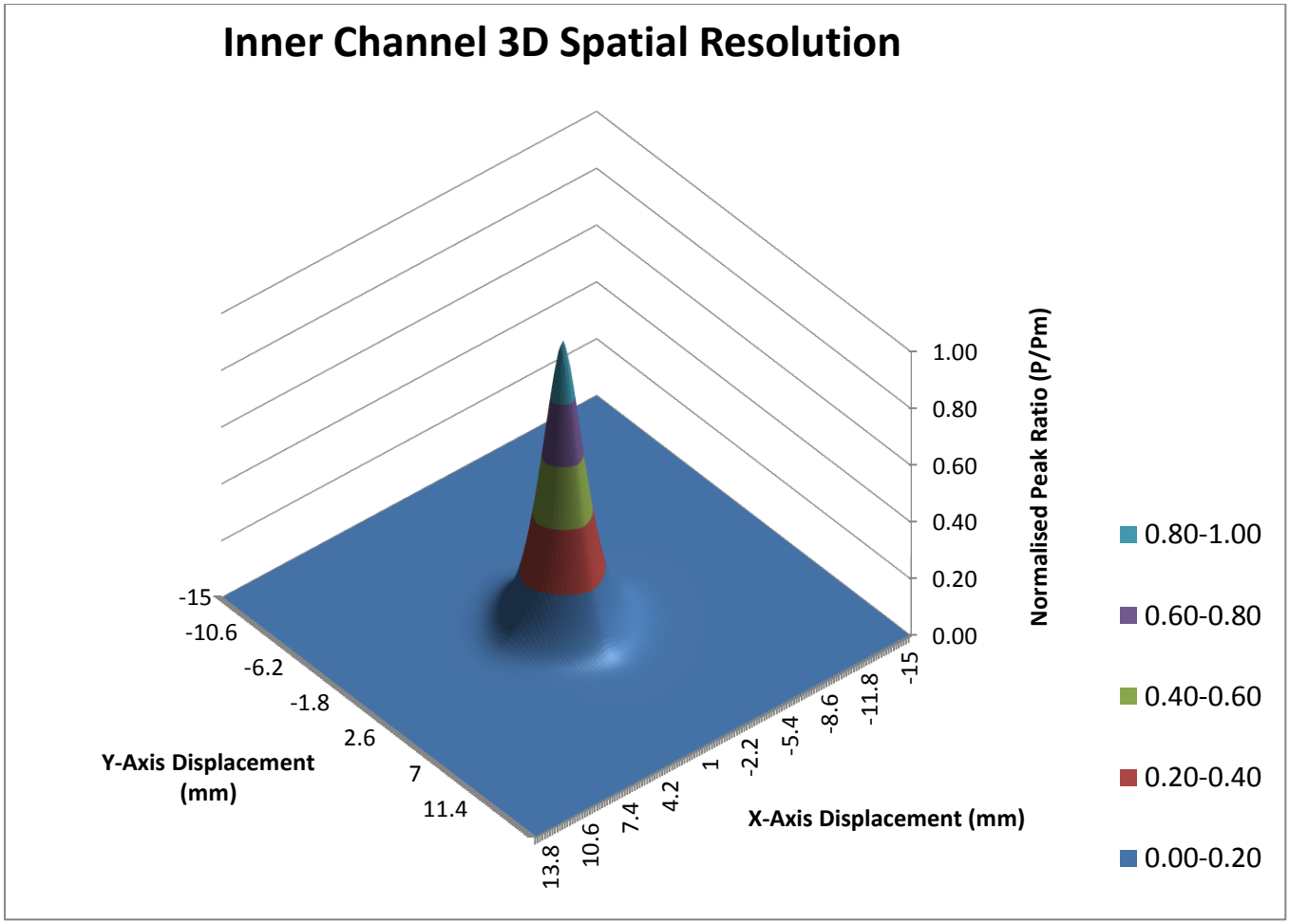


**FIG. 57:- THIS CHART IS CENTRED AT X = -0.39 MM AND Y = -0.63 MM. EXCLUDING THE BACKGROUND COUNT DOMAIN THE DEVIATION OF THE EXTRAPOLATED SPATIAL ENERGY FROM THE TRUE DATA IS <6%.**

## *XY SPATIAL RESOLUTION DISCUSSION*

The Full Width at Half Maximum (FWHM) using the extrapolated function was determined to be approximately 3.60 mm. The results correlated with the X and Y axis spatial resolutions determined in Fig. 55 and Fig. 56. The diameter of the inner scintillate was 3 mm and the diameter of the lead aperture was 0.5 mm. This information implied that a displacement $\pm$ 1.8 mm from the probe centre represented when only half of the IC was exposed to the source. Therefore only half of the photons could traverse into the IC. This data identified the additional 0.6 mm diameter of the channel as a result of inaccuracy provided by the 0.5 mm collimator aperture. The spatial resolution recorded during this project was almost double what was found in Franks study. The factorial difference was attributed to the probes closer proximity to the emission source in this study with respect to the displacement used in Franks study. The Penumbra may also have contributed to this width.

The extrapolated function was 94% accurate with the experimentally collected results and implied the FWHM resolution to be 3.60 ± 0.09 mm. The uncertainty was calculated using the difference in displacement between the measured energy point and its theoretical 6% energy difference. For a 50% counts reading at x = 1.30 mm (y = 0mm) the counts uncertainty is 3%. The displacement for 53% and 47% of maximum counts reading are x = 1.21 mm and x = 1.39 mm respectively. The displacement between these points from the ideal value of x = 1.30 mm is 0.09 mm which constitutes our displacement error. The horizontal step size for the 3D graph was 0.22mm/point i.e. approx. 5 data points were collected within 1 mm. This implies a precise localisation window based on the response difference of the device across such minute displacements, and in short time frames of 30 seconds.

The data collected for the resolution suggested the probe to be excellent for medical applications, where fast response and high accuracy are key factors to surgical success. The experimental results align with the expected outcomes for the IC and show the collimation as effective for assessing the dual function capacity for the probe.

### ***XY SPATIAL RESOLUTION FOR IC CONCLUSION***

It was implied from the results that the Liana Probe spatial resolution had a wider spatial detection window for the IC than what was recorded by Franks study. This result was expected as the probe was in closer proximity to the emission source in these tests than in Franks study and thus Penumbra was expected to impact the results. The collimation was demonstrated as effective for testing the IC with the background suppression function in effect.

It should be noted that the Liana Probes ‘A-only’, ‘A-B’ and ‘A+B’ modes were not assessed due to numerous difficulties encountered with getting the probe to work. There only time enough gather the data presented above.

## *SPATIAL RESOLUTION SUMMARY*

The Spatial Resolution FWHM was determined statistically to be 3.60 mm $\pm$ 0.09 mm. Since the area per unit data point collected was actually 0.22 $mm^2$, this statistical result for the uncertainty is surprising. This uncertainty suggests the probes fine localisation capacity was not pushed to its limit and is capable of more than was acquired during this investigation.

The FWHM determined during this study was twice the value obtained by Franks. This was most likely because of insufficient collimation material between the probe and emission source resulting in a Background Penumbra. Reduced collimation would result in a wider energy window and thus a wider energy peak would result. As the IC diameter is 3mm, 0.5 mm of the 0.6 mm could be accounted for by the aperture width of the collimator. The remaining 0.1 mm corresponds to either the uncertainty value or what may be considered the *virtual aperture width*. I.e. the width of the aperture due to reduced collimation.

This supports the Penumbra hypothesis because emissions would be expected to pass at an angle through the IC to the OC due to insufficient collimation. The FWHM resolution for the OC corresponded to this result with a value of approximately 3.80mm, where it is noted that the OC values were not acquired as accurately as the IC.

Comparing the peak height with environmental background values showed that 90% of the peak height remained resolvable. This means the probe under surgical conditions would be able to precisely identify the emission sources position as the FWHM was well above environmental background levels.

# CLOSING REMARKS

The Liana Probes design including the readout electronics and scintillator – Photodiode detectors was found to be excellent. These must be addressed so that certain factors of the Liana Probes functionality can be identified for improvement.

1. Electromagnetic Compliance

An unexpected issue of the board operation was the presence of large electronic noise. Numerous grounding connections helped resolve the issue by at minimum 10%. Using one grounding connection for resolving the Co-57 peak was impossible to achieve with any consistency. The data identifying and exploring this problem was excluded from the paper because of its inapplicability to the primary results acquired. The results acquired by this study are reliable however as the only results presented are those with the reduced noise because of the additional grounding.

2. Collimation design

The Tungsten Collimation material should be extended to thoroughly cover the top of the probe. Currently three steel washers are combined together to provide an aperture of 3mm diameter which corresponds to the position of the IC scintillate. Another suggestion is to make the Tungsten cover the base of the detector to prevent background emissions from other substances entering through the back of the probe through the electronics section.

3. Electronics Manufacture

Out of the six boards developed by this study including the one that was pre-developed (Board 0) by an earlier study. Board 6 was the only circuit able to provide consistently accurate and reliable results. Furthermore, it was also the board that

required the least maintenance. This result was directly attributable to the study as it independently manufactured these boards.

The problems associated with the board fabrication process were identified as due to:-

1. Non-professional technicians assembling the PCB's.
2. A lack of understanding associated with assembling and handling ultra-high impedance circuits.
3. Inappropriate soldering techniques and unsuitable fluxes.
4. Failure to properly clean the PCB after assembly.

It is recommended to future studies that manufacturing be performed by more experienced and capable electronics developers. This will ensure the highest performance ability of the boards which consequently will provide the highest precision results for the Liana $^{3}$DS. This will also better reflect the operational capacity of the Liana probe for its various modes once it is produced at a commercial level.

This is especially recommended to future studies investigating the probes circuit mode design as it was the only factor unable to be investigated during this study.

# RESEARCH RESULTS SUMMARY

Extensive technical and testing difficulties were experienced during the research process, however the Liana $^{3}$DS Probe was an operational success within the limits it was assessed. This was not able to include the signal processing section for the DDP function. It was anticipated however that the dual function of the probe would be effective and will be limited only by the background suppression function located within the circuit.

The FWHM obtained for the Liana Probe without the $^{3}$DS modes in effect was determined to be 3.60 mm $\pm$ 0.09 mm. This FWHM was double the value determined by Franks and theoretically was most likely because of insufficient collimation resulting in a Background Penumbra.

The Background Penumbra was not found to jeopardise the results of this study, but rather found to support the inclusion of the background suppression function. It was recommended that this technique be used for diagnosing the circuits A-B mode once the cross talk had been evaluated as suggested in this paper.

The physical phenomena managed by the $^{3}$DS electronics requires the Scintillator probe to be designed and manufactured in a specific way to achieve the best possible results. The Probes Scintillator must comprise of two co-axial like Channels and be Passively Collimated for the electronics to fine localise an emission source.

The Probes Scintillator was thoroughly tested during the course of this investigation and was found to satisfy the needs of a Background Suppression Co-Incidence circuit. The $^{3}$DS was therefore expected to operate with high precision once the Active Collimation Co-incident electronics was in effect.

# RESEARCH CONCLUSION

A criteria of seven requirements were stated and discussed in the literature review. This criteria addressed the needs for an Intraoperative Gamma Probe in the modern surgical theatre. The Liana $^{3}$DS satisfied these seven criteria in the following ways:-

1. Point source detection by the $^{3}$DS has a FWHM resolution of at least (3.60 $\pm$ 0.09) mm. This result was obtained for the A mode only.
2. Both the Passive (Tungsten/Steel) and Secondary Detector for Active Collimation were shown to be effective for supressing emissions within the intended energy range.
3. The energy FWHM was on average approx. 10% for Na-22 and Cs-137 emission sources and applied for all probes using the new circuit boards. This was approx. a 10 – 25% improvement on the resolution from Franks study using the same Scintillators.
4. A precise spectra for a point source could be acquired for a time ≥ 30 seconds, this fast response allows the surgeon to identify and remove afflicted tissue faster.
5. Across 2 hours and 15 mins the energy spectra deviated by less than 3% meaning results are 97% reproducible. The probe lifetime is estimated at 5-10 years.
6. The probe is designed to be manoeuvrable and portable.
7. Energy Windowing is available through the Active Collimation function.

The Liana $^{3}$DS has therefore demonstrated itself as capable of addressing all seven of these Criteria. The impact of its circuit logic was not assessed but is anticipated to

improve the detector functionality, especially with regards to physical localisation, significantly.

# REFERENCES

[1] G. Camilleri, B. Grima and F. Zarb, "Correlation of Number and Identification of Sentinel Lymph Nodes during Radiographer led Lymphoscintigraphy Prior to Sentinel Node Biopsy in Breast Cancer Patients," vol. 18, no. 1, 2011.

[2] M. Valsecchi, D. Silbermans, N. d. Rosa, S. Wong and G. Lyman, "Lymphatic mapping and sentinel lymph node biopsy in patiens with melanoma: a meta-analysis.," vol. 29, no. 11, pp. 1479-1487, 2011.

[3] American Cancer Society, "Cancer Facts and Figures," American Cancer Society, 2011. [Online]. Available: http://www.cancer.org/research/cancerfactsstatistics/allcancerfactsfigures/index. [Accessed 10 October 2013].

[4] P. Brader, F. Daghighian, Y. Fong, G. Mithat, L. Gonzalez and S. Gonzalez, "An Analysis of the Utility of Handheld PET Probes for the Intraoperative Localization of Malignant Tissue," Journal of Gastroinstestinal Surgery, New York City, 2011.

[5] P. Zanzonico and S. Heller, "The Intraoperative Gamma Probe: Basic Principals and Choices Available," vol. 30, no. 1, 2000.

[6] Y. Ogasawara, S. Yoshitomi, S. Sato and H. Doihara, "Clinical Significance of Preoperative Lymphoscintigraphy for Sentinel Lymph Node Biopsy in Breast Cancer," vol. 148, no. 2, 2007.

[7] D. Krag, S. Harlow, D. Weaver and T. Ashikaga, "Technique of Sentinel Node Resection

in Melanoma and Breast Cancer: Probe guided surgery and Lymphatic Mapping," vol. 24, no. 2, 1998.

[8] S. Yamamoto, K. Matsumoto, S. Sakamoto, K. Tarutani, K. Minato and M. Senda, "An intra-operative positron probe with background rejection capability for FDG-guided surgery," vol. 19, no. 1, 2005.

[9] R. Elmore, Interviewee, *Handheld Probes Inquiry - E-mail Correspondence.* [Interview]. 3 January 2013.

[10] S. Heller and P. Zanzonico, "Nuclear Probes and Intraoperative Gamma Cameras," vol. 41, no. 3, 2011.

[11] R. Raylman and A. Hyder, "A Dual Surface Barrier Detector Unit for Beta-Sensitive Endoscopic Probes," vol. 51, no. 1, 2004.

[12] S. Bonzom, L. Ménard, S. Pitre, M. Duval, R. Siebert, S. Palfi, L. Pinot, F. Lefebvre and Y. Charon, "An Intraoperative Beta Probe Dedicated to Glioma Surgery: Design and Feasibility Study," vol. 54, no. 1, 2007.

[13] T. Hickernell, H. Barber, H. Barret and J. Woolfenden, "Dual Detector Probe for Surgical Tumor Staging," vol. 29, no. 6, 1988.

[14] N. Hudina, L. Pinota, N. Dinub, Y. Charona, V. Puillb, B. Janviera, V. Chaumatb, M. Duvala, M. A. Haidara, R. Sieberta and L. Ménard, "Characterization and Optimization of silicon photomultipliers for the development of intraoperative beta probes," New Developments in Photodetection, Orsay, 2012.

[15] J. Parus, J. Kierzek, W. Raab and D. Donohue, "A dual Purpose Compton Suppresion Spectrometer," vol. 258, no. 1, 2003.

[16] A. Rosenfeld, M. Lerch, M. Chan, D. Inwood, G. Takacs, B. Lee, A. Getkin and V. Perevertaylo, "A Dual Scintillator - Dual Silicon Photodiode Detector Module for Intraoperative Gamma/Beta Probe and Portable Anti-Compton Spectrometer," in *Proceedings of the fourth international symposium on radiation safety and detection technology*, Sydney, 2008.

[17] A. Rosenfeld, M. Lerch and O. Gektin, "Dual Detector". United States of America Patent 8, 212, 220, 2012.

[18] B. Franks, "Characterisation of a New Dual Photodiode -CsI(TI) Detector to be used for Intraoperative Radioguided Surgery.," University of Wollongong, Wollongong, 2012.

[19] Nuclear Engineering - MIT, "Interactions of Photons with Matter," Massachusetts Institute of Technology (MIT), 22 January 2006. [Online]. Available: http://ocw.mit.edu/courses/nuclear-engineering/22-01-introduction-to-ionizing-radiation-fall-2006/lecture-notes/energy_dep_photo.pdf. [Accessed 7 May 2013].

[20] NucSafe, "Selection of Gamma Detector," NucSafe, 13 February 2013. [Online]. Available: http://www.nucsafe.com/cms/Selecting+Gamma+Detector/43.html. [Accessed 7 May 2013].

[21] D. Inwood, "A Scintillation Dual Detector System Featuring Active Compton Suppresion," University of Wollongong, Sydney, 2007.

[22] F. Hartmann, "Silicon Tracking Detectors in High Energy Physics," vol. 666, no. 1, 2011.

[23] A. E. G. H. W. S. Giuliano Mariani, Radioguided Surgery, Springer, 2007.

[24] A. Flynn, "Invesitgation and Characterisation of a Dual Anti-Comptonfor Anti-Terrorism Applications," University of Wollongong, Wollongong, 2011.

[25] D. Morton and A. Chan, "The Concept of Sentinel Node Localisation: How it all Started," vol. 30, no. 1, 2000.

[26] M. Tsuchimochi and K. Hayama, "Intraoperative gamma cameras for radioguided surgery: Technical characteristics, performance parameters, and clinical applications,," ELSEVIER, 4 June 2012. [Online]. Available: http://dx.doi.org.ezproxy.uow.edu.au/10.1016/j.ejmp.2012.05.002. [Accessed 12 January 2013].

[27] A. Goyal, R. Newcombe and R. Mansel, "Role of Routine Preoperative Lymphoscintigraphy in Sentinel Node Biopsy for Breast Cancer," vol. 41, no. 2, 2004.

[28] E. Hoffman, M. Tornai, M. Janecek, B. Patt and J. Iwanczyk, "Intraoperative Probes and Imaging Probes," in *Emission Tomography:- The Fundamentals of PET and SPECT*, Los Angeles, Academic Press, 2004.

[29] B. Martin, Nuclear and Particle Physics: An Introduction, Chippenham: John Wiley & Sons Ltd., 2009.

[30] L. Fass, "Imaging and Cancer:- A Review," vol. 2, no. 2, 2008.

[31] E. Hoffman, M. Tornai, C. Levin, L. MacDonald and C. Holdsworth, "A dual detector beta-ray imaging probe with gamma-ray background suppression for use in intra-operative detection of radiolabeled tumors," vol. 409, no. A, 1998.

[32] G. F. Knoll, Radiation detection and measurement, vol. 4, Hoboken: John Wiley & Sons, 2010.

[33] M. Benettia, A. Tarollib, G. Giacominib and G. D. B. C. Piemonteb, "Simulation and characterization of different setups for gamma ray detection using SiPMs and LYSO scintillators," vol. 658, no. 1, 2011.

[34] P. Brader, Y. Fong, M. Gonen, L. Gonzalez, S. Gonzalex and V. Strong, "Novel handheld PET probes provide intraoperative localization of PET-avid lymph nodes," Surgical Endoscopy, New York City, 2011.

[35] M. Hunt, B. Shank, B. McCormick, J. Yahalom, M. Graham and G. Kuthcher, "The use of Lymphoscintigaphy in Treatment Planning of Primary Breast Cancer.," vol. 17, no. 3, 1989.

[36] N. Clinthorne, R. Garcia-Parra, M. Picchio, M. Piert and L. Wang, "Performance of beta- and high-energy gamma probes for the detection of cancer tissue in experimental surgical resection beds," Annals of Nuclear Medicine, Milan, 2011.

[37] N. Hartsough, H. Barret, H. Barber and J. Woolfenden, "Intraoperative Tumor Detection: Relative Performance of Single-Element, Dual-Element and Imaging Probes with Various Collimators," vol. 14, no. 2, 1995.

[38] V. Strong, C. Galanis, C. Riedl, V. Longo, F. Daghighian, J. Humm, S. Larson and Y. Fong, "Portable PET probes are a novel tool for intraoperative localization of tumor deposits," vol. 3, no. 2, 2009.

[39] R. Moadel, "Breast Cancer Imaging Devices," vol. 41, no. 3, 2011.

[40] WikiBooks, "Basic Physics of Digital Radiography/The Patient," WikiBooks, 22 April 2013. [Online]. Available: http://en.wikibooks.org/wiki/Basic_Physics_of_Digital_Radiography/The_Patient. [Accessed 07 May 2013].

[41] Saint Gobain Crystals, "Compact CsI (TI) Photodiode Detector," Saint Gobain Crystals, 01 March 2009. [Online]. Available: http://www.detectors.saint-gobain.com/uploadedFiles/SGdetectors/Documents/Product-Configurations/Compact-CsI-Photodiode.pdf. [Accessed 7 May 2013].

[42] Crystal Gamma Probes, "Crystal Gamma Probes: Buy," Crystal Gamma Probes, 15 June 2005. [Online]. Available: http://www.surgicalprobe.com. [Accessed 11 August 2012].

[43] C. Pouroumb, "Literature Review of Detector based electronics," University of Wollongong, Wollongong, 2011.

[44] D. J. E. Parks, "The Compton Effect - Compton Scattering and Gamma Ray Spectroscopy," Dr. James E. Parks, 01 August 2009. [Online]. Available: http://www.phys.utk.edu/labs/modphys/Compton%20Scattering%20Experiment.pdf. [Accessed 7 May 2013].

[45] M. Mathew, A. Saha, T. Saleem, N. Saddozai, I. Hutchinson and A. Nejim, "Pre-operative Lymphoscintigraphy before Sentinel Lymph Node Biopsy for Breast Cancer," vol. 19, no. 1, 2009.